



**SYNTHESIS AND EVALUATION OF SILVER  
NANOMATERIALS TO ADDRESS  
MULTIDRUG RESISTANCE**

By

**Zil-e-Huma**

*A THESIS*

Submitted in partial fulfillment of the requirements for the degree of PhD  
in Chemistry from Lahore University of Management Sciences (LUMS)  
DHA, Lahore Cantt - 54792 Lahore, Pakistan

June 2021

# SYNTHESIS AND EVALUATION OF SILVER NANOMATERIALS TO ADDRESS MULTIDRUG RESISTANCE

A Dissertation Submitted to  
Department of Chemistry and Chemical Engineering  
Lahore University of Management Sciences

By

**Zil-e-Huma**  
**2014-13-0013**

In Partial Fulfillment of the Requirements for the Degree of  
Doctor of Philosophy

**June 2021**

Lahore University of Management Sciences  
D.H.A, Lahore Cantt. 54792  
Lahore, Pakistan

## Department of Chemistry and Chemical Engineering

Lahore University of Management Sciences

Lahore

### Certificate

This is to certify that the thesis entitled **“SYNTHESIS AND EVALUATION OF SILVER NANOMATERIALS TO ADDRESS MULTIDRUG RESISTANCE”** is an authentic record of research work carried out by **Ms. Zil-e-Huma**, Roll No. 2014-13-0013, under my supervision, in partial fulfilment of the requirements for the degree of PhD in Chemistry at Lahore University of Management Sciences, and that no part of this thesis has been presented for any other degree.

---

Dr. Irshad Hussain

Dated:  
10-06-2021

Professor  
(Supervisor)

## Department of Chemistry and Chemical Engineering

Lahore University of Management Sciences

Lahore

### DECLARATION

I hereby declare that the work presented in this thesis entitled "***SYNTHESIS AND EVALUATION OF SILVER NANOMATERIALS TO ADDRESS MULTIDRUG RESISTANCE***" is entirely original and was carried out by me independently under the supervision of Dr. Irshad Hussain (Professor, Department of Chemistry & Chemical Engineering, Lahore University of Management Sciences) and has not been included in any other thesis submitted for the award of any other degree.



Zil-e-Huma

2014-13-0013

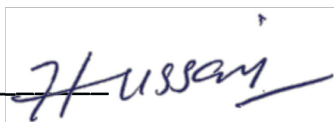
# SYED BABAR ALI SCHOOL OF SCIENCE AND ENGINEERING

## Dissertation Approval

The members of the Committee approve the dissertation entitled **SYNTHESIS AND EVALUATION OF SILVER NANOMATERIALS TO ADDRESS MULTIDRUG RESISTANCE** by **ZIL-E-HUMA**, defended on **May 31, 2021**.

It is recommended that this dissertation be used in partial fulfillment of the requirements for the degree of Doctor of Philosophy from Department of Computer Science in Syed Babar Ali School of Science and Engineering.

Dr. Irshad Hussain  
(Advisor)



Dr. Hussnain A. Janjua  
(External Examiner)

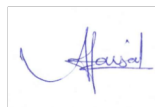


Principal  
Hussnain A. Janjua  
Applied Bioscience  
NUST, Islamabad

Dr. Shahzad-ul-Hussan  
(FDC Member)



Dr. Amir Faisal  
(FDC Member)



Dr. Shaper Mirza  
(FDC Member)



Dr. Muhammad Saeed  
(FDC Member)



*Dedicated*

*To*

*My Father*

*who had given me dreams to look forward to,*

*&*

*To*

*My Husband,*

*for his all-time encouragement and support*

## ACKNOWLEDGEMENTS

First of all, my praises and humble submission to Allah Almighty for His countless blessings, Who enabled me to complete it successfully. I offer my special thanks to the Prophet Muhammad (PBUH) who give us message to seek knowledge for the betterment of humanity and other creatures.

This dissertation marks the end of my PhD life during which I have learnt a lot as regards to research project management and scientific knowledge. I would like to express my deepest gratitude for my PhD supervisor, Dr. Irshad Hussain. I found the attitude and substance of a genius in him. Without his persistent help, guidance, valuable advices and extensive discussions, this work would not have been possible.

I am pleased to extend my indebted thanks to all the thesis committee members i.e., Dr. Muhammad Saeed, Dr. Amir Faisal and Dr. Shaper Mirza for their unwavering support and mentorship throughout my PhD projects. I want to convey my gratefulness to all other faculty members i.e., Dr. Falak Sher, Dr. Basit Yameen, Dr. Ghayoor Abbas Chotana, Dr. Salman Noshear Arshad and Dr. Muhammad Zaheer of Department of Chemistry and Chemical Engineering, SBASSE, LUMS for their occasional support and guidance.

Special thanks to Professor Vincent M. Rotello and Professor Thomas P. Davis for collaborating with us to successfully conduct a part of this research in Rotello's lab at UMass, Amherst, USA and CBNS group at Pharmaceutical department of Monash University, Parkville, Australia. I would also like to thank group fellows in these two groups especially Akash Gupta, Rubul, Ibrahim Javed, PuChun Ke, Marwin, Alexender, Aparna and Emily.

I am also extremely thankful to my all colleagues and friends especially Syed Zajif Hussain, Shazia Mumtaz, Abbass, Akhtar Munir, Muhammad Abdullah, Summayah, Hiba, Mudassir, Farhan Sohail, Mishal Khan, Uzma Hira, Soneela Asgher, Tayyaba Tariq, Mira Butt and Munazah for their continuous encouragement during my PhD. I would highly appreciate Mr. Muhammad Farooq Usman Ali for his all time and quick availability for timely submissions despite of long distances and time differences. All the support of other Academic and Lab staff members is highly acknowledged.

I would love to express kind regards to my dear parents and husband who always prayed for my success. I pay my attributes to my sister, brothers, bhabies, brother in laws, nephews, nieces and last but not the least my little champion, Dur-e-Shahwar, for being the inspiration during my entire PhD Life.

Finally, I would like to acknowledge Higher Education Commission (HEC) Pakistan for its financial assistance to conduct this research at LUMS, USA and Australia through HEC indigenous fellowship, Pak-US collaborative project and IRSIP.

*Zil-e-Huma*

## ABSTRACT

Multidrug resistance (MDR) is a major healthcare concern triggered by the extended subtherapeutic clinical conduct of infectious diseases. The resistant infections are responsible for the death of more than 0.7 million people every year and accordingly, the expected rate of death of people from drug resistant infections in 2050 is 10 million/ year. Nanoscale manipulation of metal nanoparticles has notable potential to address this concern by the tuning of nanobio interface to attack bacteria. Among the metals explored, Ag is the most effective due to certain physicochemical and morphological factors such as shape, size, composition, colloidal stabilization, aggregation behavior, surface/volume ratio, surface corona, surface coating, which when rightly tuned could benefit against numerous pathogenic bacteria by giving broad-spectrum killing profile.

In this regard, branched polyethylenimine-decorated silver nanoclusters (bPEI-Ag NCs) were produced to kill MDR pathogenic bacteria selectively by coupling the antimicrobial potential of silver with the selective virulence of bPEI towards bacteria. These Ag NCs were found very effective to kill 12 MDR clinical bacterial strains (uropathogenic) at minimal concentration of  $\sim 1$  nM compared to human fibroblast and red blood cells. The dreadful pathogens i.e., *P. aeruginosa* further challenge the situation of MDR by their innate ability to form biofilms. In this study, decrease of bacterial action and virulence through the network of extracellular amyloids was explored using silver nanoclusters (AgNCs) and nanoparticles (AgNPs) having same surface chemistry. The comparative study of these nanomaterials revealed that with the change in surface charge and size of nanoparticles, their bactericidal and antibiofilm properties can be tuned. It was further observed that at the concentration of 1  $\mu$ M or lower, both the bactericidal and antibiofilm potential of nanomaterials was linked with their structure-based bionano connections but not with silver ions discharge. This study demonstrated the biocidal ability of safe nanotechnology through the unique direction of amyloidosis inhibition. Similarly, the emerging health issue related to MDR in pneumococcal cells was also addressed by the design/development of smart and effective nanocapsules encapsulating antibiotic and silver NCs coated with organic ligands to guide the nanocapsules to the desired target. These nanocapsules have shown their

potential of efficient targeting, delivering and retaining hydrophobic drug in the desired pneumococcal strains by breaking resistive barriers electrostatically at concentrations safe to mammalian cells. This method is quite simple and easy to modify according to specific application.

Overall, this thesis supplements the available literature and suggests that silver-based nanomaterials are being recognized as a starting point for the development of novel inorganic materials-based potential antibiotic candidates to address MDR.

## خلاصہ

کثیر الادویاتی مزاحمت (ایم۔ ڈی۔ آر)، صحت عامہ کا ایک گھمبیر مسئلہ ہے جس کی بڑی وجہ متعدد بیماریوں کے علاج میں ادویات کا کثیر المیعادی ذیلی استعمال ہے۔ یہ مزاحمتی انفیکشن ہر سال 0.7 ملین سے زیادہ افراد کی موت کے ذمہ دار ہیں اور 2050 میں ایسے انفیکشن سے متاثرہ افراد کی اموات کی متوقع شرح 10 ملین سالانہ ہے۔ اس تشویش کو دور کرنے میں دھاتوں کے انتہائی مہین ذرات کا فی موثر ثابت ہو سکتے ہیں کیونکہ ان میں جوڑتور کے عمل سے بیکٹیریا پر حملہ کرنے کی قابل ذکر صلاحیت موجود ہے۔ اب تک کھوجی جانے والی دھاتوں میں، چاندی کے مہین ذرات موثر ترین پائے گئے ہیں کیونکہ اپنے طبعی-کیمیائی اور ساختی خواص جیسا کہ شکل، حجم، ترکیب، سطح اور حجم کے تناسب وغیرہ میں ردو بدل سے وہ بیکٹیریا کی مختلف انواع کو ہلاک کر سکتے ہیں۔

اس تناظر میں، پولی اتھائیلین امین کے مہلک پن اور چاندی کی اینٹی بیکٹیریل صلاحیت کو یکجا کرتے ہوئے، مزاحمتی بیکٹیریا کو ہلاک کرنے کے لیے، شاخی پولی اتھائیلین امین سے سچے چاندی کے مہین گچھے تیار کیے گئے۔ یہ گچھے ایم ڈی آر بیکٹیریا کی بارہ انواع کو کم سے کم 1 nM مقدار میں مارنے کے لئے بہت امتیازی ثابت ہوئے ہیں۔ مہلک انواع جیسا کہ پی۔ ایروجنینوزا اپنی بائیوفلم بنانے کی فطری صلاحیت کے ذریعہ ایم ڈی آر کی صورتحال کو مزید سنگین کرتے ہیں۔ اس تحقیق میں یکساں سطحی کیمیائی خواص رکھنے والے چاندی کے مہین گچھوں اور مہین ذرات کو اکسٹرا سیلولر امیلائڈز کے جال کے ذریعہ بیکٹیریا کی عمل اور مہلک پن میں کمی لانے کے لیے کھوجا گیا۔ ان مہین مادوں کے تقابلی مطالعے سے انکشاف ہوا ہے کہ مہین ذرات کے سطحی چارج اور حجم میں تبدیلی کے ساتھ، ان کی جراثیم کش اور اینٹی بائیوفیلم خصوصیات کو بھی بدلا جاسکتا ہے۔ یہ بھی مزید مشاہدہ کیا گیا ہے کہ 1  $\mu$ M یا اس سے کم کی مقدار میں، مہین مادوں کی اینٹی بیکٹیریل اور اینٹی بائیوفیلم دونوں صلاحیتیں ان کی ساخت پر مبنی بائیو نینو انٹرفیس سے منسلک تھیں لیکن چاندی کے برق پاروں کے اخراج سے منسلک نہیں۔ یہ مطالعہ محفوظ مہین ٹیکنالوجی (نینو ٹیکنالوجی) کے حیات کش خواص کا مظہر ہے۔ اسی طرح، نیموکوکلی خلیوں میں ایم ڈی آر سے متعلق ابھرتے ہوئے صحت کے مسئلے کو بھی ذہین اور موثر مہین کیپسولوں کی تیاری سے حل کیا گیا ہے۔ مہین کیپسولوں میں پوشیدہ اینٹی بائیوٹک کی نامیاتی مرکبات سے سچے چاندی کے مہین گچھوں کی مدد سے مطلوبہ نشا نے کی طرف رہنمائی کی گئی ہے۔ ان مہین کیپسولوں نے مطلوبہ نمو کوکل کی انواع کو حذف بنانے اور ان میں آب ترس دوائی کی ترسیل اور برقراری میں اپنی افادیت ثابت کی ہے۔ یہ طریقہ بہت سادہ اور آسان ہے اور اس میں مخصوص فائدوں کے حصول کے لیے ترمیم کرنا بھی آسان ہے۔

## List of Publications

### Publications (as 1<sup>st</sup> Author)

1. **Zil-e-Huma**, Akash Gupta, Ibrahim Javed, Riddah Das, Syed Zajif Hussain, Shazia Mumtaz, Irshad Hussain and Vincent M. Rotello. Cationic Silver Nanoclusters as Potent Antimicrobials against Multidrug Resistant Bacteria. *ACS Omega* **2018**, 12, 16721.
2. **Zil-e-Huma**, Ibrahim Javed, Zhenzhen Zhang, Hajira Bilal, Yunxiang Sun, Syed Zajif Hussain, Thomas P. Davis, Daniel E. Otzen, Cornelia B. Landersdorfer, Feng Ding, Irshad Hussain, Pu Chun Ke. Nano Silver Mitigates Biofilm Formation via FapC Amyloidosis Inhibition. *Small* **2020**, 16, 1906674.

### Publications (as co-author)

3. Shazia Mumtaz, Li-Sheng Wang, Sayed Zajif Hussain, Muhammed Abdullah, **Zil-e-Huma**, Zafar Iqbal, Brian Creran, Vincent M. Rotello, Irshad Hussain. Dopamine coated Fe<sub>3</sub>O<sub>4</sub> nanoparticles as enzyme mimics for the sensitive detection of bacteria. *Chemical Communications* **2017**, 53, 12306.
4. Muhammad Ahmed Mudassir, Syed Zajif Hussain, Mishal Khan, Sayed Tasmia Asma, Zafar Iqbal, **Zil-e-Huma**, Najeeb Ullah, Haifei Zhang, Tariq Mahmood Ansari, Irshad Hussain. Polyacrylamide exotemplate-assisted synthesis of hierarchically porous nanostructured TiO<sub>2</sub> microbeads for efficient photodegradation of organic dyes and microbes. *RSC Advances* **2018**, 8, 29628.
5. Farhan Sohail, Syed Hussain, Ibrahim Javed, Hafiz Shoaib Sarwar, Akhtar Nadhman, **Zil-e-Huma**, Mubashar Rehman, Sarwat Jahan, Irshad Hussain, & Gul Shahnaz. Polymeric nanocapsules embedded with ultra-small silver nanoclusters for synergistic pharmacology and improved oral delivery of Docetaxel. *Scientific Reports* **2018**, 8, 13304.
6. Muhammad Furqan, **Zil-e-Huma**, Zainab Ashfaq, Apsra Nasir, Rahim Ullah, Aishah Bilal, Maheen Iqbal, Muhammad Hashaam Khalid, Irshad Hussain, Amir Faisal. Identification and evaluation of novel drug combinations of Aurora kinase inhibitor CCT137690 for enhanced efficacy in oral cancer cells. *Cell Cycle* **2019**, 18, 2281.
7. Muhammad Farhan Sohail, Mubashar Rehman, Sayed Zajif Hussain, **Zil-e-Huma**, Gul Shahnaz, Omer Slaman Qureshi, Qandeel Khalid, Shaper Mirza, Irshad Hussain, Thomas J. Webster. Green synthesis of zinc oxide nanoparticles by Neem extract as multi-facet therapeutic agents. *Journal of Drug Delivery Science and Technology* **2020**, 59.

### Book chapter (as co-author)

8. Guotao Peng, **Zil-e Huma**, Muhammad Umair, Irshad Hussain and Ibrahim Javed. Nanosilver at the interface of biomedical applications, toxicology, and synthetic strategies. *In book: Nanosilver at the interface of biomedical applications, toxicology, and synthetic strategies* **2020**, 119-139.

## Conference Presentations

1. 2<sup>nd</sup> International Conference on Drug Development Natural & Synthetic organized at COMSATS Institute of Information Technology Abbottabad, Pakistan on August 23-25, 2015.
2. An international workshop on Nanosciences: Education and Industrial Applications at COMSTECH, Islamabad, Pakistan on December 13-15, 2016, sponsored by COMSTECH-HEC.
3. A national workshop on Advanced Materials Characterization Techniques on August 16-17, 2018, in Nathiagalli
4. 10<sup>th</sup> International Nanomedicine Conference on June 24-26, 2019, in Sydney Australia.
5. An international Conference on Recent Advances in Medical and Health Sciences on January 24-25, 2021, in Melbourne Australia.

# Table of Contents

|   |      |
|---|------|
| Certificate   | II   |
| Declaration   | III  |
| Approval  | IV   |
| Dedication  | V    |
| Acknowledgments   | VI   |
| Abstract  | VII  |
| List of Journal Publications  | XI   |
| Conference Presentations .....  | XII  |
| Table of Contents .....   | XIII |
| Table of Acronyms.....  | XVI  |
| List of Figures .....   | XVII |
| List of Schemes.....  | XXI  |
| List of Tables .....  | XXII |
| Chapter 1. ....   | 1    |
| Introduction and Background .....   | 1    |
| 1.1. Multidrug Resistance .....   | 1    |
| 1.2. Antibiotics: Possible Candidates to Control Microbial Infections ..... | 2    |
| 1.3. Emergence of Multidrug Resistance .....                                | 3    |
| 1.4. Factors Contributing to Evolving Resistance Situation .....            | 3    |
| 1.5. Mechanism of Drug Resistance Including Multidrug Resistance.....       | 6    |
| 1.5.1. Changes in Bacterial Membrane .....                                  | 7    |
| 1.5.2. The Overexpression of Efflux Pumps in Multidrug Resistant Cells..... | 8    |
| 1.5.3. Modification in Target Sites .....                                   | 8    |
| 1.5.4. Drug Modification .....  | 9    |
| 1.5.5. Horizontal Gene Transfer .....                                       | 9    |
| 1.6. Multidrug Resistance in Bacteria and Biofilms .....                    | 10   |
| 1.7. Previous Strategies to Control Multidrug Resistance .....              | 12   |
| 1.7.1. Development of New Drugs.....  | 12   |
| 1.7.2. Modification of Previous Drugs .....                                 | 13   |
| 1.7.3. Drug Combinations.....   | 13   |
| 1.8. Other forms of Multidrug Resistance .....                              | 14   |
| 1.8.1. Multidrug Resistance in Other Microorganisms .....                   | 14   |

|            |   |    |
|------------|---|----|
| 1.8.2.     | Multidrug Resistance in Cancer Cells.....   | 14 |
| 1.9.       | Advent of Nanomaterials.....  | 15 |
| 1.9.1.     | Properties of Nanomaterials.....  | 16 |
| 1.9.2.     | Types of Nanomaterials.....   | 18 |
| 1.9.3.     | Silver Nanoparticles as Potential Candidates to Address Multidrug Resistance.....   | 21 |
| 1.9.4.     | Nanoclusters: Promising Next Generation Candidates.....                             | 22 |
| 1.10.      | Mechanism of Action of Silver Nanoparticles   | 23 |
| 1.10.1.    | Membrane Disruption.....  | 24 |
| 1.10.2.    | Targeting Biomolecules and Intracellular Components.....                            | 25 |
| 1.10.3.    | ROS Generation.....   | 26 |
| 1.10.4.    | Disrupting Metabolic Pathways.....  | 26 |
| Chapter 2. | .....   | 27 |
|            | Literature Review and Scope of Thesis.....  | 27 |
| 2.1.       | Synopsis.....   | 27 |
| 2.2.       | Literature Review.....  | 27 |
| 2.3.       | Scope of this Thesis.....   | 38 |
| Chapter 3. | .....   | 40 |
|            | Experimental.....   | 40 |
| 3.1.       | Synopsis.....   | 40 |
| 3.2.       | Materials.....  | 40 |
| 3.3.       | Methods.....  | 41 |
| 3.3.1.     | Synthesis of Polyethylenimine Silver Nanoclusters (bPEI– Ag NCs).....               | 41 |
| 3.3.2.     | Synthesis of Polyethylenimine Silver Nanoparticles (bPEI– Ag NPs).....              | 42 |
| 3.3.3.     | Synthesis of bPEI– Ag NCs based Empty and Drug Loaded Nanocapsules.....             | 43 |
| 3.4.       | Physical Characterization of Nanomaterials.....                                     | 44 |
| 3.5.       | Brief Explanation of Principles Behind Used Physical Techniques and Methods.....    | 45 |
| 3.5.1.     | UV-Visible Spectroscopy.....  | 45 |
| 3.5.2.     | Zetasizer.....  | 46 |
| 3.5.3.     | Thermogravimetric Analysis.....   | 46 |
| 3.5.4.     | Inductively Coupled Plasma Optical Emission Spectroscopy.....                       | 46 |
| 3.5.5.     | Transmission Electron Microscopy and Scanning Transmission Electron Microscopy..... | 47 |
| 3.5.6.     | Scanning Electron Microscopy.....   | 48 |
| 3.5.7.     | Energy-Dispersive X-ray Spectroscopy.....   | 48 |

|  |   |           |
|--|---|-----------|
| 3.5.8.   | Helium Ion Microscopy (HIM) .....   | 48        |
| 3.5.9.   | Fluorescence Microscopy .....   | 49        |
| 3.5.10.  | Hyperspectral Imaging .....   | 49        |
| 3.5.11.  | ThT Kinetic Assay .....   | 49        |
| 3.5.12.  | Circular Dichroism Spectroscopy .....   | 50        |
| 3.5.13.  | Antibacterial Studies .....   | 50        |
| 3.5.14.  | Antibiofilm Assay.....  | 54        |
| 3.5.15.  | <i>In-vitro</i> Cytotoxicity.....   | 55        |
| 3.5.16.  | Reactive Oxygen Species Generation Study.....   | 56        |
| 3.5.17.  | Discrete Molecular Dynamics Simulations .....   | 57        |
| <b>Chapter 4. ....</b>   |   | <b>59</b> |
| <b>Synthesis and Characterization of Polyethylenimine Capped Silver Nanoclusters and Evaluation of their Antibacterial Activity .....</b>                  |   | <b>59</b> |
| 4.1.   | Synopsis .....  | 59        |
| 4.2.   | Introduction.....   | 59        |
| 4.3.   | Results and Discussion .....  | 62        |
| 4.3.1.   | Synthesis and Characterization of bPEI–Ag NCs.....  | 62        |
| 4.3.2.   | <i>In-vitro</i> Studies of bPEI–Ag NCs .....  | 63        |
| 4.3.3.   | Cell Viability and Haemolysis Assay.....  | 65        |
| 4.3.4.   | Scanning Electron Micrographs .....   | 67        |
| 4.4.   | Conclusions.....  | 68        |
| <b>Chapter 5. ....</b>   |   | <b>69</b> |
| <b>Comparative Study of Design, Synthesis and Evaluation of Silver Nanoclusters and Nanoparticles against <i>P. aeruginosa</i> Resistant Biofilms.....</b> |   | <b>69</b> |
| 5.1.   | Synopsis .....  | 69        |
| 5.2.   | Introduction.....   | 69        |
| 5.2.1.   | Bacterial Amyloidosis .....   | 69        |
| 5.2.2.   | Silver Nanoparticles: Efficient Candidates to Target Bacterial Biofilms.....                | 70        |
| 5.3.   | Results and Discussion .....  | 74        |
| 5.3.1.   | Synthesis and Characterizations of bPEI-Capped AgNPs and AgNCs.....                         | 74        |
| 5.3.2.   | <i>In-vitro</i> Interactions Between FapC and bPEI-Capped AgNPs and AgNCs.....              | 75        |
| 5.3.3.   | <i>In-silico</i> Interactions of bPEI-Capped AgNC with FapC Monomer and FapC Fragment Dimer | 77        |
| 5.3.4.   | Effect of bPEI-Capped AgNPs and AgNCs on Biofilm Formation.....                             | 79        |

|   |            |
|---|------------|
| 5.4. Conclusion .....   | 83         |
| <b>Chapter 6. ....</b>  | <b>85</b>  |
| <b>Design, Synthesis and Evaluation of Silver Nanocluster Based Levofloxacin Loaded Nanocapsules Against <i>S. pneumoniae</i>. ....</b> | <b>85</b>  |
| 6.1. Synopsis .....   | 85         |
| 6.2. Introduction.....  | 85         |
| 6.3. Results and Discussion .....   | 88         |
| 6.3.1. Drug Loading Efficiency of L-Ag NCps .....   | 90         |
| 6.3.2. Anti-Pneumococcal Activity of Nanocapsules.....  | 91         |
| 6.3.3. Mechanistic Study by Scanning Electron Microscopy and Reactive Oxygen Specie generation .....                                    | 96         |
| 6.4. Conclusion .....   | 98         |
| <b>Chapter 7. ....</b>  | <b>99</b>  |
| <b>Summary and Future Perspectives .....</b>  | <b>99</b>  |
| <b>References .....</b>   | <b>102</b> |

## Table of Acronyms

|         |  |
|---------|--|
| MDR     | Multidrug Resistance                                     |
| WHO     | World Health Organization                                |
| SEM     | Scanning Electron Microscopy                             |
| TEM     | Transmission Electron Microscopy                         |
| EDS     | Energy Dispersive Spectrometry                           |
| PEI     | Polyethylenimine   |
| CV      | Cyclic Voltammetry                                       |
| CFU     | Colony Forming unit                                      |
| AgNCs   | Silver Nanoclusters                                      |
| AgNPs   | Silver Nanoparticles                                     |
| MRSA    | Methicillin-Resistant <i>S. aureus</i>                   |
| ATP     | Adenosine Triphosphate                                   |
| DNA     | Deoxyribonucleic Acid                                    |
| RNA     | Ribonucleic Acid   |
| P-gp    | Permeability Glycoprotein                                |
| SMR     | Plasmid Transmitted Small Multidrug Resistant            |
| ABC     | ATP-Binding Cassette                                     |
| FDA     | Food and Drug Administration                             |
| Ag      | Silver   |
| PLGA    | Poly Lactic-co-Glycolic Acid                             |
| CuO     | Copper Oxide   |
| AuNPs   | Gold Nanoparticles                                       |
| ROS     | Reactive Oxygen Species                                  |
| GSH     | Glutathione  |
| MIC     | Minimum Inhibitory Concentration                         |
| OD      | Optical Density  |
| PBS     | Phosphate Buffered Saline                                |
| BSA     | Bovine Serum Albumin                                     |
| RBCs    | Red Blood Cells  |
| ECM     | Extracellular Matrix                                     |
| FapC    | Functional <i>bacterial</i> amyloids                     |
| PEG     | Polyethylene glycol                                      |
| HAADF   | High Angle Annular Dark Field                            |
| ThT     | Thioflavin T   |
| CD      | Circular Dichorism                                       |
| DMD     | Discrete Molecular Dynamics                              |
| HIM     | Helium Ion Microscopy                                    |
| ICP-OES | Inductively Coupled Plasma Optical Emission Spectrometry |
| DLS     | Dynamic Light Scattering                                 |

## List of Figures

|  |    |
|--|----|
| <b>Figure 1.1</b> Schematic illustration of steps involved in appearance of multidrug resistance in bacteria. 1- Improper dosage induces competition in bacteria and they started developing resistance, 2- Resistant bacteria flourish with more strength, 3- Spreading of resistance in medical care or by gene transfer. <sup>23</sup> .....  | 5  |
| <b>Figure 1.2</b> Diagrammatic illustration of general mechanisms adopted by bacterial cells to acquire resistance against therapeutics. ....  | 7  |
| <b>Figure 1.3</b> Schematic illustration of P-gp efflux pumps playing vital role in pushing drug out of the cell via ATP hydrolysis and causing drug resistance.....   | 8  |
| <b>Figure 1.4</b> General mechanism of interaction of nanocarriers with bacterial cells by overcoming drug resistance. ....  | 10 |
| <b>Figure 1.5</b> Diagrammatic illustration of general mechanism opted in biofilms to evade killing effect of antibiotics. <sup>39</sup> .....   | 11 |
| <b>Figure 1.6</b> A graphical illustration of time and phases involved in discovery & development of a successful medicine, which shows that it is a long developmental process with limited probability of success. <sup>41</sup> .....   | 12 |
| <b>Figure 1.7</b> Diagrammatic illustration of the properties of nanoparticles, which make them suitable candidates by alteration/modification to target resistant cells. <sup>65</sup> .....  | 16 |
| <b>Figure 1.8</b> Schematic illustration of different types of nanomaterials based on composition and their suitable properties to target MDR. <sup>87</sup> .....   | 19 |
| <b>Figure 1.9</b> Schematic illustration of antibacterial mechanism of NPs: (A) cell membrane disruption with subsequent cytoplasmic lysis; (B) interaction and dissociation of intracellular constituents; (C) disturbance in electron transport triggering electrolyte imbalance and (D) production of reactive oxygen species (ROS). <sup>122</sup> .....   | 24 |
| <b>Figure 1.10</b> The electrostatic mode of communication of bacteria with cationic silver nanoparticles that results in targeting bacteria through membrane disruption mechanism.....  | 25 |
| <b>Figure 2. 1</b> The interaction of glucosamine functionalized silver nanoparticles (GlcN-AgNPs) with Gram negative and positive bacterial cell wall surface. <sup>177</sup> .....   | 32 |
| <b>Figure 2. 2</b> Schematic illustration of the anticipated antibacterial mechanism of iodinated chitosan-Ag NP composite. <sup>181</sup> .....   | 33 |
| <b>Figure 2.3</b> Schematic representation of the synergistic antibacterial pathway of tetracycline decorated AgNPs against multidrug resistant bacteria. A four-step procedure was suggested as the major pathway leading to cell death. Pathway II represents a minor pathway and Pathway III is not operational due to tetracycline resistance by Salmonella. <sup>194</sup> .....  | 35 |
| <b>Figure 4.1</b> (a) UV-visible absorption spectrum of polyethylenimine silver nanoclusters (bPEI-Ag NCs) and polyethylenimine (PEI) showing multiple absorption peaks for Ag nanoclusters compared to those for PEI, and the inset shows bPEI-Ag NCs in 4-(2-hydroxyethyl)piperazine-1ethanesulfonic acid (HEPES) buffer (pH 7.0-9.0) is yellow under visible and blue fluorescent under UV, (b) Photoluminescence spectrum of blue fluorescent bPEI-Ag NCs showing excitation at 375 nm and emission at 430 nm, (c) Dynamic light scattering (DLS) analysis showing an average hydrodynamic diameter of 3 nm, (d) TEM micrographs of bPEI-Ag NCs showing size of 2 nm. .... | 63 |

**Figure 4.2** Fibroblast cell viability test of polyethylenimine silver nanoclusters (bPEI–Ag NCs) to test their cytotoxicity against fibroblasts, which show their safe therapeutic window..... 66

**Figure 4.3** Hemolysis study of polyethylenimine silver nanoclusters (bPEI–Ag NCs) to test their compatibility with red blood cells. .... 67

**Figure 4.4** SEM micrographs showing interaction of *E. coli* with bPEI–AgNCs at: (a) 0 h-control, (b) 4 h incubation, and (c) 8 h incubation. .... 68

**Figure 5.1** A diagrammatic representation of Ag NPs. inhibiting *P. aeruginosa* biofilms by targeting bacterial amyloid proteins (FapC)..... 73

**Figure 5.2** Physical characteristics of bPEI-capped AgNCs and AgNPs. Graphical illustrations of bPEI-capped A. AgNCs and B. AgNPs. UV–vis absorption spectra of bPEI-capped C. AgNCs and D. AgNPs. TEM micrographs of bPEI-capped E. AgNCs and F. AgNPs. Zeta potentials and hydrodynamic diameters of bPEI-capped G. AgNCs and H. AgNPs were measured twice with three repeats and no significant difference was observed in them as per one-way ANOVA analysis..... 75

**Figure 5.3** Binding between FapC and bPEI-capped AgNPs or AgNCs. A. ThT kinetic assay of FapC mixed with AgNPs or AgNCs. B. CD spectra and C. percentage secondary structure of FapC monomers, fibrils, and FapC monomers after incubation with bPEI-capped AgNPs or AgNCs, calculated using DichroWeb. D. Changes in the zeta potential of FapC monomers before and after incubation with bPEI-capped AgNPs and AgNCs. TEM micrographs of E. FapC + AgNPs and F. FapC + AgNCs. The inset shows control FapC fibers. Panels, G-H. and I-J. present the respective HAADF images and EDAX spectra of FapC + AgNPs and FapC + AgNCs. Panels K. and L. represent graphical illustrations of bPEI-capped AgNPs and AgNCs interacting with FapC. .... 77

**Figure 5.4** DMD simulations of a bPEI-capped AgNC interacting with a FapC monomer and a FapC fragment dimer. A–C. Full-length FapC monomer (R1L1R2L2R3) with and without the presence of the bPEI-capped AgNC. A. Overall secondary structure contents of the full-length FapC monomer. B. The bPEI-capped AgNC-binding probability, and the  $\beta$ -sheet and  $\alpha$ -helix propensities of each residue. C. Three representative structures of FapC in the absence (upper) and presence (lower) of the AgNC. The peptide shown as cartoon is colored rainbow from blue (N-terminus) to red (C-terminus). The core of the AgNC is shown as spheres and bPEIs as sticks. D,E. A L1R2 dimer with and without the presence of the bPEI-capped AgNC. D. Overall secondary structure contents of the dimer. E. The binding probability with bPEI-capped AgNC or AgNP, and the  $\beta$ -sheet and  $\alpha$ -helix propensities of each residue. F. Representative structures of the L1R2 dimer in the absence (upper) and presence of the bPEI-capped AgNC (lower left) and AgNP (lower right). The two peptides are colored differently. .... 79

**Figure 5.5** The effects of bPEI-capped AgNCs and AgNPs on the biofilm formation of *P. aeruginosa*. Relative biofilm formation and bacterial viability of *P. aeruginosa* PAO1 in the presence of different concentrations of bPEI-capped A,B. AgNCs and A',B'. AgNPs. C is the overlapped A & B to see the comparative response of AgNCs and C' is the overlapped A' & B' to see the comparative response of AgNPs. All of these experiments were done in triplicates in two repeats and the P values were assigned by one-way ANOVA (Bonferroni test). The statistically significant viability is indicated by P values (\*,  $P > 0.01$ ; \*\*,  $P \geq 0.001$ ; \*\*\*,  $P < 0.001$ ). Each error bar represents standard errors of means. .... 81

**Figure 5.6** Fluorescence microscopy images of *P. aeruginosa* AH298-GFP incubated with  $1 \times 10^{-6}$  M of A. AgNPs and B. AgNCs and C. untreated control that formed biofilms. A fluorescent strain of *P. aeruginosa* was used for fluorescence microscopy and ThT dye was used to stain the biofilms. Panels

D–F. represent the hyperspectral images (HSI) along with the SPR spectra of AgNPs, *P. aeruginosa* incubated with  $1 \times 10^{-6}$  M AgNPs, and *P. aeruginosa* control, respectively. .... 82

**Figure 5.7** Helium ion microscopy (HIM) and TEM micrographs of *P. aeruginosa* incubated with AgNPs (HIM: panel (A), TEM: panel (B)), *P. aeruginosa* incubated with AgNCs (HIM: panel (C), TEM: panel (D)), and *P. aeruginosa* control (HIM: panel (E), TEM: panel (F)). ROS generation by *P. aeruginosa*, relative to positive control ( $H_2O_2$ ), upon incubation with AgNPs and AgNCs (panel (G)). .... 83

**Figure 6.1** Occurrence of pneumonia in different areas of the world.<sup>360</sup> ..... 86

**Figure 6.2** Pneumococcal structure showing its various important components which was used by antimicrobials to target them..... 87

**Figure 6.3** The characterization of PEI-Ag NCs, E-Ag-NCps and L-Ag-NCps using A. UV-vis spectroscopy showing  $\lambda$ -max at 283 nm for the drug and the corresponding peak for L-Ag-NCps, B. DLS- Zetasizer displaying size of 180 and 193 nm for L-Ag-NCps and E-Ag-NCps, C. Transmission electron micrograph showing (a) PEI-Ag NCs with 2 nm, Scanning electron micrographs showing (b) E-Ag-NCps with 160 nm and (c) L-Ag-NCps with 185 nm size, respectively. .... 90

**Figure 6.4** Anti-pneumococcal activity of A. empty nanocapsules (E-Ag-NCps), B. levofloxacin loaded nanocapsules (L-Ag-NCps), C. drug against serotype 16F, D. Represents overlapped A & B to see the comparative effect of E-Ag-NCps and L-Ag-NCps on type 16F, while E. represents overlapped B & C to see the comparative effect of L-Ag-NCps and drug on type 16F. Each error bar represents standard errors of means. The statistically significant Log CFU killing was represented by P values (\*, > 0.01; \*\*,  $\geq 0.001$ ). .... 93

**Figure 6.5** Anti-pneumococcal activity of A. empty nanocapsules (E-Ag-NCps), B. levofloxacin loaded nanocapsules (L-Ag-NCps), C. drug against serotype 13, D. Represents overlapped A & B to see the comparative effect of E-Ag-NCps and L-Ag-NCps on type 13, while E. represents overlapped B & C to see the comparative effect of L-Ag-NCps and drug on type 13. Each error bar represents standard errors of means. The statistically significant Log CFU killed was represented by P values (\*, > 0.01; \*\*,  $\geq 0.001$ ; \*\*\*, < 0.001). F. Pictorial view of colonies grown on blood agar plates after 2 h incubation of treatments with type 13 showing increased death of colonies in L-Ag-NCps compared to controls. .... 94

**Figure 6.6** Anti-pneumococcal activity of A. empty nanocapsules (E-Ag-NCps), B. levofloxacin loaded nanocapsules (L-Ag-NCps), C. drug against serotype 19F, D. Represents overlapped A & B to see the comparative effect of E-Ag-NCps and L-Ag-NCps on type 19F, while E. represents overlapped B & C to see the comparative effect of L-Ag-NCps and drug on type 19F. Each error bar represents standard errors of means. The statistically significant Log CFU killed was represented by P values (\*, > 0.01). .... 95

**Figure 6.7** Anti-pneumococcal activity of A. empty nanocapsules (E-Ag-NCps), B. levofloxacin loaded nanocapsules (L-Ag-NCps), C. drug against serotype 2. D. Represents overlapped A & B to see the comparative effect of E-Ag-NCps and L-Ag-NCps on type 2, while E. represents overlapped B & C to see the comparative effect of L-Ag-NCps and drug on type 2. Each error bar represents standard errors of means. The statistically significant Log CFU killed was represented by P values (\*, > 0.01; \*\*,  $\geq 0.001$ ; \*\*\*, < 0.001). F. Pictorial view of colonies grown on blood agar plates after 2 h incubation of treatments (L-Ag-NCps, E-Ag-NCps, drug) with type 2 showing increased death of colonies compared to controls. .... 96

**Figure 6.8** The possible mechanism involved in killing of bacterial cells was studied by (A) SEM images of (a) Pneumococcal serotype 2 control cells, (b) pneumococcal cells showing stress response in the

form of long chains, (b') pneumococcal cells with pits on their surface due to L-Ag-NCps targeting, (c) the complete lysis of pneumococcal serotype 2 cells with designed nanocapsules (L-Ag-NCps), (B) and ROS generation playing effective role in pneumococcal serotype 2 targeting, which is truly attributed to silver content of nanocapsules (L-Ag-NCps). Each error bar represents standard errors of means. The statistically significant killing by ROS production was indicated by P vaues (\*\*,  $\geq 0.001$ ). ..... 98

## List of Schemes

|  |    |
|--|----|
| <b>Scheme 3.1</b> A general schematic route for the synthesis of blue fluorescent AgPEI NCs by silver mirror reaction and their purification by dialysis. ....   | 42 |
| <b>Scheme 3.2</b> A general schematic route for the synthesis of AgPEI NPs by chemical reduction method and their purification by precipitation method. ....   | 43 |
| <b>Scheme 3.3</b> A general schematic route for the synthesis of AgPEI NCs based empty (E-Ag NCps) and levofloxacin-loaded nanocapsules (L-Ag NCps) by emulsion dispersion method and their purification by lypholization.....       | 44 |
| <b>Scheme 3.4</b> A schematic illustration of various steps involved in antibacterial study including culturing, purification, inoculation and estimation of bacteria.....   | 52 |
| <b>Scheme 4.1</b> A general scheme presenting the synthesis of blue fluorescent branched polyethylenimine-coated Ag NCs (bPEI–Ag NCs) by chemical reduction method and their potential bactericidal action.....                      | 62 |
| <b>Scheme 6.1</b> Schematic illustration includes A. synthesis of bPEI–Ag NCs, B. emulsification to form nanocapsules (E-Ag-NCps and L-Ag-NCps), C. targeting of pneumococcal strains by nanocapsules (E-Ag-NCps and L-Ag-NCps)..... | 89 |

## List of Tables

|   |    |
|---|----|
| <b>Table 4.1</b> A table presenting MIC data of polyethylenimine silver nanoclusters (bPEI–Ag NCs) .....  | 65 |
| <b>Table 6.1</b> A. MIC of AgPEI NCs and drug against four different pneumococcal serotypes B. The concentration of AgPEI NCs and drug loaded into E-Ag-NCps/L-Ag-NCps used for anti-pneumococcal activity..... | 92 |

# Chapter 1.

## Introduction and Background

### 1.1. Multidrug Resistance

Bacterial Resistant infections are responsible for the death of more than 0.7 million people every year and accordingly, the expected rate of death of people from drug resistant infections in 2050 is 10 million/ year.<sup>1</sup>

Multidrug resistance (MDR) is the tendency of bacteria to develop broad-spectrum tolerance against drugs/antimicrobials, and in return make treatments ineffective resulting in persistent infections.<sup>2</sup> It is a global concern, and a coordinated action is needed to control the emergence and spread of MDR.<sup>3</sup> In United States, resistant bacteria are responsible for 60% of nosocomial infections.<sup>4</sup> *P. aeruginosa*, a Gram-negative bacterium, is a major cause of infections and death in people with compromised immune system, for example cystic fibrosis patients and hospital acquired infections.<sup>5,6</sup> Almost 40% of *S. aureus* strains collected from hospitals are MRSA, methicillin-resistant *S. aureus* and a few are even resistant to a wide range of antibiotics such as vancomycin and carbapenems. If bacterial species continues to develop resistance to drugs, then even simple infections such as common cold as hospital acquired infections, can prove to be fatal for humans in addition to surgeries. Insusceptibility to conventional antibiotics is expected to keep on increasing, and the condition may get more worst with the growth of MDR bacteria strains.<sup>7,8</sup> MDR, therefore, intensifies the general cost of treatment and resource depletion to fight resistant infections.

According to WHO report after epidemic of typhoid fever in Pakistan since November 2016, over-all 5274/8188 cases have been testified as extremely drug resistant (XDR), which is the susceptibility of bacteria to just one/two antimicrobial categories compared to multidrug resistant (MDR) bacteria which were non-susceptible to atleast one antibiotic. Out of these XDR isolates, 30 were linked to patients with Pakistan travel history, and this XDR

strain of *S. typhi* has now made people sick globally. As Pakistan is among the least spending nations on healthcare all round the world, these epidemics will result in complete disaster; and since infectious diseases respect no borders, this could circumvent other countries too. The quick actions were needed to protect our health care system from complete disaster against these superbugs.<sup>9</sup> Likewise, every year in United States, two million patients are empirically treated against hospital-acquired contaminations with 99,000 expiries at charge of about \$35 billion.<sup>10</sup> Virtually, 30% of these contagions are Methicillin-resistant *S. aureus*, and these are resistant to penicillin, methicillin and all other  $\beta$ -lactams. Additionally, 440,000 novel cases of MDR-TB emerge every year globally, instigating at-least 150,000 demises.<sup>11</sup> Gonorrhoea is heading for top incurable bacterial infection, as failure of most recent generation cephalosporin has been stated from 10 nations.<sup>12</sup>

## **1.2. Antibiotics: Possible Candidates to Control Microbial Infections**

The “golden era” of antibiotic development, which began in 1928 with Fleming's discovery of penicillin was followed by rapid commercialization and manufacture of many new antibiotics like streptomycin, sulfonamide. With this advancement, it then seemed like that infectious diseases would soon be a memory of past.<sup>13</sup> However, as correctly indicated by Fleming, the bacteria continued to evolve and, once susceptible bacteria started to develop resistance.

Antimicrobials belong to two large categories including bactericidal drugs- that causes bacterial death and the bacteriostatic drugs that prevents bacterial growth.<sup>14</sup> Among bactericidal drugs, Quinolones target bacteria by inhibiting DNA replication through DNA–topoisomerase complexes as this process is catalyzed by topoisomerases.<sup>15</sup> Rifampicins also target bacteria by inhibiting RNA synthesis via blocking transcription process through binding with  $\beta$ -subunit of RNA polymerase. Antibiotics can also work by interrupting translation of proteins by using 50S and 30S inhibitors. 50S inhibitors like clinolamides, amphenicols, and macrolides work by blocking initiation step of translation, whereas 30S inhibitors like amino cyclitols block the entry of aminoacyl tRNAs into ribosomes. Nowadays, many of us take antibiotics for granted that any infective disease is treatable by antibiotic therapy.

Antibiotics are produced at an estimated annual production of ~100,000 tons worldwide, and their frequent usage has an immense influence on the life of bacteria on earth.<sup>16</sup>

### **1.3. Emergence of Multidrug Resistance**

The scientists were capable to temporarily control the outburst of epidemics by the introduction of antibiotics (e.g. Penicillin and its derivatives) and consequently improve the quality of life. Although, finding of penicillin in the beginning of 20<sup>th</sup> century led to a substantial drop in infectious diseases, till 1991 when 1.3% of strains were tested to be penicillin resistant by the Center for Disease Control and Prevention, USA. The ratio of resistant bacterial strains continued to rise universally and presently reported occurrence of only penicillin resistance is 12.7% (Latin America), 14.7% (Europe) and 15.9% (North America), respectively. Later, strains resistant to penicillin were also seen resistant to other antimicrobials such as macrolides, whereas macrolides resistance have more medical significance than penicillin.<sup>17, 18</sup> Advent of drug resistance is the supreme frightening situation in the era of chemotherapy. Chemotherapy is the forefront approach to put down most of the human ailments but this survival battle between pathogenic microorganisms and humans makes many of the microorganisms resistant to most of the vulnerable drugs.<sup>19</sup> In 2011, WHO declared MDR microorganisms in top three threats to humans.<sup>20, 21</sup> The Lancet Infectious Diseases Commission by Laxminarayan and colleagues have cautioned about the antibiotic usage and their resistance, that “we are at the dawn of a post antibiotic era”, with “almost all disease causing bacteria resistant to the antibiotics commonly used to treat them”.<sup>22</sup>

### **1.4. Factors Contributing to Evolving Resistance Situation**

In low and middle-income countries (LMICs), MDR is the foremost health concern and is linked with a lot of aspects, some of them are listed in **Figure 1.1**. In underdeveloped countries like Pakistan, medicines are accessible over-the-counter, and are generally consumed arbitrarily without doctor’s prescription. Additionally, doctors prescribed medicines are also not taken and recommended by the doctor and are discontinued on

disappearance of symptoms. This unrestrained usage of non-prescribed drugs increases the selection pressure and causes resistance.<sup>23-26</sup> In 1976, Stamey et al. stated the appearance of resistance against fluoroquinolones owing to under-dosage of antibiotics. The optimization of appropriate antibiotic dosages can help significantly in this regard.<sup>27</sup> Furthermore, bacteria present in the environment are also exposed to different harsh environment which include, nutritional competition with other common dwellers of the same niche, exposure to reactive oxygen species and heavy metals. Such conditions, in the absence of antimicrobials, serves as selective pressure for bacterial mutations. Mutations thus made can also contribute to antimicrobial resistance by mechanisms that are not known yet.

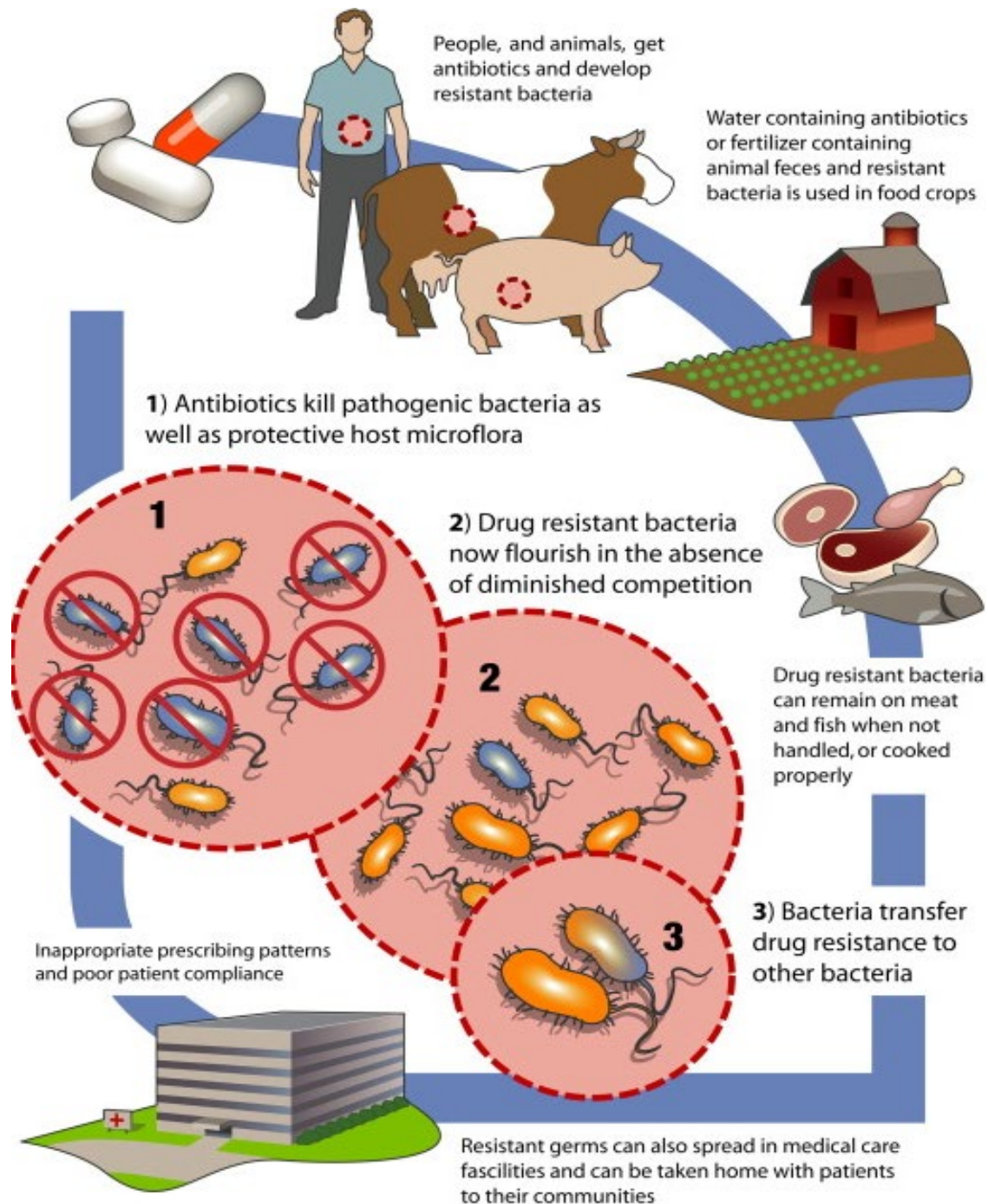


**Figure 1.1** Schematic illustration of steps involved in appearance of multidrug resistance in bacteria. 1- Improper dosage induces competition in bacteria and they started developing resistance, 2- Resistant bacteria flourish with more strength, 3- Spreading of resistance in medical care or by gene transfer.<sup>23</sup>

Increased rate of hospitalization can also lead to the spread of infections. The careful observation and separation of patients is required to control the spread of MDR microbes.

In addition, bacterial cells can transfer genetic material by vertical (parents to siblings) and horizontal gene transfer (conjugation, transduction, transformation) among same or different bacterial species. For instance, there are millions of deaths reported back in 1968 in Guatemala owing to the spread of *Shigella* containing a plasmids with several antibiotic resistant factors.<sup>28</sup> Extreme usage of antimicrobial drugs in dairy, poultry and farming enhances exposure of microorganisms/ cells to them, which makes them more prone to resistance.<sup>29</sup> The wastewater treatment plants, communal or industrial waste heaps, foods rich in bacteria are all other important causes of bacterial transmission and indirect reasons behind the appearance of MDR.<sup>30</sup>

### **1.5. Mechanism of Drug Resistance Including Multidrug Resistance**

Microbial infections, particularly drug resistant infections, are posing serious healthcare challenge across the globe. The appearance of multidrug resistant (MDR) strains of microbes with the shortage of novel and effective antibiotics is a distressing phenomenon for the entire humanity. The rapid increase of multiple antibiotic resistant microbial strains calls for the development of new biocidal agents and approaches to obstruct growth of microbes. The resistant microorganisms are constantly evolving in an effort to preserve their existence.<sup>11, 13</sup> Towards that, bacteria have developed several mechanism to evade killing by antimicrobials. For example, in United States, *Pseudomonas aeruginosa* was the prominent cause of casualties due to gram-negative bacteria. At first this bacterium, developed inherent resistance by means of fluctuations in genetic makeup. This drops outer membrane permeability, which results in improved basal minimal inhibitory concentration making it useless against many communal antibiotics. This triggers several secondary adaptive resistance procedures like enzymatic drug alteration and stimulation of efflux pumps. Additionally, acquisition of transmissible traits by horizontal gene transfer further worsen the situation. General ways to acquire resistance by bacteria are listed below in **Figure 1.2**.

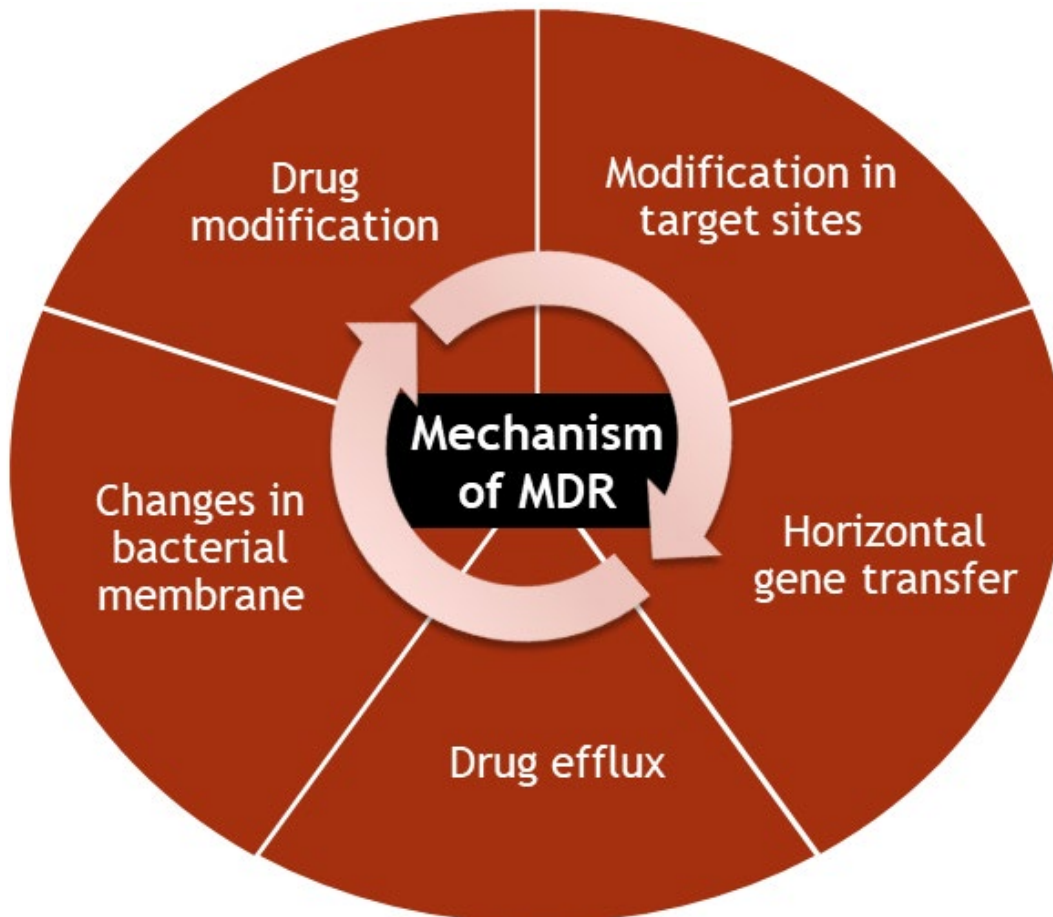


**Figure 1.2** Diagrammatic illustration of general mechanisms adopted by bacterial cells to acquire resistance against therapeutics.

### 1.5.1. Changes in Bacterial Membrane

The foremost resistive structures in case of bacteria are capsule, cell wall and cell membrane, which prevent the entry of drug enter into bacterial cell to perform its action. In gram negative bacteria, cell membrane is composed of lipid bilayer and is further covered by outer membrane of lipopolysaccharides presenting a primary obstacle to the entrance of hydrophilic drug molecules. The bacterial cell is further covered by cell wall, which comprises of several layers of peptidoglycan. The  $\beta$ -lactam antibiotics target cell wall production in bacteria by preventing peptide bond formation via blocking assembly of glycan subunits resulting in bacterial cell lysis.<sup>31</sup> These small hydrophilic antibiotic molecules get their entry into cell via porin channels in the outer membrane. The decrease in the number of porins

resulted in reduced entry of corresponding antibiotic and hence resistance is developed to the corresponding class of antibiotics by changes in membrane structure.<sup>32</sup>

### 1.5.2. The Overexpression of Efflux Pumps in Multidrug Resistant Cells

The major and most predominant mechanism of drug resistance consists of overexpression of efflux pumps in cells surface, which actively transfer drug molecules outside the cell thereby increasing minimum inhibitory concentration. The efflux pumps belongs to five key families i.e., the resistance-nodulation cell-division family, small MDR family (SMR), multidrug, toxic and antibiotics compound extrusion family, major facilitator family and ATP-binding cassettes family (ABC). The most important efflux pumps to target MDR are P-glycoprotein (P-gp) pumps, which comes in ABC binding cassettes category. P-gp are uniporter, propelling pumps that are derived by ATP hydrolysis. **(Figure 1.3)** Regular role of P-gp is to safeguard against noxious chemicals however, their excessive expression in MDR cells promotes chemotherapy failure.<sup>13</sup>

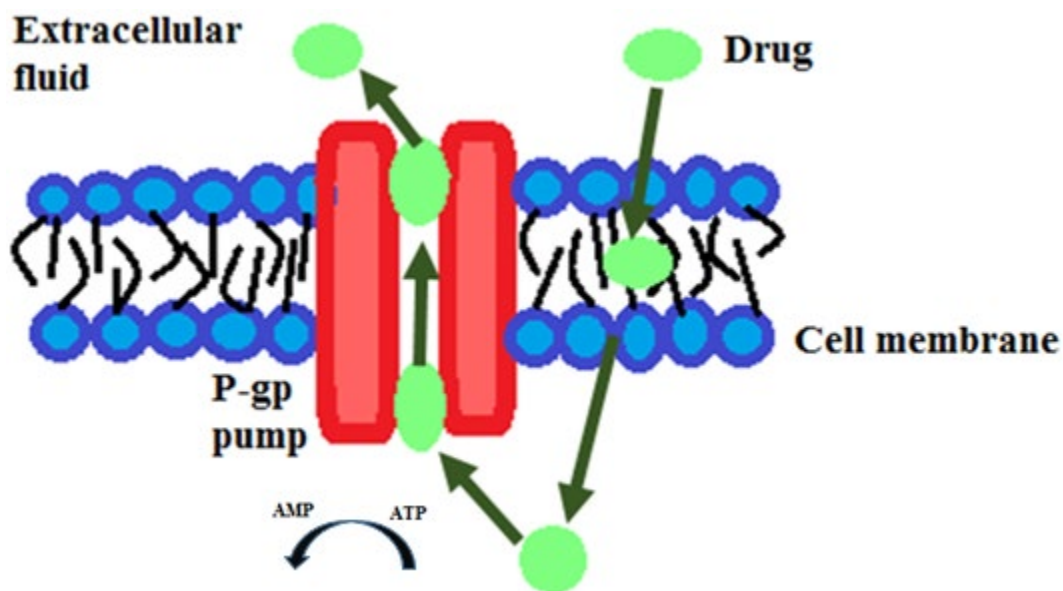


**Figure 1.3** Schematic illustration of P-gp efflux pumps playing vital role in pushing drug out of the cell via ATP hydrolysis and causing drug resistance.

### 1.5.3. Modification in Target Sites

Many strategies were opted by microorganisms to change drug target sites to minimize the interaction of drugs with target site. It may include protection or modification of targeted

site. There are many genetic factors found in bacterial chromosomes that code for specific proteins. The best example of target protection is tetracycline resistance factors, developed in various plasmids with broad-range transposons. Another method to cut antibiotics action is the modification in target points for related antibiotic families. These may involve mutations in genes coding for target sites, bypassing of target sites or chemical alterations of the metabolic pathways using several enzymes, which are normally attached with antibiotics to abolish their influence.<sup>11</sup>

#### **1.5.4. Drug Modification**

The chemical modification of the therapeutic molecules by various enzymes is the most effective approach adopted by bacteria. Various enzyme-catalyzed chemical responses includes phosphorylation (chloramphenicol, aminoglycosides), adenylation (lincosamides, aminoglycosides), and acetylation (streptogramins, chloramphenicol, aminoglycosides).  $\beta$ -lactam resistance is the destruction of antibiotic moieties with  $\beta$ -lactamases.  $\beta$ -lactamases ultimately break cyclic amide bond (called lactam ring) and make lactam ring in antimicrobials useless.<sup>33</sup>

#### **1.5.5. Horizontal Gene Transfer**

Horizontal gene transfer is one of the important mechanisms used by resistant bacteria to spread the infection. The contaminations triggered by penicillin-resistant *S. aureus* disclosed that mechanism behind this resistance is the transmission of strains via penicillinase-encoded plasmid, which result in rapid spread of resistant microbes.<sup>34</sup>

All above-mentioned features contribute towards the multidrug resistance (MDR). It is clear that the emergence of resistance is a trend and the bacteria are poised to develop resistance against each antibiotic group sooner or the later. For this reason, in addition to developing new class of antibiotics (possibly inorganic nanoparticles), there is a genuine need to develop drug delivery vehicles to control the efficient transport of antibiotics/therapeutic agents at the targeted site to deliver accurate dose to the bacteria by bypassing above-mentioned pathways (**Figure 1.4**).

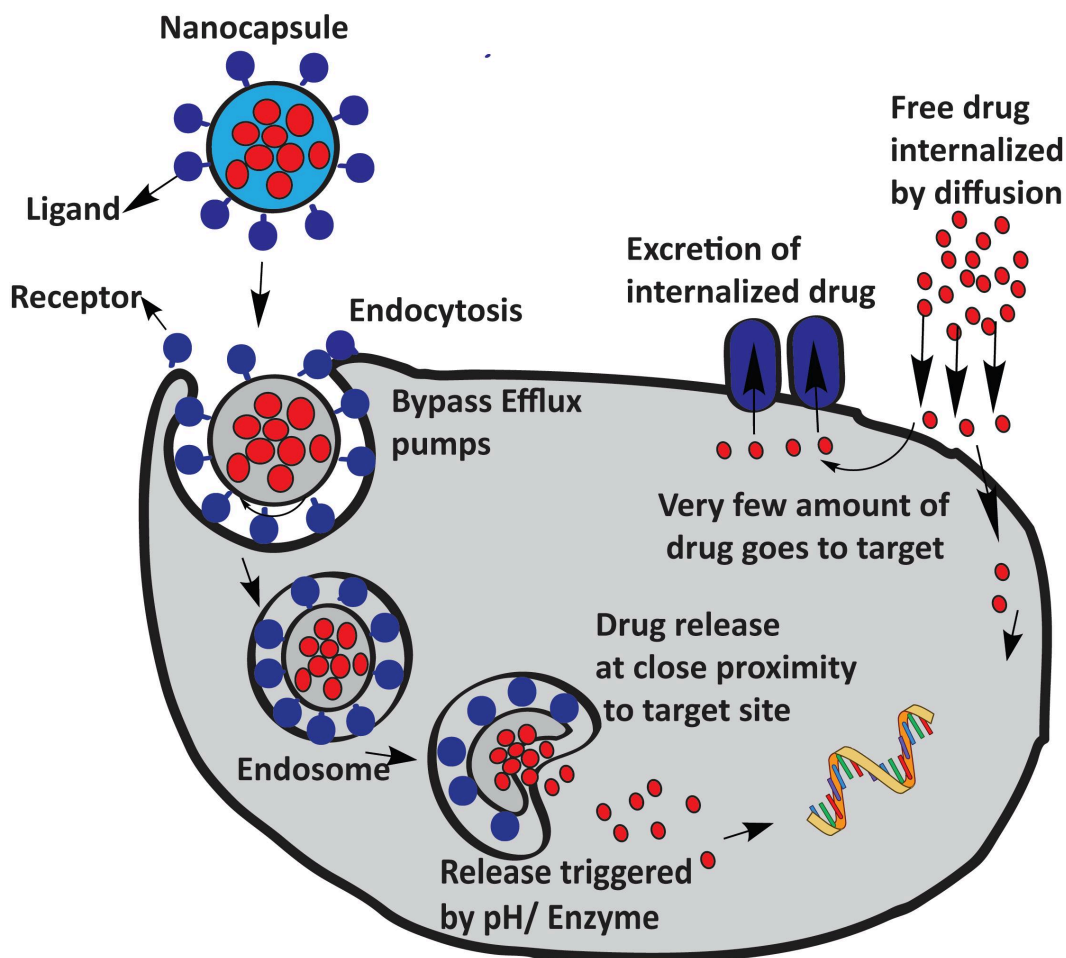


**Figure 1.4** General mechanism of interaction of nanocarriers with bacterial cells by overcoming drug resistance.

### 1.6. Multidrug Resistance in Bacteria and Biofilms

Multidrug resistant (MDR) organisms are mostly hard to treat, in particular Gram-negative organism. Colistin, a lipopeptide and fellow of the polymyxin family, is presently employed as a last-line medicine for the control of MDR Gram-negative microbial infections. Bacterial cells generally grow in two arrangements i.e., planktonic, which involves free swimming isolated bacterial cells that are not bound to any surface. The other arrangement is biofilm, which includes multicellular sessile cells living in the form of communities.<sup>35, 36</sup>

Microbial biofilms are extremely resistant bacterial communities that are very difficult to destroy (**Figure 1.5**). These strong biofilms are commonly found on artificial implantations and indwelling curative devices like dental implants, arthro-prostheses and urinary

catheters. The spread of biofilm can happen on dead or alive tissues, resulting in chronic wounds, otitis media and endocarditis. These stubborn infections and their associated ailments are difficult to handle due to strong resistance in biofilms against host immunogenic responses and also the extracellular polymeric materials in these biofilms hinder the permeation of antibiotics. Present practices to eradicate biofilms on synthetic surfaces consist of sterilizing the site using bleach or any other corrosive means. These biomedical biofilms are much more challenging to treat due to increased health maintenance expenses and rare patient's approval owing to the hostile treatment options. This problem is further intensified by the dramatic rise in the spread of drug resistant microbes.<sup>37, 38</sup>

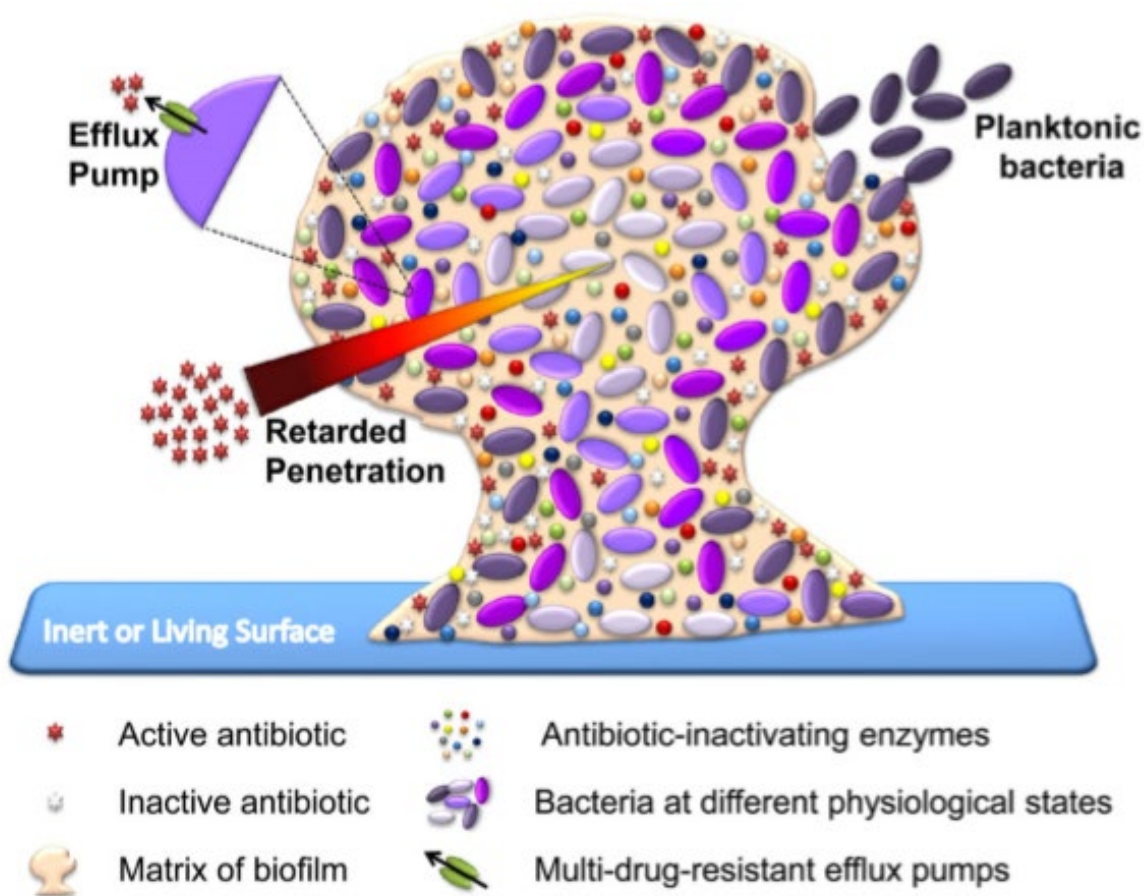


**Figure 1.5** Diagrammatic illustration of general mechanism opted in biofilms to evade killing effect of antibiotics.<sup>39</sup>

## 1.7. Previous Strategies to Control Multidrug Resistance

To address MDR, it was essential to adjust pharmacokinetics and pharmacodynamics of drugs to enhance their efficacy, reduce toxicity and, meanwhile, limit the possibility of developing resistance. Some of the previously adopted strategies in this regard are highlighted below.

### 1.7.1. Development of New Drugs

The development of new drugs was originally thought to target resistance, but it is an extensive, laborious and costly process with limited possibility of success (**Figure 1.6**).<sup>24</sup> Over the past several decades, the drug discovery and development have been falling swiftly. Approximately, 16, 14, 10, and 7 novel antibiotics were approved during 1983–1987, 1988–1992, 1993–1997, and 1998–2002, whereas just 5 and 2 were approved during 2003–2007, 2008–2012, and 2012-onwards is the end of the golden age in which older drugs were reconsidered or used in combinations, respectively.<sup>40</sup> Inappropriately, pharmaceutical companies are hesitant to put in substantial resources for the discovery of novel antibiotics because pathogens are likely to redevelop resistance within a short time.

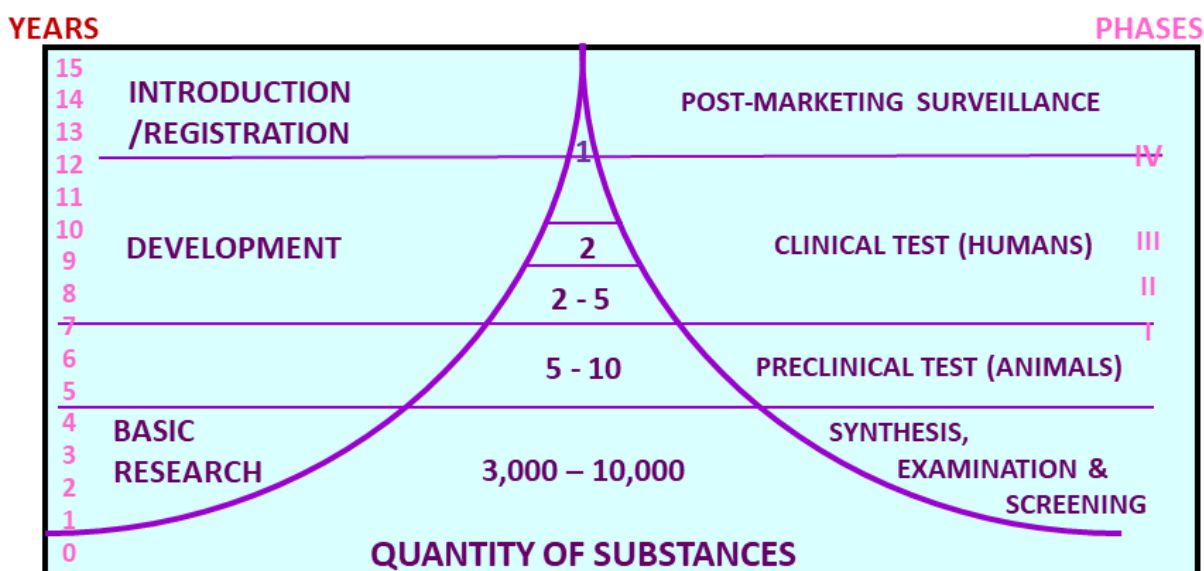


**Figure 1.6** A graphical illustration of time and phases involved in discovery & development of a successful medicine, which shows that it is a long developmental process with limited probability of success.<sup>41</sup>

### 1.7.2. Modification of Previous Drugs

A race started in synthetic chemistry to increase the potency of already reported drugs by introducing new functional moieties, while keeping the family same. As a result, numerous new compounds were produced with slight modifications. The resistant microbes, however, are very smart in developing resistance even against related families of drugs. The situation turned out to be even worse when novel structurally linked antibiotics were found not much effective to treat resistant infections. These findings and the reluctance of pharmaceutical companies to develop new antibiotics are posing a real threat to medicinal chemistry.<sup>42</sup>

### 1.7.3. Drug Combinations

Combinatorial action of an antiseptic cocktail is known to collectively regulate the action of respective components by pursuing bacteria from two different faces. This effective technique could be offered to bacteria as a next tough evolutionary barrier to cross.<sup>43</sup> However, the infectious pathogens can evolve over time, many of them have acquired resistance to the prescribed and almost all new antibiotics.<sup>44</sup> Combination therapy for the time being overwhelmed the problematic resistance and was immensely valued in treating extremely invasive pathogenic infections.<sup>45</sup> It may include antibiotic-antibiotic mixing or antibiotic-adjuvant mixing (Augmentin) and was quite useful in targeting various channels of resistance instantaneously. The right model of antibiotic-antibiotic mixing is the management of *M. tuberculosis* contagions by using four separate drugs in combination, directing four different goals whereas, augmentin is best example of antibiotic-adjuvant amalgamation.<sup>46</sup> The problematic part in combination therapy is that it is likely to modify the pattern of antimicrobial resistance in a predictable way, which may decrease its efficacy with time. Steering several paths of resistance by combination therapy, might just speed up evolution, where microbes will discover altered biological routes to persist.

The multidrug resistance is an area of universal concern. Consequently, there is vital need to develop means that can either be used to potentiate the outcome of present drugs or can be used openly to destroy pathogens, without prompting resistance in them.

## **1.8. Other forms of Multidrug Resistance**

Different microorganisms/ cells opt different strategies to become resistant to various drugs. Some of these forms are discussed below.

### **1.8.1. Multidrug Resistance in Other Microorganisms**

The microbial membrane behaves as the primary defence line against foreign attack. World Health Organization (WHO) has reported that, in the previous 4 years, 12 countries in Asia, Africa and the Americas have exceeded suitable levels of drug resistance against the two backbone drugs of HIV treatment: nevirapine and efavirenz. This form of drug resistance in viruses could emerge due to patchy or poor delivery of drugs and is totally unacceptable.<sup>47</sup> Fungi are important for the conservation of global ecological balance, but they can also target particular hosts and cause damage. Fungicides are available and mostly used against fungal infections but the appearance of multidrug resistant (MDR) fungal infections is also posing a big threat to public health.<sup>48</sup>

### **1.8.2. Multidrug Resistance in Cancer Cells**

One of the severe danger to human well-being, causing universally tens of millions of expiries annually, is cancer and chemotherapy is the finest means to approach it. Although, most of the chemotherapeutic approaches display toxicity and specificity concerns which are leading to multidrug resistance.<sup>49, 50</sup> In cancer, multidrug resistant cells become resistant to chemotherapeutic drugs, which results in minimal cell death along with spreading of tumors. This is the major obstacle in clinical treatment of cancer as it results in cross-resistance to many mechanically and structurally different chemotherapeutics. Chemosensitization is the pathway used now a days to make tumor cells more sensitive to chemotherapeutic drugs by simultaneously delivering the drug and inhibiting the pathway used to develop resistance.<sup>51, 52</sup> Although many delivery carriers can upregulate the concentration of the drug in cancer tissue, resistance mechanisms and cellular obstacles may still limit the general efficacy of the chemotherapeutics.<sup>53</sup> Chemotherapeutic delivery systems are also susceptible to other limitations such as sudden release and possible off-site toxicity.<sup>54</sup> Each year, ~90,000 fresh cases for breast tumor are spotted in Pakistan with 47 % demise rate.<sup>55</sup>

The condition is not even respectable in the advanced world making it a severe universal health problem but the developed countries are considering it extremely serious unlike the developing/deprived world.<sup>56</sup> The failure of current tumor healing approaches by means of small molecules is largely due to the delayed diagnosis of the emerging cancer, small circulation period of the therapeutic agents, absence of the directed delivery of the chemotherapeutic agents to the damaged cells/ tissues and the successive intake of anticancer drugs by the tumorous tissues/ cells.<sup>57</sup> Drug resistance and the toxicity of chemotherapeutics to the healthy cells are even more distressing and cause serious health problems together with poor efficiency and serious side effects such as reduced white blood cell number and even the failure of heart in few cases. In order to address this issue, first liposomal nanomedicine i.e., Doxil, was introduced in the market in 1995, which is actually doxorubicin enclosed in liposomal protective coating. It shows improved antitumor activity with reduced toxicity as compared to doxorubicin.<sup>58</sup> Doxil and abraxane are amongst the few US FDA permitted antitumor drugs, which provide enhanced therapeutic efficacy and comparatively fewer side effects owing to the conjugation of directed groups with DOX and paclitaxel respectively, but even these drugs are not much capable to address numerous concerns including multidrug resistant tumor cells.<sup>59, 60</sup>

## **1.9. Advent of Nanomaterials**

At present, nanotechnology seems to be ready to invade several aspects of our lives. It is already presenting favorable solutions to the challenges in several fields of biomedical sciences and technology.<sup>61</sup> For example, it improves the activity of convenience goods like antifog layers on lenses and glasses, skin-maintenance products, stain or wrinkle-resistant dresses and several others. It is playing an effective role in various parts of clinical and medical research, for example timely detection and monitoring of various diseases and their subsequent treatment, and the development of vaccines and more effective therapeutics. In recent times, nanomaterials have emerged as the most stimulating and proficient candidates to monitor and guard human wellbeing and address ailments.<sup>62</sup> The nanoparticulate based formulations have been demonstrated as encouraging platforms for

the management of microbial infections.<sup>63, 64</sup> The nanostructured materials hold numerous benefits, which make them powerful candidates for building improved approaches to fight pathogens, even the resistant ones.

### 1.9.1. Properties of Nanomaterials

Nanomaterials possess unique chemical and physical properties depending on their nanoscale features that make them attractive candidates for many intriguing applications including those in biomedical sciences (**Figure 1.7**). Some of the factors affecting the properties of nanomaterials are briefly discussed below:

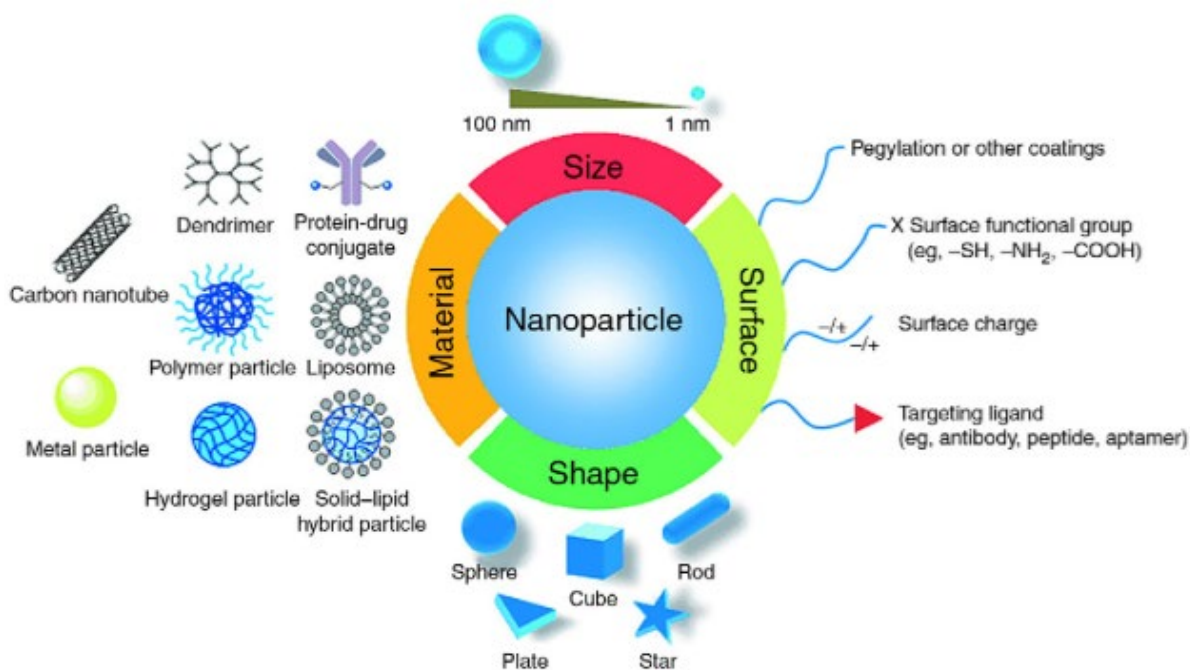


**Figure 1.7** Diagrammatic illustration of the properties of nanoparticles, which make them suitable candidates by alteration/modification to target resistant cells.<sup>65</sup>

#### 1.9.1.1. Size of Nanoparticles

Nanomaterials are extremely competent transporters in biological systems owing to their small size (at least one facet in nano regime), fine matching with biomolecules which allows them to bypass biological obstructions efficiently. It is further known that the biocidal potential of AgNPs is enhanced as their surface area increases i.e., reducing their size. Smaller the size of nanoparticles, the more active moieties they have on their surface, which

enhance their antibacterial potential.<sup>66-76</sup> Atomically precise nanoparticles synthesized by efficient control over their size and structure are called as nanoclusters.<sup>77</sup> Metallic nanoclusters having several to hundred atoms possess unique molecule-like properties. Small molecule protected nanoclusters hold stronger potential in biomedical applications as compared to the larger ones. These are new class of functional nanomaterials having applications in energy, sensing, environment, catalysis, medicine and imaging. Commonly used synthetic methodologies for nanoclusters are direct metal reduction in the presence of strong capping ligands, ligand exchange or metal exchange reactions.<sup>78</sup> The NPs in 5–50 nm size regime are known to be bacteriostatic and bactericidal at different doses.

#### **1.9.1.2. Surface Charge of Nanoparticles**

The initial nanomaterials interaction with cellular membranes includes electrostatic grip to interact with the anionic lipid head groups with subsequent insertion aided by its hydrophobic remainders into the hydrophobic membrane interior. Both sides of the bacterial cytoplasmic membranes are full of anionic lipids, such as, phosphatidylserine, cardiolipin and phosphatidylglycerol. However, the external leaflet of eukaryotic cytoplasmic cell membrane is made of zwitterionic lipids such as cholesterol or phosphatidylcholine and phosphatidylethanolamine. The alterations in cytoplasmic membranes charge can perhaps be best to exploit for selective killing of bacteria and this can be achieved by the adjustment of surface charge and hydrophobicity of nanoparticles.<sup>79</sup>

#### **1.9.1.3. Shape of Nanoparticles**

The shape of nanoparticles has a dominant influence on their properties. Studies related to the antibacterial properties have shown reduced nanotoxicity of silver nanospheres in comparison to nanowires.<sup>80</sup> Composite materials, such as Ag NPs impregnated silicon nanowires, are also effective antimicrobials.<sup>81</sup> Similarly, Ag nanoparticles based carbon nanotubes are quite beneficial to hit antibiotic resistant microbes with insignificant cytotoxicity.<sup>82</sup> The star-like silver nanoparticles also demonstrate significant antibacterial properties.<sup>83</sup> Sadeghi et al. have demonstrated that nanoscale Ag plates manifest enhanced bactericidal potential for *S. aureus* and *E. coli* in comparison to Ag nanorods and

nanoparticles.<sup>84</sup> The prismatic silver nanoparticles reported by Fouzia et al. present outstanding antimicrobial properties. The spherical AgNPs are more prone to target bacteria due to their high probability to attach and disrupt membrane permeability.<sup>85</sup> These findings demonstrate that the antibacterial potential of given nanoparticles are significantly enhanced by increasing their anisotropy, all other factors being constant.

#### **1.9.1.4. Surface Modification of Nanoparticles**

The selection of the nanoparticle exterior coating can be chemically tuned to attain target specificity and selective delivery of antibiotics to the required spot. The surface modulation of nanoparticles can be exploited to trick the resistant micro-organisms to uptake hidden drug. Nanoparticles chemistry offers surface conjugation with a variety of small organic molecules to articulate the toxicity concerns. The studies show that tuning the surface chemistry of NPs exterior can control their communication with bacteria and in-turn promote their antimicrobial efficiency both in single and mixed therapies. In contrast, the hydrophobic part of surface ligands of NPs/NCs supports their entry into the lipid bilayer of bacteria and results in indiscriminate toxicity. A decent control over the charge to hydrophobic proportion of ligands on NPs/NCs surface has been a common and fairly successful approach to enhance their bactericidal efficiency.

#### **1.9.1.5. Chemical Nature of Nanomaterials**

The intrinsic properties of the nanoparticles (e.g., optical, redox and magnetic, etc.) are estimated by the chemical composition of the internal core. The generation of free radicals by metal NPs/NCs is dependent on the nature of their core and there is enough primary evidence that some forms of metal NPs/NCs are highly effective to kill even the resistant microbes by the creation of free radicals in their surrounding area upon interaction with an external stimulus (e.g. light).<sup>86</sup>

#### **1.9.2. Types of Nanomaterials**

The splendid range of therapeutics has produced a plethora of diverse nanoparticle based chemotherapeutic materials comprising of polymers, lipid-based formulations, dendrimers,

inorganic nanoparticles, or carbon nanostructures, and many formulations including additional categories, such as nanoparticles encapsulated in polymer capsules to enhance their biocompatibility, stability and targeted delivery (**Figure 1.8**). Some of these categories are briefly described below.

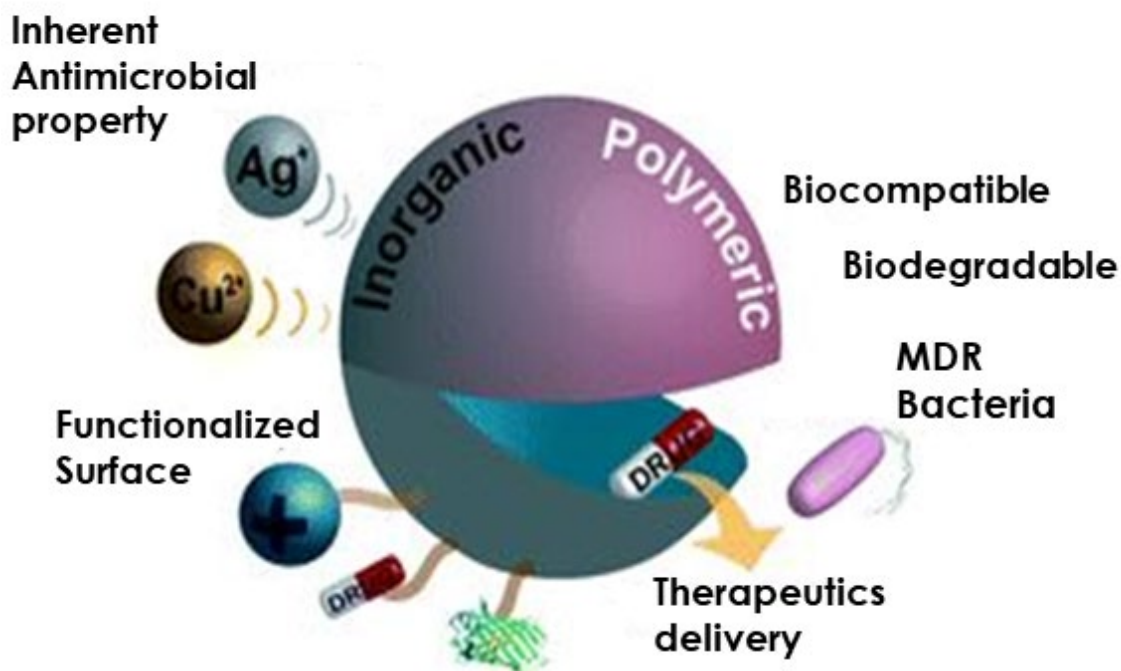


**Figure 1.8** Schematic illustration of different types of nanomaterials based on composition and their suitable properties to target MDR.<sup>87</sup>

#### 1.9.2.1. Liposomes

Liposomes are globular vesicles having a diameter ranging from 20 nm to micrometers, comprising of single or additional phospholipid bilayers, and having hydrophilic surface and interior cavity. The key benefit is that they are prepared from natural, non-immunogenic, non-toxic, and recyclable phospholipids and can encapsulate or bind various drug molecules in their cavity, hydrophobic assembly and even on their surface. Liposomes are among the best known and extensively explored platforms for drug delivery systems. Apart from their multiple benefits, liposomal antibiotics are prone to a few limitations such as their instability and low loading in the liposomes. Another important problem is the synthetic limitation of stable liposomes. The purification techniques used for liposomal antibiotics do not permit

the use of high temperature, radiations or chemicals, as lipids are usually unstable towards heat and simply undergo unwanted hydrolysis and oxidation reactions.<sup>88</sup>

#### **1.9.2.2. Polymeric Nanomaterials**

Polymeric nanomaterials were initially introduced in order to increase stability and drug loading efficiency of nanoscale materials. The rich chemistry of polymer nanoparticles facilitates the physical capture, encapsulation or chemical conjugation of a wide range of bioactive agents. The polymers used in nanomaterials are either synthetic or natural. For example, poly(lactide-co-glycolide) (PLGA) copolymers have been permitted by FDA for numerous biomedical applications. It has been demonstrated that co-encapsulation of isoniazid, rifampicin and pyrazinamide in PLGA nanoparticles displays comprehensive fumigation in only 4 doses and were comparable to 46 oral doses of free drug.<sup>89</sup> Even though polymeric nanomaterials have revealed their capability to improve the transport of antibiotics both intracellularly and extracellularly, a lot more efforts are needed to realize their clinical presentations.

#### **1.9.2.3. Metallic Nanomaterials**

Various metals in size regime of nanoparticles are extremely effective for many pharmacological actions, but exploring their therapeutic efficiency is essential with reference to their toxicities. Among metals as nanoparticles, gold, silver, copper/ copper oxide are considered much better for biomedical applications over other metals, thanks to their good renal clearance and low toxicity. The suitable functionalization of AuNPs with small molecule ligands can control antimicrobial resistance in bacteria by modulating genes expression as reported by Feldheim and coworkers.<sup>90</sup> Gu et al. also reported vancomycin decorated gold nanoparticles, which manifests improved antimicrobial activity against vancomycin resistant bacteria.<sup>91</sup> In a recent study, CuO NPs also demonstrated their antimicrobial potential by the generation of holes in bacterial cell wall, which is related to their electrostatic interaction and the successive reduction of Cu on bacterial surface.<sup>92, 93</sup> In addition ROS based bacterial killing by Cu ions is also reported when applied in wound bandages to the resistant infections.<sup>94</sup> More recently, copper nanoparticles have also been

reported as efficient material for lipid peroxidation, protein oxidation and DNA degradation.<sup>95, 96</sup> Copper oxide nanoparticles generally display decent antimicrobial properties but are less effective than silver nanoparticles except in a few cases i.e. *B. subtilis* and *B. anthracis* were found highly vulnerable to CuO whereas *E. coli* and *S. aureus* are highly susceptible to Ag. Silver has extensively been used in antimicrobials and by further decrease in size in the form of nanoparticles, enhances its surface area and antimicrobial properties. Among other metals, iron oxide, zinc oxide and manganese oxide nanoparticles have also been tested as good biocidal agents especially with reference to their size, shape and surface chemistry.<sup>95, 97</sup> In general, metal NPs play important role to manipulate usual antibiotic resistance pathways like efflux pump facilitated exclusion of antibiotics from the bacterial cells. The combination of NPs and antibiotics offers a good alternative method to hit MDR bacteria by escaping the regulatory problems linked with former bioconjugate assemblies, which additionally improves existing therapeutic approaches. These reports highlighted that the toxicological and pharmacological power of metal nanoparticles in health sector is based on the nature of core material, particles shape, size and their surface chemistry.

### **1.9.3. Silver Nanoparticles as Potential Candidates to Address Multidrug Resistance**

Silver nanoparticles are promising antimicrobial candidates at concentrations where they are not toxic to human cells. This emerging property of silver nanoparticles is adjusted by size and surface functionalization to tune bio-nano interface interactions. The antibacterial efficacy of AgNPs increases with decrease in size owing to enhanced potential to release Ag ions and atoms.<sup>98</sup> There is also a direct connection between the surface charge and biocidal property of AgNPs, specifically the more positive are generally considered to be more toxic. AgNPs are capped with positively charged ligands due to their ability to promote membrane permeability and reduce drug efflux in bacteria.<sup>99</sup> The actual problem with these metals is toxicity when used in excess. Silver is considered to break the resistance by ion releasing effect and thus has extraordinary multipharmacological, antimicrobial potential even against resistant variants.<sup>100</sup> The silver-based nanomaterials are finding an increased usage as antimicrobials due to the exceptional chemistry of silver interfacing with microbes.<sup>101</sup> Raulin was the first one to report the antibacterial ability of silver in 1869. He witnessed that there

is complete stop in growth of *A. niger* in silver vessels.<sup>102</sup> Elvio Amato synthesized glutathione (GSH) stabilized AgNPs showing MIC of 180 and 15 µg/mL against *S. aureus* and *E. coli*, respectively. He inferred that this antimicrobial potential was due to AgNPs instead of Ag ions.<sup>103</sup> Kaiyuan Zheng designed a hybrid by the conjugation of AgNPs with an antibiotic. This hybrid displayed an enhanced bacterial killing than controls. These NPs use membrane disruption and DNA disinfection to kill bacterial cells as manifested by LIVE DEAD and TUNEL assay. The continuous generation of ROS further restrict microbes to develop resistance.<sup>104</sup> A large number of reports are already available to validate AgNPs antimicrobial potential against resistant pathogens i.e. *E. coli*, *E. faecalis*, *B. subtilis*, *P. aeruginosa* and *K. pneumonia*. All these findings show that silver based nanomaterials have great potential to be used as broad spectrum antibiotics with minimum bacterial resistance reported.

#### **1.9.4. Nanoclusters: Promising Next Generation Candidates**

Metal nanoclusters (NCs) display distinct chemical and physical properties in between single atoms and bulky nanocrystals.<sup>105</sup> Commonly used synthetic methodologies for nanoclusters are direct metal reduction in the presence of ligands, ligand exchange or metal exchange reactions. Small molecule protected nanoclusters hold stronger potential in biomedical applications as compared to the larger ones.<sup>93, 106</sup> Since the first report by Burst et al. a series of gold nanoclusters (Au<sub>19</sub>, Au<sub>24</sub>, Au<sub>25</sub>,) have been efficiently synthesized and characterized.<sup>107, 108</sup> Many reports are available for silver nanoclusters synthesis as well (Ag<sub>9</sub>, Ag<sub>11</sub>, Ag<sub>44</sub>), but they are still facing challenges in terms of their reproducible synthesis and precise control over their composition which limit their applications.<sup>109, 110</sup> Numerous reports are available on antibacterial role of metal nanoclusters especially of Ag, which are widely exploited in this regard. These metal nanoclusters (NCs) enter the resistant cells owing to their reduced size and biocompatible surface chemistry and break resistance by using multiple mechanisms.<sup>111, 112</sup> Few of the distinctive electronic properties of NCs can be credited to the binding of organic ligands to metal atoms. Many proteins and other bioactive molecules have been widely used as stabilizing/capping agents for metal nanoparticles because of strong metal-thiol interactions.<sup>113-115</sup> The living organisms take in metal species to make their mineral structures by a natural process of biomineralization.<sup>116, 117</sup> Inspired by

this method, microorganisms have natural ability to intake inorganic metals and reduce them into zerovalent metal nanoparticles.<sup>118, 119</sup>

### **1.10. Mechanism of Action of Silver Nanoparticles**

Nanoparticles own a universal way of toxicity to bacteria, which is mostly missing for mammalian cells.<sup>120</sup> In this respect, AgNPs have gained much consideration and have been demonstrated as efficient antimicrobial against approx. 650 microorganisms. Metal nanoparticles are referred as next-generation antimicrobials due to their remarkable potential to target MDR bacteria. Metal nanoparticles/nanoclusters generally lead to membrane disruption in bacteria by directly connecting to it whereas eukaryotic cells phagocytose them and afterwards expel/degrade them via lysosomal fusion. Mostly nanomaterials act on bacterial cells by direct surface connection without deep penetration and by inducing reactive oxygen species generation. Both of these action mechanisms have absolute power to address major resistance mechanisms used by bacteria and for that reason are, less liable to resistance than previous antibiotics.<sup>121</sup> The mechanism behind AgNPs action is rather complex. The silver nanoparticles first stick to the cellular envelope, and then breach into the microbial cell, promoting the production of ROS and finally inducing discrepancies in transduction of signals to destroy cells. There are four distinct mechanisms used by AgNPs for antibacterial action (**Figure 1.9**), which are briefly described below.

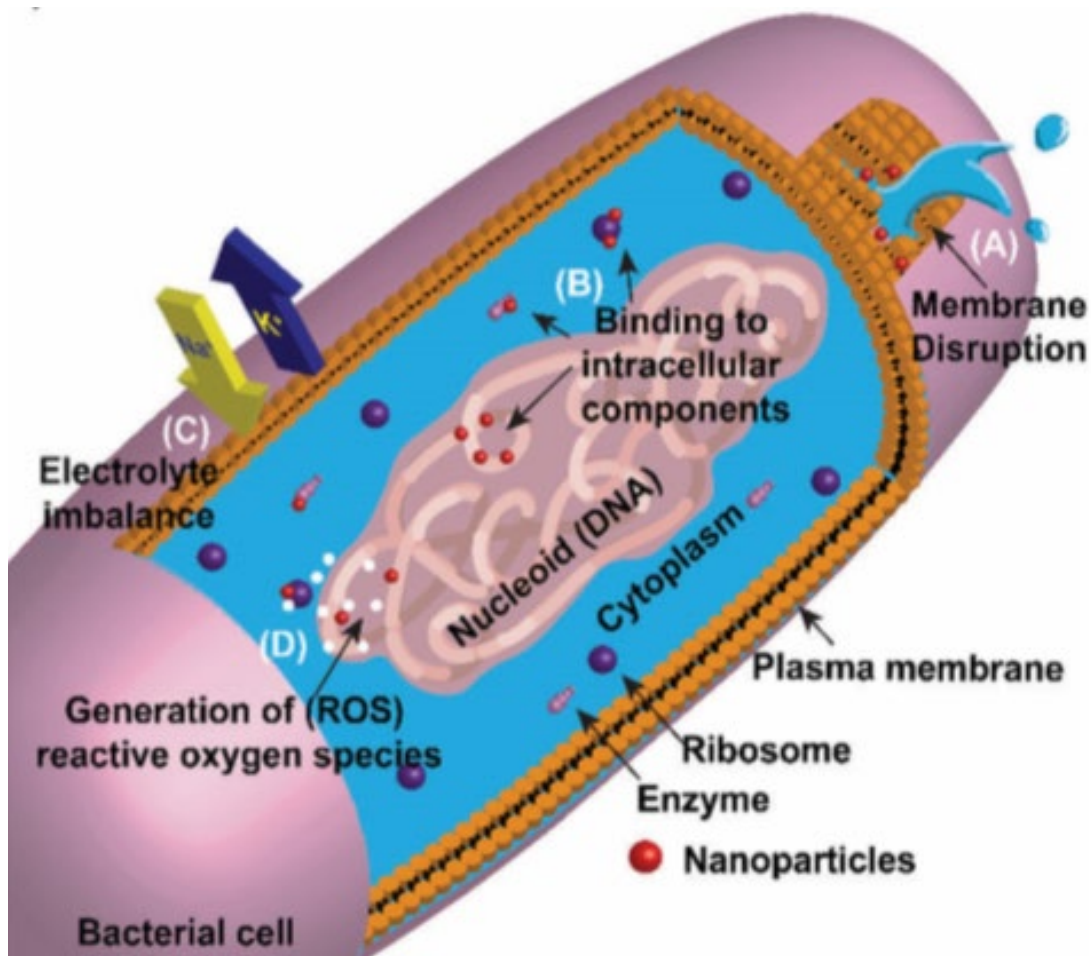


**Figure 1.9** Schematic illustration of antibacterial mechanism of NPs: (A) cell membrane disruption with subsequent cytoplasmic lysis; (B) interaction and dissociation of intracellular constituents; (C) disturbance in electron transport triggering electrolyte imbalance and (D) production of reactive oxygen species (ROS).<sup>122</sup>

### 1.10.1. Membrane Disruption

At first, cationic silver nanoparticles stick to bacterial cells via electrostatic interactions, as microbial membrane is composed of lipid bilayer and has overall negative charge (**Figure 1.10**).<sup>123</sup> This adherence results in changes in cell morphology followed by cell rupture and lysis. In addition to electrostatic interactions, silver nanoparticles can also interact with sulphur group containing proteins in membranes, attributed to increased affinity of Ag with sulphur, and cause irreversible changes. These membrane disruptions can be viewed as pits on bacterial cells surface and have been confirmed by TEM.<sup>124-126</sup>

Moreover, silver can also act by disturbing transport of potassium ions, causing increased membrane permeability that leads to further pronounced outcomes i.e., cellular leakage of ions, sugars, proteins and energy basins. This antimicrobial potential of silver nanoparticles is based on the cell wall composition and the presence of outer membrane. The increased vulnerability of Gram-negative bacteria to silver based antimicrobials is because of difference in membrane composition of bacterium compared to Gram-positive bacteria.

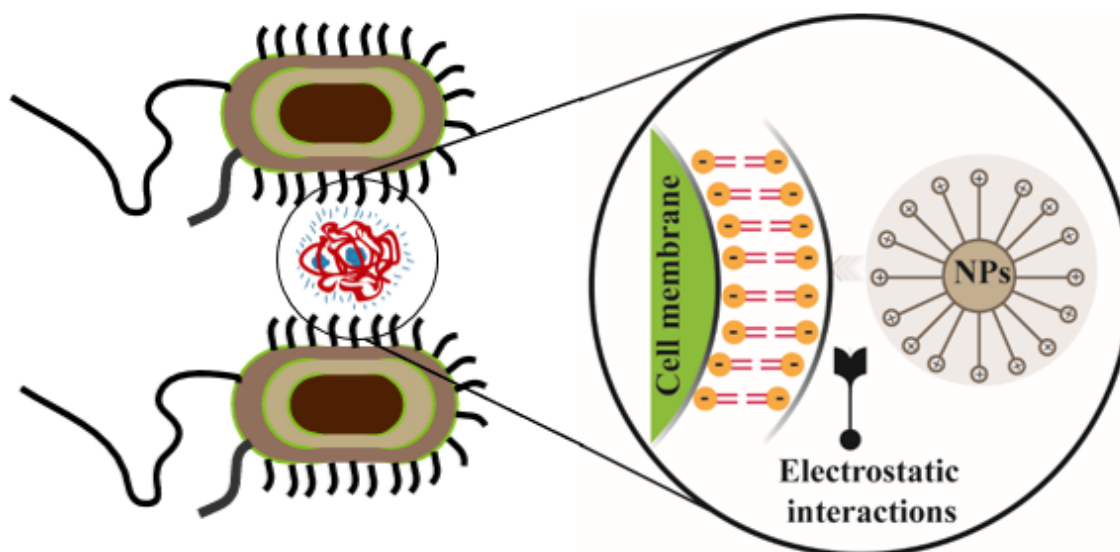


**Figure 1.10** The electrostatic mode of communication of bacteria with cationic silver nanoparticles that results in targeting bacteria through membrane disruption mechanism.

### 1.10.2. Targeting Biomolecules and Intracellular Components

After initial adherence to cellular membrane, nanoparticles penetrate deep inside the cells and almost disturb all cellular machineries. Due to high affinity of AgNPs with mercapto group, it leads to deactivation and denaturation of proteins, DNA, ribosomes and other biomolecules. This DNA disinfection indirectly affects cell division. Ribosomes play a very important role in protein synthesis and their denaturation leads to inhibition of translation. Similarly, AgNPs can also spoil sugar metabolism by deactivating phosphomannoses by releasing  $\text{Ag}^+$  ions causing strong bactericidal outcomes.<sup>127</sup>

### **1.10.3. ROS Generation**

In cells, ROS were generated normally by mitochondria and Fenton reaction. Like other heavy metals, silver also intensifies oxidative stress via production of additional reactive oxygen moieties and many other free radicals. The amplified ROS generation leads to cell death. Silver ions further disturb the cellular oxidative levels by inhibiting respiratory enzymes and affecting mitochondrial membrane. This increase in ROS production results in hyper-oxidation of lipids, protein and DNA leading to the death of bacteria.<sup>128</sup>

### **1.10.4. Disrupting Metabolic Pathways**

Silver nanoparticles may also affect cellular growth by disrupting many metabolic pathways. For example, they interfere with bacterial growth by dephosphorylating tyrosine residues on peptide chains and subsequently target cellular signaling. Phosphorylation and dephosphorylation of proteins play a major part in cell cycle, DNA's recombination, replication and cellular metabolism. Therefore, interruption in these pathways affects enzymatic action and finally bacterial growth inhibition.<sup>129</sup>

## Chapter 2.

### Literature Review and Scope of Thesis

#### 2.1. Synopsis

This chapter comprises of two parts. The 1<sup>st</sup> part covers literature review highlighting the importance of silver-based nanoparticles. The 2<sup>nd</sup> part presents scope of this thesis to assist in breaking MDR in different bacterial varieties through silver-based nanomaterials.

#### 2.2. Literature Review

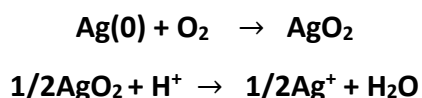
Silver has been used since long as an antimicrobial to prevent spoilage and fight infections, and Ag ions and Ag-based materials are known to be lethal for Gram-positive and Gram-negative microbes.<sup>130</sup> Initially, this might appear intuitive as metals and their complexes were usually recognized for application as catalysts or materials and are frequently linked with toxicity.<sup>131</sup> In the late 19<sup>th</sup> century, the earliest scientific paper relating the therapeutic usage of silver is accredited to F. Cr  d  , who used 1% silver nitrate solution as an eye drops in infants, removing blindness triggered by postpartum eye infections, and to treat internal antiseptis in 1901.<sup>132</sup> Later in 1965 0.5% silver nitrate was used for the management of burn injuries.<sup>133</sup> This treatment worked well at this stage to govern *P. aeruginosa* infection, but then the appearance of resistance to silver nitrate<sup>134</sup> provoked a variation in formulation leading to the use of silver sulphadiazine – a mixture of sulphonamide and silver instead.<sup>135</sup> Klasen suggested that such combinations function by slow discharge of Ag<sup>+</sup> as the major antiseptic whereas sulfadiazine assists generally to retain Ag<sup>+</sup> in solution form and avoid the formation of light-sensitive black colloidal Ag<sup>0</sup> on the skin - once more a severe cosmetic issue with AgNO<sub>3</sub>-based stuff as patients reported skin blackening issues. On the other hand, Klasen also recommended that microbial resistance to silver-sulphadiazine established quickly primarily due to the antibiotic constituents.<sup>136</sup> Recently, the British National Formulary approved the use of silver nitrate (40–95%) and

silver sulphadiazine (1%) for exterior use for management of infections on wounds.<sup>137</sup> These pre-historic benefits of silver in different forms supports its active role in antimicrobials.

The appearance of resistance in bacteria against antibiotics is quite challenging for the drug companies and healthcare professionals. In the previous decades, however, the merely permitted antiseptic along with newly exposed teixobactin was linezolid.<sup>138</sup> One of the major way to develop microbial resistance is the alteration of antibiotics target.<sup>139</sup> For instance, alteration of cell wall constituents induces resistance against vancomycin, whereas alterations in structure of ribosomes hinder tetracycline.<sup>140</sup> In the same way, bacteria can also overexpress enzymes like aminoglycosides and  $\beta$ -lactamases to destroy antibiotics. Moreover, increased expression of efflux pumps supports bacteria to escape several antibiotics simultaneously. Numerous pathogens, for example *C. pneumonia*, exist within the cellular compartments in host cells to protect themselves from antibiotics which are usually limited to extracellular space.<sup>141, 142</sup> So, there is a dier need of new category of materials to target micro-organisms by overcoming different barriers simultaneously.

The antibacterial formulations as nanoparticles (NPs) can be suitable candidates to interact with bacteria intimately and could be employed as efficient bactericidal materials owing to their improved reactivity because of higher surface to volume ratio.<sup>143, 144</sup> There are approx. 100 nanomedicines permitted by FDA and many are under clinical trials.<sup>145</sup> To start with, researchers varied the essential core of nanomaterials to produce antimicrobials with varying mode of action. The silver nanoparticles play an extraordinary oligodynamic role among all other metals.<sup>146, 147</sup> Bajaj et al. stated the development of antibacterial dipeptide-functionalized Ag or Au nanohybrids. They observed improved MIC (0.37–0.93 $\mu$ M) by Ag nanoparticles capped with dipeptides against *S. aureus* compared to the dipeptides or Ag nanoparticles alone (controls), respectively. A synergistic response was observed by dipeptides and Ag combination nanoparticles. In comparison, the dipeptide-decorated Au nanoparticles presented no bactericidal response suggesting that the core material plays a vital role.<sup>148</sup> The Sun group has also reported a series of comprehensive studies on the mode of action and targets of silver based antimicrobials.<sup>149, 150</sup> All these studies supports the use of silver based nanomaterials in connection with their prehistoric antimicrobial applications.

Silver in nano-size manifest better antibacterial potential than bulk metal and ionic silver.<sup>151, 152</sup> For instance, silver-based nanoparticles use free Ag<sup>+</sup> ions as an active agent to work as antimicrobials. Alvarez and co-workers proved that anaerobic environment prevent Ag(0) oxidation and thus Ag<sup>+</sup> leakage in Ag NPs suspension, and hence no detectable antibacterial effects on *E. coli* even at thousands of times (7665 times) increased concentration than the minimum harmful concentration of Ag<sup>+</sup> ions (0.025 mg/L), whereas under aerobic environment these Ag NPs displayed thousands of times improved minimum lethal concentration:



This finding led to the conclusion that the biocidal potential could be managed by controlling the Ag<sup>+</sup> release profile by adjusting the silver nanoparticles shape, size and surface chemistry together with the apparent coating.<sup>153, 154</sup> Xiu et al. reported similar findings for AgNPs acting as antimicrobials against *E. coli* under aerobic vs anaerobic conditions. They concluded that their antibacterial action solely depends on Ag<sup>+</sup> ions release instead of AgNPs themselves even at thousands of times elevated concentrations.<sup>155</sup> Later on studies revealed that Ag<sup>+</sup> and Ag NPs both can pass through the bacterial cell membrane using porin proteins resulting in rupturing of cell membrane, pit formation and cytoplasmic escape.<sup>156</sup> This all resulted in recommendation by Alvarez and coworkers to use Ag NPs as antimicrobials because of their reduced ability to bind with naturally occurring ligands compared to Ag<sup>+</sup> and therefore resulted in improved delivery of Ag<sup>+</sup> in bacterial cytoplasm using the acidic cell membrane.<sup>157</sup>

The current scenario of MDR emphasizes the growing scientific interest to reconsider silver nanomaterials owing to their wonderful therapeutic history.<sup>158</sup> AgNPs were widely used as antibacterials against various MDR and non-MDR varieties of bacteria owing to their decreased sensitivity in contrast to free ions.<sup>159</sup> They acquire their bactericidal action through a lot of opposing metabolic and biochemical routes, thus manifesting MDR reversal in a variety of MDR resistant strains. The AgNPs show a variety of biological activities due to their innate antibacterial potential for both antibiotic sensitive and resistant strains.<sup>160</sup> In recent times, AgNPs appeared to have profound scientific interests by offering innovative

pathways for reversing microbial resistance and are being suggested as novel class of antibiotics.<sup>161</sup> Normally, the antibiotics can only target one fixed feature of bacteria while silver ions can bind non-specifically to various proteins and DNA etc. by different ways, thus targeting bacteria at once in several components of their structure and metabolism.<sup>162</sup> It is well-known that free Ag ions, leached from silver nanomaterials, generally stick to the cell membrane moieties, disrupt their membrane potential and cause excessive proton seepage.<sup>163, 164</sup> Pal et al. further supported that the inorganic metal nanoparticles are also responsible to form irregular pits on bacterial wall to support ions penetration into the cytoplasm.<sup>165</sup> So, the AgNPs are quite suitable candidates compared to silver ions, bulk silver and other inorganic metals to target MDR bacteria.

With reference to the synthesis of AgNPs in this thesis, chemical reduction approach was used which generally involved the transformation of Ag<sup>+</sup> ions into colloidal and stable monodispersed nanoparticles by inorganic or an organic reducing agent in a suitable aqueous/organic medium containing an appropriate stabilizing agent. Usually, ascorbate ions or citrate ion or a powerful reducing agent like borohydride can change the Ag<sup>+</sup> ions to metal atoms.<sup>166-168</sup> Consequently, the initially formed Ag<sup>0</sup> atoms aggregate to form oligomeric clusters that grow during the course of reaction to produce AgNPs.<sup>169</sup> The stabilizing agents with -COOH, -OH, or -SH functional groups display significant interactions with the nanoparticles surface.<sup>170-172</sup> They also accelerates the particle growth while it is binding to the nanoparticles surface and inhibit their agglomeration in solution form.<sup>173</sup> The capping agents preserve the dispersed state of nanoparticles without affecting their surface attributes. Dondi et al. planned a simple single-step synthetic method for the production of size and shape controlled AgNPs by tollens reagent by a principal resorcinol ether core enclosed by triazole sugar ligands, which stimulate nucleation, growth, and dispersion phases for the synthesis of AgNPs. This scheme is useful for the preparation of AgNPs in the size range from 25 to 50 nm.<sup>174</sup> To get further reduction in the size of nanoparticles to make nanoclusters, the ratio of ligand to metal was increased along with the optimization of various reaction conditions like temperature, reaction time, stirring rate etc.

Silver nanoparticles are already well acknowledged for their antibiotic potential in reduced concentrations against different multidrug resistant varieties of *E. coli*, *P. aeruginosa*, *P. mirabilis*, and *S. enterica*.<sup>175</sup> They show increased antibacterial power due to high affinity with bacteria which is attributed to their high surface area/volume ratio, tunable surface chemistry, and the ability to load various drugs.<sup>176</sup> AgNPs capped with various ligands i.e., glucosamine (Figure 2.1), polyethyleneimines, peptides, and chitosan usually presented an improved antibacterial activity, which is relatable to their increased intake by bacterial cells due to better binding capacity of nanoparticles.<sup>177-179</sup> Similarly, 14 nm spherical Ag NPs having chitosan as a stabilizer were made by slow addition of NaBH<sub>4</sub> to a fast stirring metal salt solution (500 rpm). These AgNPs act as strong disinfectant at 25 μM concentration, which is quite high compared to this thesis findings, against Salmonella bacteria of concentration 10<sup>8</sup> colony-forming units (CFU) mL<sup>-1</sup>.<sup>180</sup> There is still room available in optimization of AgNPs to attain nanoparticles/nanoclusters with further size reduction to have improved antibacterial potential.

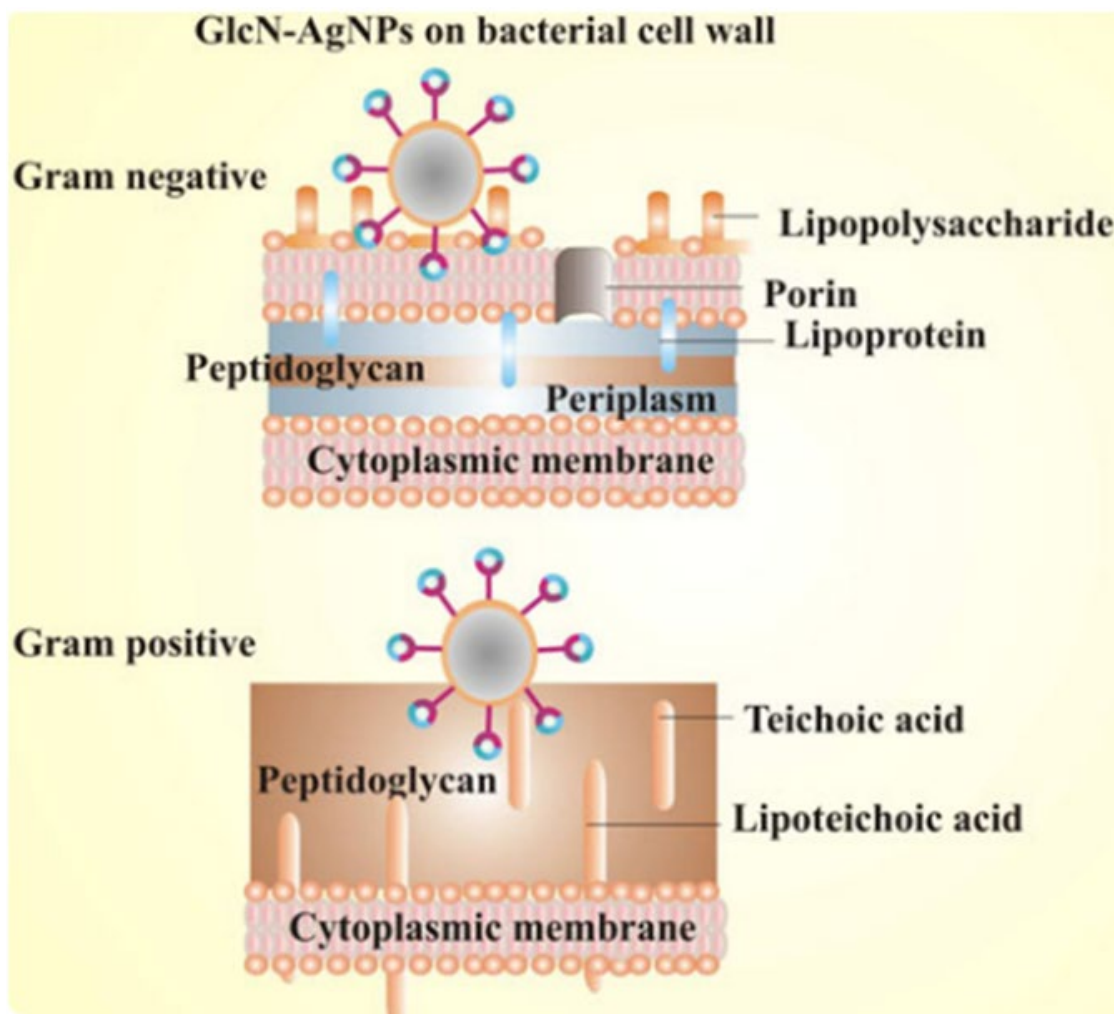


**Figure 2. 1** The interaction of glucosamine functionalized silver nanoparticles (GlcN-AgNPs) with Gram negative and positive bacterial cell wall surface.<sup>177</sup>

Banerjee et al. described that the bactericidal potential of AgNPs can be uplifted by coating them with a variety of polymers such as cationic polysaccharides and chitosan (Figure 2.2).<sup>181</sup> Li's group reported the synthesis of positively charged polymer (2-(dimethylamino)ethylmethacrylate (DMAEMA) functionalized silver nanoparticles (AgNPs@PDMAEMA-C4) by silver nitrate reduction, which showed good antibacterial activity at concentrations that were not lethal to the mammalian cells. The bactericidal role of these nanoparticles (AgNPs@PDMAEMA-C4) was greatly increased due to the joint antibacterial and multivalent action of the nanoparticles and polymer. These nanoparticles improved the cytoplasmic membrane permeability and successive penetration into the bacterial cells to obstruct intracellular enzyme functioning, leading to the cell death.<sup>182</sup>

Similarly, compared to the anionic hyaluronic acid-modified particles, aminocellulose coated nanoparticles with a cationic surface presented improved interaction with microbial membranes, causing more cell wall deterioration and antibacterial activity.<sup>183</sup> Recently, nanoparticles have been functionalized with cationic and hydrophobic alkyl chains to improve bacterial membrane injury. The longer alkyl chains play important role in improving hydrophobicity of nanoparticles that facilitated their uptake through the cell membrane and thus resulted in lowering their bacterial minimum inhibitory concentration (MIC).<sup>184</sup> All this shows positively charged silver nanoparticles with hydrophobic capping works as efficient antimicrobials.

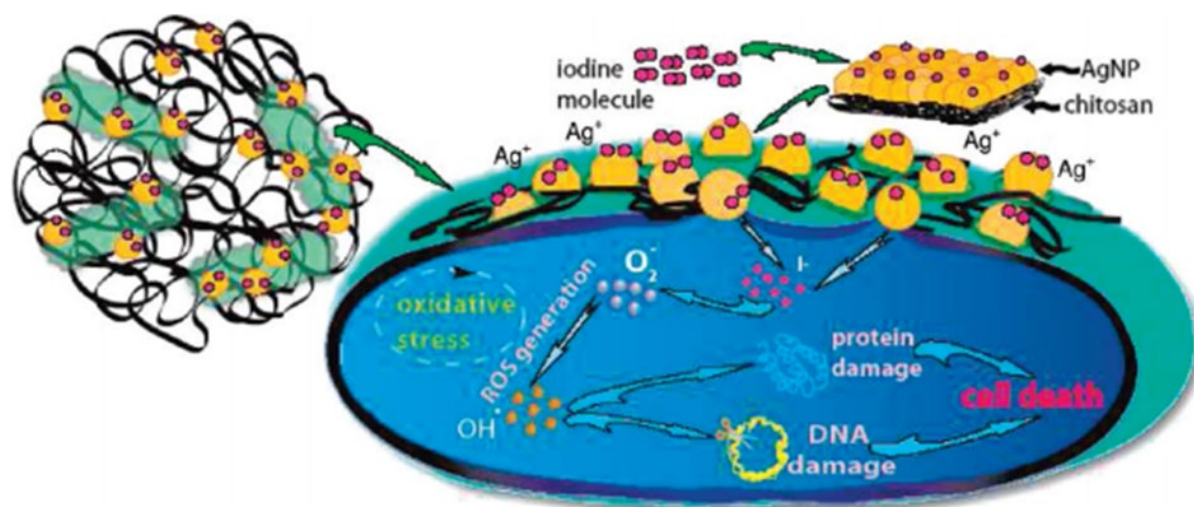


**Figure 2. 2** Schematic illustration of the anticipated antibacterial mechanism of iodinated chitosan-Ag NP composite.<sup>181</sup>

Improving the stability of silver nanoparticles in the growth medium promotes their toxicity by giving them more time for retention on bacterial media, otherwise, the aggregation of nanoparticles lead to the reduced biocidal potential.<sup>185, 186</sup> Gnanadhas et al. decorated AgNPs with the bovine serum albumin (BSA) to enhance their stability in a variety of intracellular pH and and showed great potential as antimicrobials and drug delivery systems.<sup>187</sup> Conversely, a few ligand-functionalized silver nanoparticles even though have better stability and are fairly uniform in size but were found less bioactive because the capping agent slowed down the discharge of silver ions.<sup>188</sup> Kooti et al. observed that coating of graphene oxide on Ag nanoparticles inhibited their aggregation quite effectively and this nanocomposite can also release loaded ciprofloxacin in a controlled way. The zone of

inhibition for this nanocomposite was improved over 2-fold in comparison to the control without ciprofloxacin, and far more than that of the ciprofloxacin alone. Hence, properly coated AgNPs show improved stability and antibacterial activity.<sup>189</sup>

Morones et al. have evaluated antibacterial role of silver nanoparticles ranging in size 1–100 nm against *E. coli* by growing them to mid-log phase. They observed that the nanoparticles in 1-10 nm range were the best in showing direct interaction with bacteria and the concentrations higher than 75  $\mu\text{g mL}^{-1}$  were deadly for bacteria.<sup>190</sup> So, smaller the size of silver nanoparticles higher is their antibacterial potential.

Moreover, AgNPs reportedly show a significant synergism with a few well-known antibiotics (Figure 2.3).<sup>191</sup> The therapeutic formulation of AgNPs with the relatively ineffective antibiotics showed a pronounced synergistic outcome along with playing a broad-spectrum role.<sup>192</sup> Ping et al. observed that the least administrable dose of the drug also dropped as a result of AgNPs in the combination.<sup>193</sup> Similarly, Deng et al. reported a four-step route to reveal the AgNP-antibiotic synergistic mechanism by employing  $\beta$ -lactam antibiotics: kanamycin, tetracycline, enoxacin, and neomycin. They found that the AgNPs make complex with antibiotics thus improving their interaction with the targeted cells. It increases the level of Ag<sup>+</sup> ions nearby the target cells ultimately causing their death.<sup>194</sup> These antibiotic combinations with AgNPs not just increases the absorptivity of the antibiotics to the respective cells, but also improves their bioavailability. In addition, Sharifi-Rad et al. used a combination of allicin (a naturally occurring bactericidal compound rich in garlic) with biocidal Ag nanoparticles in mice for the treatment of MRSA skin infection. This ointment showed a good synergistic response against MRSA infection. The bacteria shows no growth for the combination treatment compared to AgNPs alone, allicin alone, and control bacteria.<sup>195, 196</sup> So, such combination treatments are also good alternatives to work against MDR bacteria.

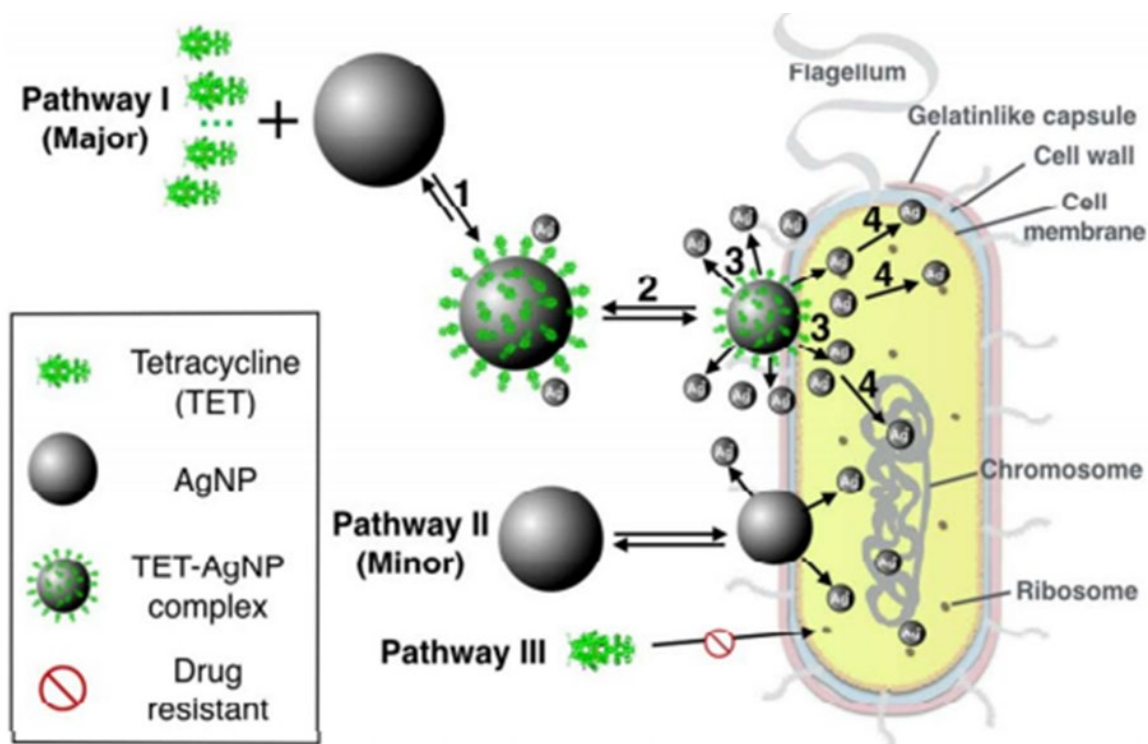


**Figure 2.3** Schematic representation of the synergistic antibacterial pathway of tetracycline decorated AgNPs against multidrug resistant bacteria. A four-step procedure was suggested as the major pathway leading to cell death. Pathway II represents a minor pathway and Pathway III is not operational due to tetracycline resistance by Salmonella.<sup>194</sup>

The Gram-positive bacteria are often tested to be less prone to silver nanoparticles compared to Gram-negative owing to the difference in composition of peptidoglycan layer.<sup>197, 198</sup> In Gram-positive bacteria, the increased negative charge due to phosphates and carboxylates of the polymeric teichoic acids deactivates the bioactive  $Ag^+$  ions released by AgNPs thus rising the AgNPs resistance.<sup>199</sup> Furthermore, the Gram-negative bacteria with hydrophobic lipopolysaccharide-loaded outer membranes provide additional defense against the penetration of various hydrophilic bactericidal agents.<sup>200, 201</sup> Bacteriological infections usually present much low pH (4.5) because of their hypoxic environment. The acidic atmosphere of microbial infectious spots can be coupled to the designing of pH subtle drugs. The histidine residues in pegylated poly L-histidine micellar nanoparticles get protonated at 6.5 pH and develop strong interactions with the anionic bacterial cell membrane, so silver NPs coated with histidine/ groups which can be protonated like amines can work as better antimicrobial agents.

Some bacterial strains have developed additional protective measures to escape the AgNPs mediated loss by the construction of biofilms. A dense glycocalyx sheath in these biofilms sticks bacterial cells colony to a hard sedentary surface through loose van-der Waals forces and accelerates the maturation of microbial biofilm.<sup>202</sup> This highly viscous glycocalyx matrix increases antibiotic resistance in bacterial strains by hindering antibiotic molecules diffusion to deeper bacterial community using a range of routes.<sup>203</sup> In this context, a variety of coatings on silver nanoparticles have been evaluated with useful results and some of these are summarized below:

- (i) Starch coated AgNPs disrupt biofilms developed by *S. aureus* and *P. aeruginosa*;<sup>204</sup>
- (ii) Citrate functionalized AgNPs of variety of sizes were found to prevent biofilms formation by *P. aeruginosa*;<sup>205</sup>
- (iii) Polyvinylpyrrolidone (PVP) coated silver NPs revealed good antibacterial potential against *P. aeruginosa*, *S. aureus*, *E. coli* and *B. subtilis*;<sup>206</sup>
- (iv)  $\beta$ -cyclodextrin is also an active functionalizing and stabilizing ligand that enhances anti-biofilm activity of AgNPs while decreasing their toxicity against mammalian cells.<sup>207</sup>

Kalishwaralal et al. observed 95%-98% decrease in biofilm formation against *S. epidermidis* and *P. aeruginosa* using AgNPs. Hence, it was deduced that AgNPs have potential to detach *S. epidermidis* and *P. aeruginosa* quite rapidly and effectively, introducing clinical alternative therapies.<sup>204</sup>

A few reports relating the AgNPs attacking bacterial biofilms without affecting the mammalian cells sustainability are also available. For example, citrate-functionalized AgNPs exhibit synergistic response with aztreonam against biofilms of *P. aeruginosa*. This response is the result of an increased permeation of the drug into biofilm matrix.<sup>205</sup> Various AgNPs coated medical devices and surgical masks, are now in clinical trials with quite favorable outcomes.<sup>208-210</sup> In addition, the biocidal potential of silver nanoparticles is also dependent on the type of bacterial strain, concentration and structure of cell wall.<sup>211</sup> As stated earlier, dose/concentration is a key factor for the application of nanoparticles as an antibacterial agent. Generally, the toxicity of Ag NPs is dependent on their concentration. The average dietary exposure of Ag-NPs is predicted as 70–90 $\mu$ g/day. The oral nanoparticles

that skip the absorption route reach the colon where they possibly affect the structure and function of gut microbes, upsetting the toxicity and production of bacterial metabolites.<sup>210</sup> Vila et al. observed a concentration of 100 µg/mL of 8 nm sized Ag-NPs to show 20% cytotoxicity against Caco-2 cells.<sup>213</sup> Another study presented that most of the Ag NPs were dissolved before reaching the stomach and most of the discharged ions were bound to the food matrix. This makes silver ions less bioavailable and consequently reduced toxicity.<sup>214</sup>

Moreover, the low therapeutic indices of AgNPs against host mammalian cells can restrict their extensive practice in biomedical applications. For this purpose, zebrafish embryos were tested by different concentrations of silver nanoparticles for 4 days and merely a rise in toxicity was detected for 40 nm nanoparticles. This could be attributed to the holding of silver in intestine, which is dependent on the size of particles and agglomerates.<sup>215</sup> Wilding et al. tested oral administration of 20 and 110 nm silver nanoparticles capped with PVP and citrate for 28 days in mice and found no effect on gut microbiome at antimicrobial concentrations.<sup>216</sup> This shows that effectively capped AgNPs of different sizes were quite safe against gut microbes compared to free Ag ions.

Researchers also fabricated zwitter ionic ligands decorated silver NPs with varying charge positions, one with cationic outermost layer and the other with cationic inner termini of the ligand. It was observed that NPs with positive charge on the surface showed improved antibacterial potential compared to the NPs with cationic inner side. Hence, silver nanoparticles with cationic surface act as potent antimicrobials.

The NPs surface chemistry plays an important role in making them soluble in the blood stream and thus giving them a “stealth effect” against the body’s usual defense system. The phagocytic system can remove the nanoparticles from blood unless they were suitably engineered to skip recognition. Another significant biological hurdle to nanoparticle-based systems is the opsonization. In the blood, opsonin proteins quickly stick to the nanoparticles, letting the macrophages from the defense system to bind and eliminate NPs from circulation.<sup>217</sup> To address this issue, various pathways have been employed to hide nanoparticles from the natural defense system. Among these approaches, the preferred one is the covering of polysaccharides e.g., chitosan or the grafting or adsorption of hydrophilic

polymers for example poloxamers (e.g. pluronic-F68) or PEG on the nanoparticles surface.<sup>218-220</sup> These coverings build an 'uncharged cloud' of hydrophilic groups on the surface of particle that prevent plasma proteins adsorption and improve the retention time of nanoparticles in the circulatory system. When Ag-NPs come in connection with proteins, a protein corona is formed on their surface and this reduces their entry into cells and consequently losses cellular toxicity.<sup>221</sup> Gil-Sánchez et al. assessed that the glutathione-capped silver nanoparticles show less agglomeration compared to nanoparticles with polyethylene glycol capping and were also less lethal to colon cells.<sup>222</sup> Hence, capping of AgNPs with ligands having balanced hydrophobic and hydrophilic constituents is important.

### **2.3. Scope of this Thesis**

The major focus of this thesis is on the designing of silver-based functional nanoscale materials as substitute and non-conventional materials to address the multidrug resistance challenge. It is of supreme interest to inspect the antibacterial potential of ultra-small silver nanoclusters and nanoparticles to acquire a proper knowledge of its mechanism of action. With the decrease in particle size, there is an increase in specific surface area exposing a big number of atoms on the surface accessible for photochemical, biochemical, and redox reactions along with physicochemical connections with cells. Cationic nanoparticles firmly stick to the bacterial cells surface, leading to their merging in cell wall, whereas no adherence is noticed for the anionic nanoparticles in Ag nanoparticles case. The shape is likely to play a significant role in dealing with the bacterial interaction. The spherical shaped ultrafine AgNPs give an increased surface area for interaction with the membrane and bacterial cell wall quite effectively.

The bottom up method is generally used for the synthesis of silver nanoparticles. In this method, NPs/NCs are produced by self-assembling of atomic scale components. The best approach employed here to control specificity, cytotoxicity, and breaking resistance through nanomaterials is shielding of bioactive portion of NPs/NCs with biocompatible polymers like polyethylenimine. These nanomaterials are employed in targeting multidrug resistant bacteria and their resistant biofilms. There is an increased interest and demand for the

introduction of non-conventional supplies, which can not only increase the pharmacokinetics and bioavailability of the pre-existing drugs and their derivatives, but can also target the bacteria by methods that limit the possibility to grow resistance against them.<sup>223</sup> In this regard, nanoclusters (NCs) are also used efficiently in making stabilized nanocapsules to load resistant antibiotics. These nanocapsules are used to effectively target resistant bacteria. This technology have great potential to be expanded to therapeutic surface engineering of nanostructures and more potent systems, with the ultimate goal to develop clinically viable products.

The overall objectives of this thesis are:

- Synthesis and characterization of silver nanoclusters and nanoparticles functionalized with polyethylenimine.
- Testing of silver nanoclusters against multidrug resistant bacterial strains and evaluation of their killing mechanism.
- Comparative study of silver nanoclusters and nanoparticles against *P. aeruginosa* resistant biofilms and evaluation of their working mechanism.
- Design, synthesis and characterization of silver nanocluster based levofloxacin loaded nanocapsules and their testing against different pneumococcal strains with evaluation of their working mechanism.

## Chapter 3.

### Experimental

#### 3.1. Synopsis

This chapter comprises of two parts. The 1<sup>st</sup> part covers the materials, experimental protocols and the basic characterization of the nanomaterials reported in this thesis. The 2<sup>nd</sup> part presents brief description of the basics of different analytical techniques and methods used for the analysis of nanomaterials.

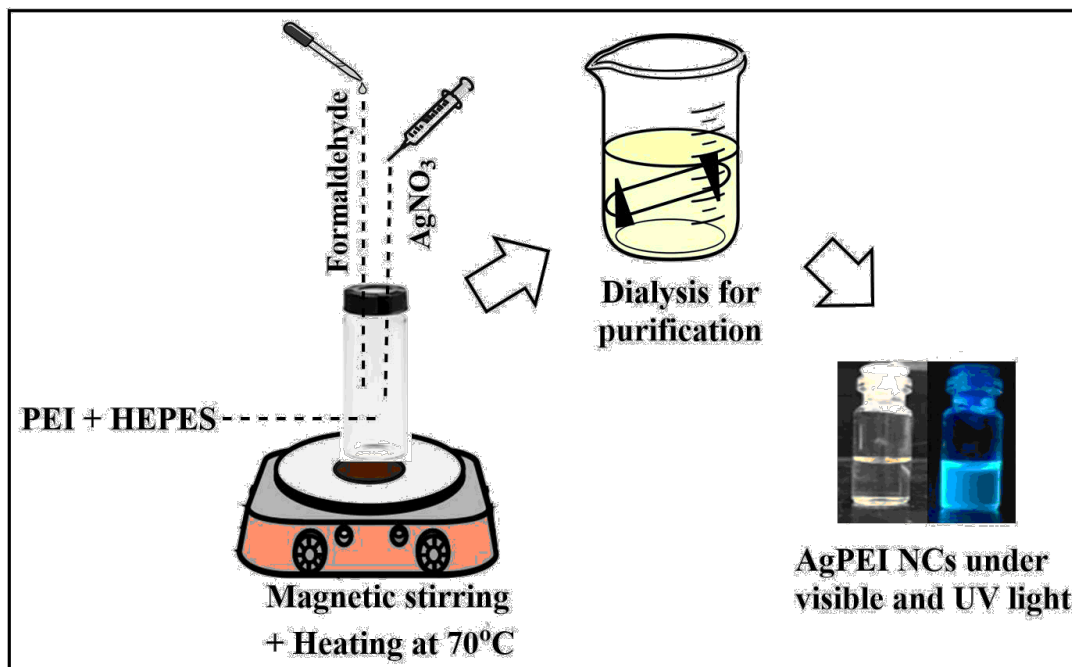
#### 3.2. Materials

Hyperbranched polyethylenimine (bPEI) (Mr 800, 99%), silver nitrate, 4-(2hydroxyethyl)piperazine-1-ethanesulfonic acid (HEPES), formaldehyde (30 wt %), phosphate-buffered saline (PBS 7.4 pH), levofloxacin, sodium dodecyl sulfate (SDS), peppermint oil, resazurin, yeast extract, Todd hewitt broth, cation-adjusted Mueller-Hinton broth CAMHB (BD, Sparks, MD, USA), crystal violet and dialysis membranes (molecular weight cut-off (MWCO) 1 kD) were obtained by Sigma-Aldrich. All the solvents used in study were of analytical grade. Millipore water with a resistivity of 18.2 M $\Omega$  was used to prepare all aqueous formulations. All bacterial strains in chapter 4 were harvested in the Cooley Dickinson Hospital Microbiology Laboratory (Northampton, MA, USA). NIH 3T3 cells (ATCC CRL1658) and Dulbecco's modified Eagle's medium (DMEM) (DMEM; ATCC30-2002) were purchased from ATCC, and fetal bovine serum (SH3007103) was purchased from Fisher Scientific. FapC was produced from *P. aeruginosa* (PAO1) according to reported literature and stored in 6 M GdmCl. All bacterial strains (chapter 6) were collected from Chughtai Lab (CL). All CFU counts in chapter 6 were log-transformed before analysis and multiple comparison between groups mean log<sub>10</sub> CFU counts were made by one way analysis of variance (ANOVA) with Bonferroni's post-test.

### 3.3. Methods

#### 3.3.1. Synthesis of Polyethylenimine Silver Nanoclusters (bPEI–Ag NCs)

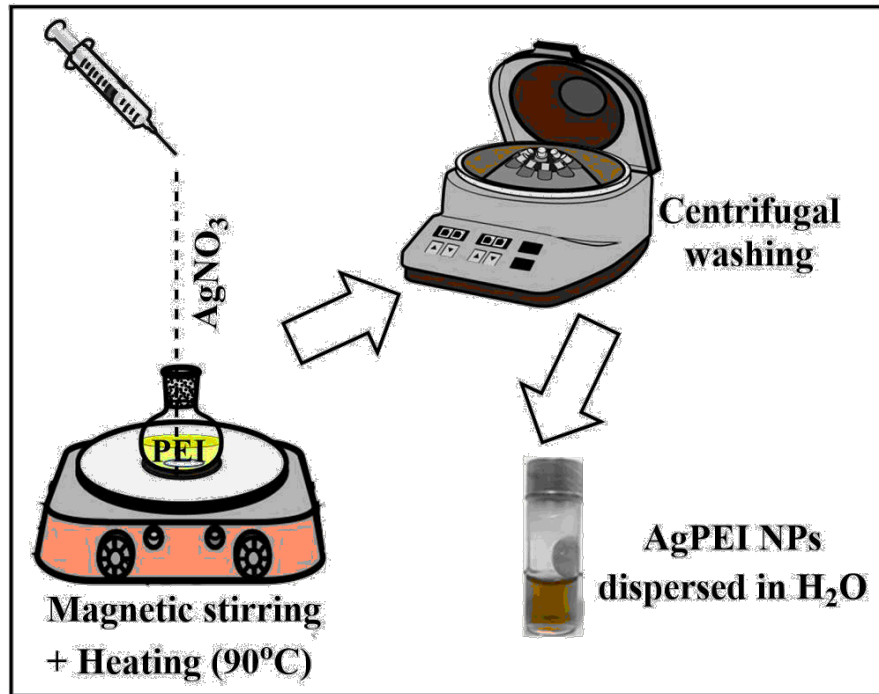
Nanoclusters (bPEI–Ag NCs) were prepared using a modified silver mirror reaction (**Scheme 3.1**). Briefly, 1 mL aqueous solution of bPEI (0.094 g), 50  $\mu$ L of HEPES (1 M), and 950  $\mu$ L of H<sub>2</sub>O were vigorously stirred for 2 min followed by a dropwise addition of 2.5 mL of AgNO<sub>3</sub> (0.01 M). Silver ions were first sequestered in bPEI forming a bPEI–Ag complex, which is resistant against reduction under basic conditions (pH 9.0) even with NaBH<sub>4</sub>. The pH was adjusted to 7 with the HEPES buffer, resulting in a change of solution color from colorless to light yellow because of the formation of a complex. At neutral pH, the reduction potential for the Ag<sup>+</sup>/Ag system is 0.799 V, whereas that for Ag(NH<sub>3</sub>)<sup>+</sup>/Ag is 0.379 V.<sup>224, 225, 226</sup> Formaldehyde (100  $\mu$ L) (30%) was then slowly added, and the reaction mixture was stirred for 10 min at 70 °C. PEI can etch the larger Ag NPs to smaller Ag NCs; hence, upon prolonged incubation of the reaction mixture (24 h), polyethylenimine coated silver nanoclusters (bPEI–Ag NCs) were obtained.<sup>227</sup> The bPEI–Ag NCs were purified by dialysis in deionized water using a 1 kD (MWCO) membrane for 24 h and stored in dark at 4 °C for further use. UV–vis absorption spectra of bPEI–Ag NCs show absorption peaks at 268 and 354 nm, which correspond to Ag NCs; however, pure PEI shows only one absorption peak at 260 nm, which overlaps with that of the absorption of glass cell. The complete wavelength scan showed that the corresponding excitation and emission wavelengths for bPEI–Ag NCs were 375 and 430 nm, respectively. Pure bPEI also displayed similar excitation and emission peaks, but the fluorescence intensities were about 1/60th of those exhibited by bPEI–Ag NCs.



**Scheme 3.1** A general schematic route for the synthesis of blue fluorescent AgPEI NCs by silver mirror reaction and their purification by dialysis.

### 3.3.2. Synthesis of Polyethylenimine Silver Nanoparticles (bPEI– Ag NPs)

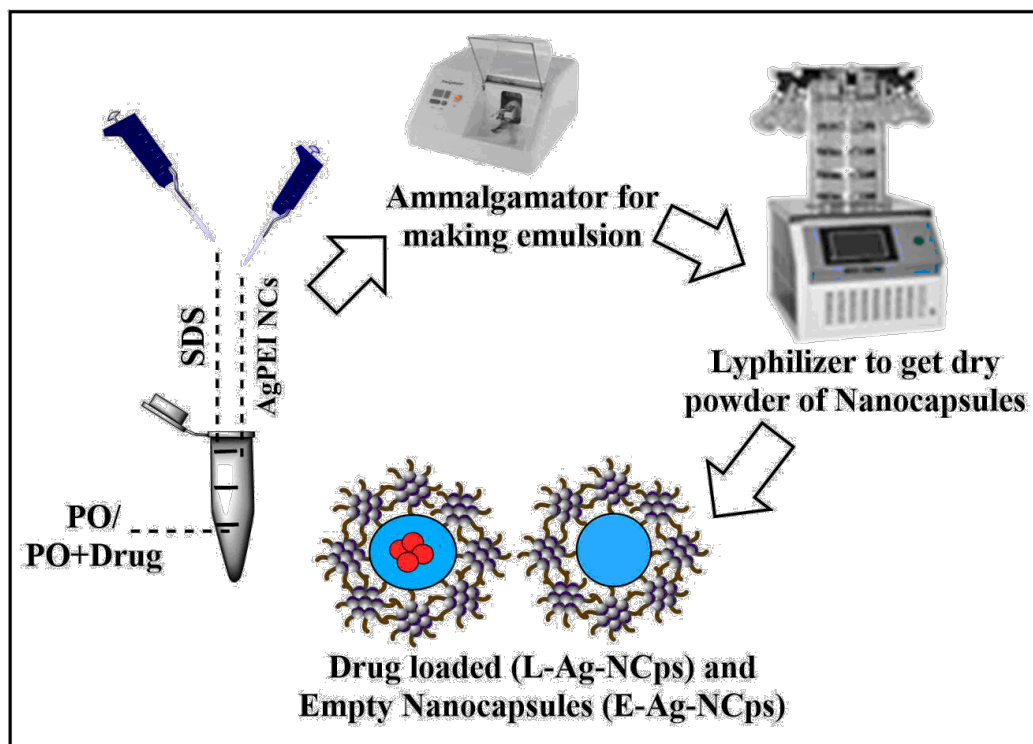
For the synthesis of bPEI-capped AgNPs, an aqueous solution of bPEI (0.1 M, 5 mL) was heated up to 90 °C followed by a quick addition of AgNO<sub>3</sub> (0.15 M, 5 mL). The reaction mixture was stirred continuously at 90 °C for 1 h, resulting in a change of color from colorless to yellow and then dark brown. The bPEI-capped AgNPs were cooled down to room temperature, purified by centrifugal washing (3×, 16,000 *g* for 30 min), and dispersed in water (**Scheme 3.2**). The UV-Vis spectra of the resulted particles displayed a peak around 415 nm indicating the formation of AgNPs.<sup>228</sup> The nanoparticles were stored in dark at 4 °C for further use. The Ag NCs were synthesized at 70 °C, and the absorption peaks at 268 and 354 nm due to Ag NCs were disappeared upon further increasing the temperature and a new absorption peak emerged at 400 nm (surface plasmon resonance), which corresponds to silver nanoparticles.



**Scheme 3.2** A general schematic route for the synthesis of AgPEI NPs by chemical reduction method and their purification by precipitation method.

### 3.3.3. Synthesis of bPEI– Ag NCs based Empty and Drug Loaded Nanocapsules

A total of 50  $\mu\text{L}$  peppermint oil, SDS (50  $\mu\text{L}$ , 70mg/ mL) and 14  $\mu\text{L}$  of PEI- Ag NCs (37  $\mu\text{M}$ ) was added in 890  $\mu\text{L}$  of a water and agitated by an amalgamator at 5000 rpm for 100 s to form an emulsion. 1 mL of emulsion was added in 4 mL of deionized water and incubated for 10 min to afford nanocapsules (Ag-NCps). Similarly, levofloxacin loaded nanocapsules (L-Ag-NCps) were prepared by using 50  $\mu\text{L}$  of peppermint oil drug solution (10mg/1mL) instead of peppermint alone. These nanocapsules were lyophilized for further characterization and activity (**Scheme 3.3**).



**Scheme 3.3** A general schematic route for the synthesis of AgPEI NCs based empty (E-Ag NCps) and levofloxacin-loaded nanocapsules (L-Ag NCps) by emulsion dispersion method and their purification by lyophilization.

### 3.4. Physical Characterization of Nanomaterials

A UV–visible spectrophotometer (Shimadzu; UV-1800) was used to measure UV–visible absorption spectra of nanomaterials and drug loading efficiency of nanocapsules in the wavelength range of 200–800 nm. Fluorescence measurements of nanoclusters were carried out using a fluorescence spectrophotometer coupled with a multiplate reader (PerkinElmer; Enspire 2300). The thermogravimetric analysis (TGA) were conducted using a Shimadzu DTG-60AH analyzer to quantify organic ligand grafted on the nanoparticle surfaces. The dynamic light scattering (DLS) measurements of nanomaterials were conducted to confirm their size and stability using a Zetasizer system (Malvern, Nano ZSP) at room temperature (25 °C) with folded capillary zeta cells, and were recorded with Zeta software 7.03. The concentrations of silver in nanomaterials was determined using inductively coupled plasma optical emission spectroscopy (ICP-OES) (iCAP 6000 Series, Thermo Scientific). Transmission electron microscopic analysis was performed using a JEOL 7C transmission electron microscope

operating at 80 keV. The interaction of bacteria with Ag NCs at different time intervals was studied using a field-emission scanning electron microscope (FEI; Nova Nano SEM-450) equipped with a STEM detector operating at 10 kV. In chapter 5, the interactions between nanoparticles and bacterial amyloid protein (FapC) was studied via transmission electron microscopy (TEM, aggregate morphology assessment), energy-dispersive X-ray spectroscopy (EDAX, for elemental analysis), high-angle annular darkfield (HAADF) imaging (for elemental imaging and analysis), and circular dichroism (CD) spectroscopy (for analyzing secondary structure of protein). In addition, TEM, helium ion microscopy (HIM) and fluorescence microscopy was used for more detailed study of *P. aeruginosa* (PAO1) biofilm architecture.

### **3.5. Brief Explanation of Principles Behind Used Physical Techniques and Methods**

#### **3.5.1. UV-Visible Spectroscopy**

This technique was employed here:-

1. To confirm nanocluster/ nanoparticle synthesis by peak location ( $\lambda_{\max}$ ) and number of peaks.
2. To estimate drug loaded into nanocapsules using drug as standard.
3. To check optical density of bacteria which was used to estimate their concentration.

Silver nanoparticles show prominent surface plasmon peak at 400-500 nm as mentioned in Chapter 5, which shift towards longer/shorter wavelength with increase/decrease in size. The formation of silver nanoclusters were confirmed by the appearance of cluster of peaks in lower UV region along with the absence of surface plasmon peak.<sup>229</sup> This response changes with variation in size, shape and dispersity of nanoparticles.<sup>230, 231</sup> In Chapter 6, the concentration of corresponding drug loaded into nanocapsules was estimated by comparing absorbance at  $\lambda_{\max}$  of control drug i.e. levofloxacin. Similarly, optical density (OD) is the measurement of time taken by light of specific wavelength, in this case 600 nm, as it is safe for bacterial cells, to pass through sample. It is used in this thesis to estimate concentration of bacterial culture in all *in-vitro* bacterial analysis.

### **3.5.2. Zetasizer**

Hydrodynamic diameter is the size of a particle in solution state including surface functionalization or coatings. The measurement of hydrodynamic size and zeta potential is quite useful to determine overall size of nanomaterials (including the surface coating and surface bound solvent molecules on nanoparticles in solution) and surface potential for many biological applications including the development of nanomedicine where nanoparticles are required to interact physiologically with proteins.<sup>232</sup> A very dilute (PDI<0.5) and clean/filtered solution of silver nanoclusters, silver nanoparticles and nanocapsules was used to measure their size and zeta-potential in a folded capillary cell.

### **3.5.3. Thermogravimetric Analysis**

This technique is generally used to analyze the purity of sample and to quantify organic coating (in this case bPEI) grafted on the nanoparticle surfaces.<sup>233</sup> For this purpose, 100  $\mu$ L solutions of AgNCs or AgNPs were placed on a platinum pan. The samples were kept at 80 °C for 30 min to remove water and then the weight losses were measured from 80 to 700 °C at a rate of 10 °C/min under inert atmosphere of nitrogen. The measurements were conducted using a Shimadzu DTG-60AH analyzer.

### **3.5.4. Inductively Coupled Plasma Optical Emission Spectroscopy**

Inductively coupled plasma optical emission spectroscopy (ICP-OES) is an analytical technique used for elemental detection and quantification. The plasma is used as an ionization source, which is generated by flowing high frequency alternating current in induction coils surrounding quartz torch filled with argon. The resulting alternating magnetic field generates ignition in torch and initiates ionization of argon gas. These charged particles move in circular patterns under the influence of magnetic field, resulting in increased collisions with neutral atoms and generate stable plasma of about 6000-7000 K. The sample is injected by peristaltic pump into the spray chamber through a nebulizer. In this chamber, samples undergo atomization and ionization. The electrons undergo many excitations in these samples due to high temperature and then relax to give characteristic emissions. These emissions are recorded as emission spectrum through spectrometers. The emitted light is

passed through optical chamber, where it is separated into specific wavelengths. Finally, the intensities of all wavelengths are measured through detectors. The concentration of Ag in AgNCs and AgNPs was determined using inductively coupled plasma optical emission spectroscopy (ICP-OES) (iCAP 6000 Series, Thermo Scientific). The samples (1 mL) were digested by adding 9 mL of HNO<sub>3</sub> (68%) and heating at 190, 150 and 100 °C (30 min at each step). The dried layer was reconstituted in 1 mL (4%) HNO<sub>3</sub> and analyzed by ICP-OES. The corresponding concentration of Ag in AgNCs and Ag NPs is 8.95 µg/mL and 0.034 µg/mL.

### **3.5.5. Transmission Electron Microscopy and Scanning Transmission Electron Microscopy**

Transmission electron microscopy is a microscopic technique, which uses high voltage electrons beam to pass through the sample and observe size and morphology of the nanoparticles, and also to analyse their interaction with the bacterial cells. Scanning transmission electron microscope (STEM) is a combination of TEM and SEM technique. It enables simultaneous measurement of secondary electrons, scattered electrons, characteristic X-rays and transmitted electrons. This makes STEM suitable for annular dark field imaging and energy dispersive X-ray mapping (EDX). One of the modification of dark field STEM is high-angle annular dark field imaging (HAADF). It gives high contrast images with good resolution.

The sample used for TEM needs proper preparation. The dilute solution of nanomaterials were analyzed by preparing sample grid by placing a 5 µL drop of each sample on a glow-discharged copper grid and then blotting it off after 1 min. The grid was negatively stained for 30 s with uranyl acetate (1%) and excess stain was blotted off. The prepared grid was air dried and imaged by TEM using an FEI Tecnai F20 microscope operated at 200 kV. Similarly in chapter 5, FapC was incubated with AgNCs or AgNPs at the same molar ratios as for the ThT assay and incubated for 120 h to analyse their interaction with TEM.

The TEM samples of treated and untreated bacterial cells in chapter 5, were prepared by incubating the cells with nanoparticles for 24 h, and washing them via repeated centrifugation. The grid was prepared by using 5 µL of each sample as described for the nanoparticles. This was done to see the clear effect of nanoparticles on morphology of bacterial cells and their biofilms.

### **3.5.6. Scanning Electron Microscopy**

The samples for SEM were prepared by placing a drop of a clean and dilute solution of nanoclusters/nanoparticles/nanocapsules incubated with bacteria on carbon coated copper grids, followed by air-drying. The bacteria on copper grids were then fixed using 2.5% solution of glutaraldehyde (prepared in normal saline), followed by subsequent dehydration using a series of acetone dilutions, i.e., 30, 50, 70, 80, 90, and 100% for 10 min each.<sup>234</sup> The obtained SEM micrographs gives illustration of the interaction of silver nanomaterials with bacterial cells.

### **3.5.7. Energy-Dispersive X-ray Spectroscopy**

Energy-dispersive X-ray spectroscopy (EDX) uses basic phenomena of X-ray emission. After radiating the sample with electron beam, the emitted X-rays are used for the composition analysis of samples.<sup>235</sup> The similarly prepared copper grid for TEM was used to image EDX mapping spectra for silver nanomaterials with an FEI Tecnai F20 microscope. The spectra show characteristic peaks for Ag and Cu (grid), with no impurity.

### **3.5.8. Helium Ion Microscopy (HIM)**

Helium ion microscope uses helium ion beam as a source of illumination. The mass of He is  $\sim 10^4$  times more than that of electron, and at the same voltage its wavelength is 100 times shorter. This property of He is used in HIM to acquire images with high-resolution using low energy beams.<sup>31</sup> Helium ion microscopy (HIM) was performed to image the surface morphology of fixed bacterial cells and their biofilms. Briefly, bacterial cells were treated with the nanoparticles for 24 h and then fixed by adding 200  $\mu$ L of 2.5% paraformaldehyde. The bacterial cells were washed thrice via centrifugal washing and resuspended in PBS (0.1 M, pH 7.4). The bacterial cells were placed on poly-L-lysine-treated glass slides and incubated for 1 h. The slides were washed with excess DI water and then dehydrated with gradually increasing concentration of ethanol, i.e., 10, 20, 30, 50, 70, 90, 100 and 100% with 30 min incubation at each step. The slides were dried and imaged under HIM (Orion NanoFab, Zeiss, USA).

### **3.5.9. Fluorescence Microscopy**

Fluorescence microscopy is the type of optical microscopy and is used to image fluorescent samples or the samples labeled with fluorescent dyes (fluorophore). In chapter 5, a fluorescent strain of *P. aeruginosa* (AH298-GFP) was employed to visualize the biofilm formation and viability of bacteria treated with AgNPs and AgNCs, respectively. After 24 h incubation of the bacteria with 1  $\mu$ M of the nanoparticles (with respect to Ag content), 5  $\mu$ L (100  $\mu$ M) of ThT dye was added to the culture and incubated for another 10 min. Excess ThT dye was removed by centrifugal washing (5,000 *g* for 5 min, thrice) and bacterial cells were suspended in PBS (0.1 M, pH 7.4). 10  $\mu$ L of this bacterial suspension was placed on poly-L-lysine-coated cover slips and imaged under the GFP channel of a fluorescence microscope (Nikon, Eclipse Ti).

### **3.5.10. Hyperspectral Imaging**

Hyperspectral imaging (HSI) was performed to detect the surface plasmon resonance (SPR) spectra of AgNPs in AgNPs-treated bacteria. For this, bacterial cells were incubated with AgNPs for 24 h and then 10  $\mu$ L of the culture was placed on a poly-L-lysine-coated glass slide, covered with a coverslip and imaged under an HSI dark field microscope (CytoViva) attached with a PixelFly CCD camera. Images were processed via ENVI 4.8 software. AgNPs alone were used as a control and a spectral library generated from AgNPs was averaged to single mean spectra and scanned against AgNPs-treated bacterial samples. No scattering spectra were observed from untreated bacterial control.<sup>236</sup>

### **3.5.11. ThT Kinetic Assay**

ThT kinetic assay involves the use of benzothiazole salt to picture and quantify the existence of protein aggregates in bacterial biofilms termed as amyloids. Thioflavin T (ThT) consists of a benzathiole and a benzylamine ring linked through a C-C bond. When ThT is excited at 440 nm, the free rotation of rings result in quenching of excited state. However, when they are in connection to amyloids, they show characteristic emission at 485 nm due to the immobilization of rings.

A ThT kinetic assay is described in chapter 5 and was performed by preparing a 50  $\mu$ L aqueous solution containing 75  $\mu$ M ThT and 50  $\mu$ M of FapC, in the presence or absence of AgNCs or AgNPs (1  $\mu$ M), in a 96-well plate. The plates were incubated at 37 °C for 120 h without agitation and ThT fluorescence (excitation: 440 nm/emission: 485 nm) was recorded at different time points. ThT kinetic parameters of rate of fibrillization ( $k$ ), time to reach half of the saturation point ( $T_{1/2}$ ) and lag time were calculated as described.<sup>237</sup>

### **3.5.12. Circular Dichroism Spectroscopy**

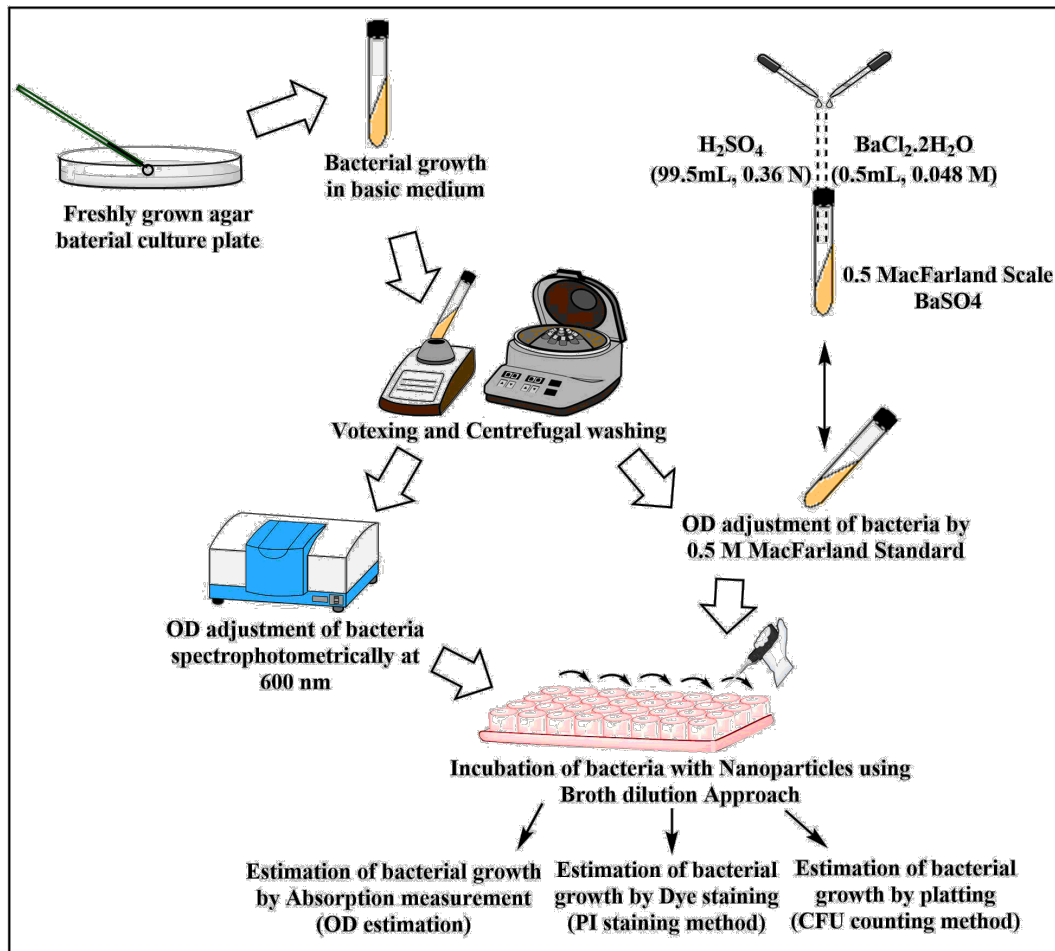
The CD spectroscopy was used in this study for secondary structure ( $\alpha$ -helix,  $\beta$ -sheets,  $\beta$ -turns, random coils) elucidation of Fap C protein in chapter 5. The peptide bonds backbone of proteins usually absorb in far-UV region (180-250 nm). They mostly show two absorption bands including high intensity  $\pi$  to  $\pi^*$  transitions at  $\sim$ 190 nm and low intensity  $n$  to  $\pi^*$  transitions at  $\sim$ 210 nm. To determine the secondary structure of FapC monomers, fibrils and FapC fibrillated with or without AgNCs/AgNPs, 200  $\mu$ L of each sample, same as for the ThT assay, was transferred into a CD cuvette. CD spectra were recorded from 190-240 nm, with a 1 nm step size. The data were deconvoluted and percentage secondary structures were obtained by Dichroweb.<sup>238</sup>

### **3.5.13. Antibacterial Studies**

Planktonic bacteria are a form of bacteria, which cause disease in human beings; they also contaminate medical devices and food items. The silver nanoparticles/nanoclusters were used to destroy these planktonic bacteria, together with multidrug resistant strains. The methods commonly used for assessing the antibacterial action of nanoparticles comprise of minimum inhibitory concentration (MIC), minimum bactericidal concentration (MBC), broth dilution assay, colony-forming unit (CFU) quantification and live/dead assay. The standard protocol is generally modified by changing the culture media, temperature, treatment periods and bacterial counts in different studies for the optimization of a variety of nanoparticles against different bacterial strains.<sup>239</sup> MIC value is marked as the lowermost concentration of the antibacterial agent (nanoparticles/nanoclusters/antibiotics) that

prevents the visible growth of the tested bacteria, and it is generally expressed in mg/L or  $\mu\text{g/mL}$ . The antibacterial activity increases with the decrease in MIC.<sup>239</sup>

Serial dilution approach is the most suitable one for the estimation of MIC. The simplest antibacterial vulnerability testing approach is broth micro-dilution method.<sup>241</sup> This method was used in this study to quantitatively measure the concentration of nanoparticles needed as an antibacterial agent against bacteria in the broth medium. It is well recognized that the kind of growth medium, the inoculum preparation technique, size of inoculum and the incubation time can impact MIC values. This approach allows the bioassay to be executed as a standardized methodology in order to value clinical relevance of these results. This process involves making two-fold dilutions of the nanoparticles in a growth medium distributed in a 96-well microtitre plate. Then, each well is inoculated with bacterial culture of specific  $\text{OD}_{600}$  prepared in the similar medium. After mixing well, the inoculated plate is incubated under appropriate conditions depending upon the nanoparticles nature and bacterial type. The key advantages of the micro-dilution approach are the reproducibility and the miniaturization of the test that favors economy in context of reagents and space. For the estimation of MIC endpoint, inspecting devices can support reading micro-dilution plate and recording outcomes with high aptitude to determine bacterial growth in the wells (**Scheme 3.4**).<sup>241</sup>



**Scheme 3.4** A schematic illustration of various steps involved in antibacterial study including culturing, purification, inoculation and estimation of bacteria.

For this purpose, as described in Chapter 4, different bacterial strains were grown overnight in the lysogeny broth and their optical density (OD) was measured at 600 nm after washing them with PBS to separate viable bacteria. A solution of bPEI–Ag NC was prepared in eight different concentrations ranging from 16–0.03 nM by serial dilution method.<sup>20</sup> The Ag NCs were incubated with  $5 \times 10^5$  cfu/mL bacteria (Table 4.1) for 16 h in an incubator at 37°C on shaking platform maintained at 275 rpm. The media and bacteria without bPEI–Ag NCs were employed as negative and positive controls, respectively. Finally, after 16 h, the OD<sub>600</sub> was measured again to check the concentration of living bacteria.<sup>242</sup>

Furthermore, numerous colorimetric procedures based on the use of different dyes have been established. Tetrazolium salts, 2,3-bis {2-methoxy-4-nitro-5-[(sulfenylamino) carbonyl]-2H-tetrazolium-hydroxide} (XTT) and 3-(4,5-dimethylthiazol-2-yl)-2,5-

diphenyltetrazolium bromide (MTT) are frequently used for the detection of MIC endpoints in antibacterial micro-dilution assays. To detect bacterial viability after 16 hour incubation, the flow cytometry technique was used. Briefly bacteria were mixed with, double stains containing propidium iodide (PI), an intercalating agent and a fluorescent dye. The experiment works on the following principal where, live bacteria with intact cell membranes will only be stained with FITC- the green fluorescent dye. The dye is small and is freely diffusible through the bacterial membrane. Propidium iodide which is an intercalating reagent will only get inside the cell if the membranes are already compromised. Binding of Propidium iodide will stain the DNA red. Dead or dying cells will stain bright red due to significant influx of Propidium iodide whereas cells that are intermediate will stain orange indicating some retention of FITC along with PI. Cells staining green are alive cells where the membranes are intact enough to keep the propidium out of the cell. In this perspective in Chapter 5, *P. aeruginosa* (wild-type reference strain PAO1) was freshly subcultured onto cation-adjusted Mueller-Hinton agar (CAMHA, containing 25 mg/L Ca<sup>2+</sup> and 12.5 mg/L Mg<sup>2+</sup>) and incubated at 35 °C for 24 h. Random colonies (2-3) were selected and grown in 10 mL cation-adjusted Mueller-Hinton broth (CAMHB, containing 25 mg/L Ca<sup>2+</sup> and 12.5 mg/L Mg<sup>2+</sup>) overnight, from which early-log-phase growth was obtained. The OD<sub>600</sub> of the culture was adjusted to 0.5 MacFarland standard and 100 µL of the bacterial suspension was mixed with 100 µL of different concentrations of AgNPs or AgNCs (prepared by dilutions in CAMHB) and incubated for 24 h at 35 °C. A bacterial viability assay was performed by propidium iodide (PI) staining. Briefly, 1 µL of 2 mg/mL PI solution was added to each well and incubated for 20 min. Excess dye was removed by centrifugal washing at 5,000 g for 5 min and bacterial cells were resuspended in phosphate-buffered saline (PBS, 0.1 M, pH 7.4). Fluorescence corresponding to the PI-stained dead cells was recorded by excitation at 535 nm and emission at 617 nm. The percentage dead cells were recorded relative to the positive (0.1% Triton X 100) and negative (untreated) controls.<sup>243</sup>

The minimum bactericidal count (MBC) is marked as the lowermost concentration of nanoparticles required to destroy 99.9% of the final bacterial inoculum. The MBC can be calculated after running broth micro-dilution assay by sub-culturing some sample from wells,

and producing negative bacterial growth after 24 h incubation on the non-selective agar plates to estimate the number of viable bacterial cells (CFU/mL). In Chapter 6, different pneumococcal strains were inoculated in 5 mL tube in THY medium and grown to  $OD_{600}$  0.2 (stationary phase) at 37°C. These cultures were then collected by centrifugation (5000 g, 4 min) and washed thrice with PBS and finally suspended in 15 mL of THY to get stock solution. 50  $\mu$ L of diluted culture was pipetted out in each well in 96 well plate and incubated with different concentrations of nanocapsules (L-Ag-NCps, E-Ag-NCps and drug). Further, 30  $\mu$ L of THY was added as a media in all dilutions. The plate was incubated at 37°C for 2 h in triplicates; however, similar experiment was repeated twice on separate days. After incubation, all of the samples were further diluted 10 folds to calculate CFU by plating. Finally, plated NCps concentration ranged from 13 nM to 128 nM. All these steps were used to calculate MBC for respective samples.

#### **3.5.14. Antibiofilm Assay**

In addition to planktonic bacteria, biofilm formation also play a vital role in letting down clinical therapeutic treatment. Biofilms are bacterial aggregates enclosed in extracellular polymeric matrix, and are communal adaptations opted by most of the bacterial varieties in pathological and natural habitats. They provide a defensive system leading to the existence of microorganisms in harsh situations. Biofilms are responsible for considerable increase in drug resistance among bacteria and biofilm-related toxicities are also hard to treat.

In chapter 5, biofilm formation was assessed by crystal violet assay. Briefly, 100  $\mu$ L of bacterial suspension ( $OD_{600}$  adjusted to 0.5 MacFarland standard) was incubated at 35 °C with 100  $\mu$ L of different concentrations (1-0.03125  $\mu$ M) of AgNPs or AgNCs. The medium was gently removed after 24 h and the wells were washed with PBS (0.1 M, pH 7.4) thrice. The microplates were air dried and then biofilms were stained with crystal violet (0.1%, 200  $\mu$ L) for 15 min. Excess crystal violet dye was removed and the wells were washed again with PBS (0.1 M, pH 7.4) to remove traces of unbound dye. The biofilms stained with crystal violet were dissolved in acetic acid (200  $\mu$ L, 33%) and transferred to new microplates. The absorbance was recorded at 595 nm, corresponding to the crystal violet-stained biofilms.

Percentage biofilm formation was calculated relative to the positive and negative controls, similar to the viability assay.

### **3.5.15. *In-vitro* Cytotoxicity**

Cytotoxicity is an essential safety parameter to assess the practical usage of nanomaterials. There are numerous possible methods to expose AgNPs to individuals like dermal application, blood circulation (intravenous inoculation), inhalation (respiratory tract exposure), oral administration (gastrointestinal tract exposure), etc.<sup>244</sup> All of these routes ultimately lead silver nanoparticles to blood circulation, which resulted in their accumulation in various organs like liver, kidney, lungs, and brain etc. Cell viability assessment is the most frequently used technique to estimate the toxicity profile of Ag NPs/NCs.<sup>245</sup> Usually, the ratio of dead cells is related directly to the cellular toxicity of nanoparticles. In general, these tests use chemicals and are related to differential exclusion, inclusion, or conversion of dye or dye precursors, which can be converted enzymatically to visible colour of dye in viable cells. In chapters 4 and 5, cytotoxicity potential of Ag NCs and Ag NPs were estimated by assays alamarBlue and live/dead cells assays. The Alamar blue assay (resazurin), a fluorometric indicator of cellular metabolic activity, involves the reduction of resazurin form to resorufin using mitochondrial enzymes, like NADPH dehydrogenase. Resazurin is blue in color and is non-fluorescent molecule while resorufin is red and highly fluorescent molecule. The corresponding fluorescence of these components can be observed at 560/ 590 nm excitation/ emission wavelengths to estimate cell viability.<sup>246, 247</sup>

In Chapter 5, live/dead assay is used for the estimation of cell viability similar to the previous bacterial viability protocol. Human embryonic kidney 293 (HEK 293 from ATCC) cells were cultured in complete Dulbecco's modified Eagle's medium (DMEM) with 15% fetal bovine serum (FBS) to estimate cellular viability. For this assay, poly-L-lysine (70  $\mu$ L) was coated on a costar black/clear bottom 96 well plate, incubated for 30 min at 37 °C and washed with DI water. 200  $\mu$ L of the cells (density: 10,000 cells) were added to the wells. The cells were incubated at 37 °C for 24 h to attain 70-80% confluency. After replenishing the media, 1  $\mu$ M propidium iodide (PI) dye, dissolved in DMEM, was added to the wells and incubated for 30 min. Samples of 25  $\mu$ M FapC and 5  $\mu$ M AgNCs or AgNPs (200  $\mu$ L) were added into the wells.

All samples were observed in triplicate in two repeats and estimated in a live cell chamber (5% CO<sub>2</sub>, 37 °C) by Operetta (PerkinElmer, microscope objective: 20× PlanApo; numerical aperture: 0.7) after 14 h of treatment. The ratio of dead to total cell count was calculated by a built-in function, bright-field mapping of Harmony High-Content Imaging and Analysis software. The measurement was performed at 5 reads/well. Untreated cells were used as the control.

Nanoparticles are ultimately expected to come into systemic circulation and possibly interact with circulatory components like blood vessels, blood cells, and the heart.<sup>248</sup> In chapter 4, the compatibility of Ag PEI NCs was tested against human erythrocytes. Citrate-stabilized human whole blood (pooled, mixed gender) was purchased from Bioreclamation LLC, NY, and immediately processed. For this purpose, 10 mL of phosphate-buffered saline (PBS) was added to the blood (2 mL) and centrifuged at 5000 rpm for 5 min. The supernatant was carefully discarded, the red blood cells (RBCs) were dispersed in 10 mL of PBS, and the solution was kept on ice during the procedure. The RBC solution (0.1 mL) was added to 0.4 mL of the bPEI–Ag NC solution in PBS in a 1.5 mL centrifuge tube (Fisher) and mixed gently by pipetting. RBCs incubated with PBS and water were used as negative and positive controls, respectively. All bPEI–Ag NC samples as well as controls were prepared in triplicate. The mixture was incubated at 37 °C for 30 min with gentle shaking at 150 rpm. After incubation, the solution was centrifuged at 4000 rpm for 5 min and 100 µL of the supernatant was transferred to a 96-well plate. The absorbance of the supernatant was measured at 570 nm using a microplate reader (Spectra Max M2, Molecular Devices) with absorbance at 655 nm as a reference.<sup>249</sup>

### **3.5.16. Reactive Oxygen Species Generation Study**

Reactive oxygen species (ROS) are the usual byproducts of metabolism produced by respiring organisms. Although slight changes in ROS levels can be adjusted by cells natural antioxidant defenses such as glutathione/glutathione disulfide ratio (GSH/GSSG), surplus ROS production possibly lead to oxidative stress. These extra free radicals can target membrane lipids and initiate membrane breakdown, DNA damage and also affect mitochondrial functioning. Metals like Ag behave as catalysts and produce ROS in the

presence of dissolved oxygen. In this perspective, silver nanoparticles can also catalyze reactions using oxygen producing surplus free radicals. Carlson et al. suggested that silver nanoparticles in eukaryotic cells may hinder the antioxidant security system by directly interacting with GSH, connecting GSH reductase or affecting other GSH conservation enzymes. All this could possibly bring drop in GSH/GSSG levels and, consequently, upsurge ROS cellular levels.<sup>250</sup>

In this perspective, ROS generation study was done against different *bacterial* cells using 2,7-dichlorofluorescein diacetate (DCFH-DA) or resazurin assay. For this purpose, bacterial cells were grown to a specific OD<sub>600</sub> and incubated with Ag NPs, Ag NCs and controls for specific duration. The culture was then washed and their absorbance/ fluorescence was recorded at specific wavelength.

### **3.5.17. Discrete Molecular Dynamics Simulations**

In Chapter 5, discrete molecular dynamics (DMD) simulations was done for studying molecular details of bacterial amyloid protein (FapC) and nanoparticles binding. Discrete Molecular Dynamics is a rapid and predictive molecular dynamics algorithm, which has been used to study protein aggregation and nano-bio interface and detailed description of the DMD algorithm can be found elsewhere.<sup>236, 251-254</sup>

Based on previous study, an AgNC comprising 38 silver atoms was reconstructed with a diameter of  $\approx 1$  nm.<sup>255</sup> The Ag (111) surface with five layers of atoms was used to approximate the relatively flat surface of an AgNP with a much larger radius. Each layer comprised of 648 silver atoms with a dimension of  $\approx 7.0 \times 6.8$  nm<sup>2</sup>. To model the bPEI molecule, a generation-3 PEI dendrimer was started with.<sup>254</sup> Based on previous study, terminal ethylenimine groups were randomly deleted iteratively until reaching the MW of  $\approx 800$  Da as in the experiment. To construct the bPEI–AgNC complex, initial binding simulations of one AgNC were performed with 9 bPEI molecules at 300 K. Up to 3 bPEI molecules were found to bind the AgNC strongly. For the bPEI–AgNP complex, an initial DMD simulation started with 12 bPEI molecules covering the surface, and it was found that only 9 bPEI molecules were able to stay bound. Thus, an AgNC bound with 3 bPEI molecules and the nano-sized Ag (111) surface covered with 9 bPEI molecules approximating an AgNP were used in the further simulations.

In addition to the N-terminal signaling sequence, FapC is comprised of three homologous repeat sequences (R1-R3) separated by two linker regions (L1-L2). We used the R1L1R2L2R3 region from the FapC sequence of the *Pseudomonas* strain UK4 (175 amino acids in total) in our computational modeling. For the full-length FapC (R1L1R2L2R3), equilibrated conformations were obtained with initial relaxation simulations at room temperature starting from a fully-stretched conformation. A cubic box with the periodic boundary condition and a dimension of 12 nm was used. To ensure sufficient sampling, 10 independent simulations with different initial configurations were performed for a FapC monomer with and without the presence of a bPEI-capped AgNC. Each independent simulation lasted 350 ns at room temperature.

The two fragments i.e., L1R2 and L2R3 were used separately to model the dimerization process in FapC aggregation and evaluate the impact of the bPEI-capped AgNC on FapC aggregation. For each dimer simulation in the presence and absence of the bPEI-capped AgNC, 20 independent simulations each of 300 ns were performed. A simulation box with each dimension of 15 nm was used. The last 50 ns trajectories of all independent simulations, where the corresponding steady states were reached, were used in statistical analysis.

## Chapter 4.

# Synthesis and Characterization of Polyethylenimine Capped Silver Nanoclusters and Evaluation of their Antibacterial Activity

## 4.1. Synopsis

This chapter presents polyethylenimine stabilized silver nanoclusters (bPEI-Ag NCs) as potential candidates to target pathogenic bacteria. The 1<sup>st</sup> part covers the introduction and background of this project. The 2<sup>nd</sup> part includes the discussion of results of physical and chemical characterization, antibacterial activity, cytotoxicity study against fibroblast cells and erythrocytes, and the mechanistic study supported by SEM and live/dead assay of these nanoclusters.

## 4.2. Introduction

Pathogenic bacteria with acquired resistance are responsible for millions of infections and thousands of deaths worldwide.<sup>256</sup> The prominent clinical reason for the development of MDR bacterial strains as previously mentioned is the long-term, subtherapeutic exposure of microbes to antibiotics.<sup>257, 258</sup> Multidrug resistant “superbugs”, both Gram-positive (such as *E. faecium*) and Gram-negative (including *K. pneumoniae*, *A. baumannii*, *P. aeruginosa*, and *Enterobacter*) species, lead to serious community health hazards. In the United States alone, annually 2 million patients are victimized by hospital-acquired infections with 99 000 annual deaths, causing economic burden of \$35 billion a year.<sup>259, 260</sup> Significantly, ~60% of nosocomial (hospital-related) infections in the United States are caused by multidrug resistance (MDR) bacteria.<sup>261, 262</sup> Recently, in developing countries like Pakistan, 71% infections of newborn babies are caused by MDR bacteria. Initially, the development of new antibiotics and antibiotic combinations was sufficient to address different pathways of resistance simultaneously.<sup>259, 260</sup> However these strategies are changing the pattern of antibacterial resistance in a predictable manner, resulting in the loss of efficacy of current clinical treatments.<sup>263</sup> This continuous rise of multiple-antibiotic-resistant bacterial strains

drives the search for new antimicrobial agents and methods to control the growth of MDR bacterial strains. The eventual goal of this study was to develop cost-effective, potent, safe, readily available, and easily synthesized alternatives to the conventional antibiotics that are increasingly becoming ineffective against MDR pathogens.<sup>264-266</sup>

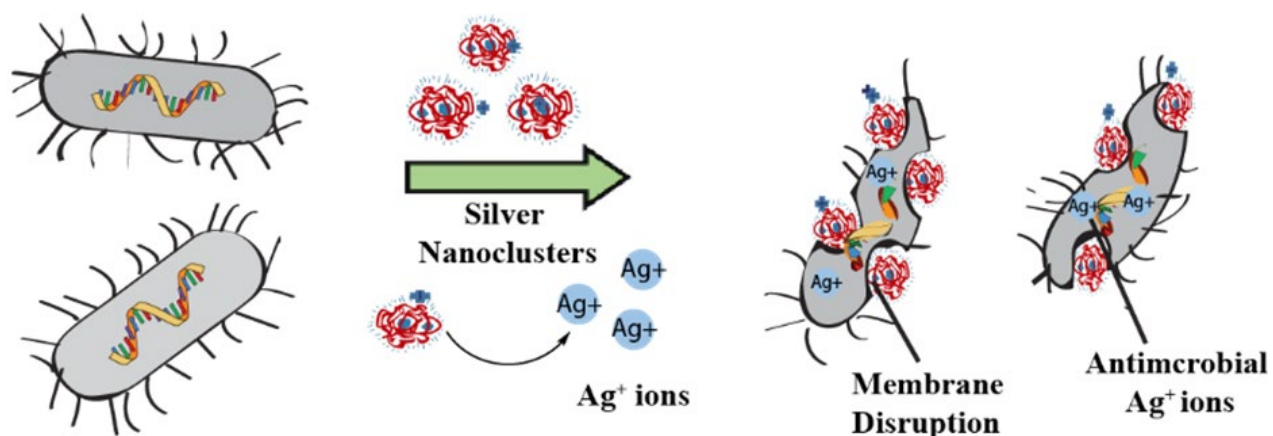
Targeting bacterial membrane using cationic, hydrophobic nanoparticles (NPs); peptidoglycan-recognizing agents; metals; and inhibitors of ATPase can provide an efficient strategy to control these superbugs.<sup>20, 267, 268</sup> Nanoparticles provide an efficient platform to target MDR bacteria owing to their high surface-to-volume ratio, facile surface modification, and controllable size.<sup>201, 269</sup> The nature of the core material, size, and surface chemistry play significant roles in the antibacterial properties of nanoparticles. The configuration of nanoclusters makes them highly reactive, which in combination with their small dimensions (comparable to the size of most active biological species e.g., DNA, proteins) can induce serious damage to the cells and microorganisms.<sup>270</sup> For example, nanoparticles have been reported to be responsible for the generation of reactive oxygen species (ROS), the depletion of intracellular ATP and the inhibition of DNA replication.<sup>258</sup> Moreover, they can interfere with respiratory enzymes in microbes and alter the membrane potential causing their death.

Metals, especially silver (Ag), have promising antimicrobial potential arising from dissolved Ag<sup>+</sup> ions that are effective against a wide range of MDR strains.<sup>271</sup> Decreasing the size of NPs improves their surface-to-volume ratio, leading to an enhancement in their dissolution and hence antimicrobial activity.<sup>272-274</sup> Surface charge is also important, with cationic nanoparticles serving as efficient self-therapeutic antimicrobial candidates that induce cellular membrane disruption.<sup>184, 275</sup> This ability to lyse bacteria with reduced mammalian cell toxicity involves the adjustment in the proportion of surface charge and hydrophobicity.<sup>184, 266, 276</sup> Increasing the biocompatibility of cationic antimicrobial agents through a rational design by encapsulating bioactive molecules using biocompatible polymers like polyamidoamine, chitosan, and branched polyethylenimine (bPEI) is an attractive research direction in this regard.<sup>277-281</sup>

bPEI is a positively charged and highly basic polymer widely used in non-viral gene delivery and therapy both *in-vivo* and *in-vitro*. Due to high cellular uptake and endosomal escape, it

shows good transfection efficiency.<sup>282</sup> Higher toxicity of high molecular weight bPEI (HMW bPEI) limits its applications, whereas lower molecular weight bPEI (LMW bPEI) shows less toxicity but poor transfection ability as well. Furthermore, LMW bPEI shows enhanced cellular uptake and transfection ability but reduced cytotoxicity, when it is conjugated to inorganic carriers i.e., silica, iron oxide, and gold etc.<sup>283</sup> Combinations of antimicrobials can synergistically increase the therapeutic efficacy.<sup>284</sup>

We, therefore, set out to use a combination of PEI and silver in the form of silver nanoclusters (Ag NCs) to target MDR bacteria (**Figure 4.1**).<sup>282</sup> In this work, we synthesized blue fluorescent cationic silver nanoclusters coated with low molecular weight bPEI (bPEI–Ag NCs) and characterized these polymer-coated nanoclusters using optical measurements and electron microscopic techniques. The prepared nanoclusters demonstrated pronounced antibacterial activity against 12 multidrug uropathogenic (pathogens associated with urinary tract infections) strains of bacteria. Scanning electron microscopy (SEM) imaging showed that bPEI–Ag NCs target bacteria through the membrane disruption mechanism. Significantly, these silver nanoclusters exhibited minimal hemolysis toward red blood cells and low toxicity against mammalian cells at doses lethal to the bacteria, making them promising therapeutics for bacterial infections.

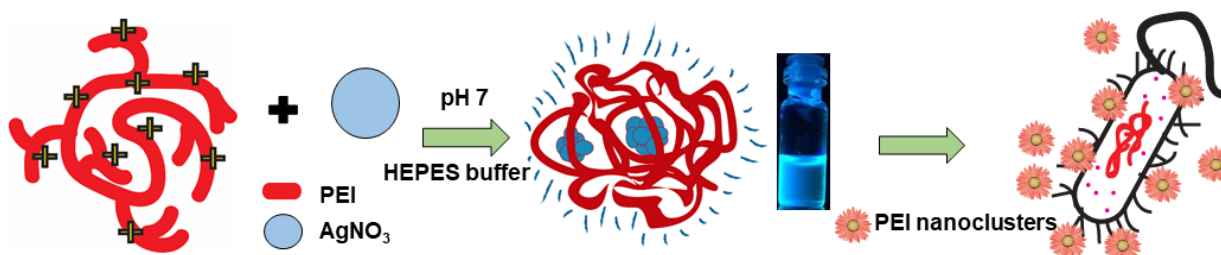


**TOC 4.1** Table of content presenting the pictorial view of bacterial cell targeting with bPEI-Ag NCs.

## 4.3. Results and Discussion

### 4.3.1. Synthesis and Characterization of bPEI–Ag NCs

The bPEI–Ag NCs were synthesized through a one-pot, single-step chemical reduction method (**Scheme 4.1**).



**Scheme 4.1** A general scheme presenting the synthesis of blue fluorescent branched polyethylenimine-coated Ag NCs (bPEI–Ag NCs) by chemical reduction method and their potential bactericidal action.

These silver nanoclusters were further characterized for their absorption and photoluminescence properties, sizes, and morphologies. The solutions of bPEI–Ag NCs were light yellow under visible light and displayed blue fluorescence under UV illumination at 365 nm. The absorption spectrum showed two absorption bands at 268 and 354 nm (**Figure 4.1a**). The absorption peak at 354 nm corresponds to the oligomeric silver species. The absence of the surface plasmon resonance band of larger Ag NPs between 400 and 500 nm indicates the formation of smaller Ag nanoclusters.<sup>285</sup> The maximum fluorescence emission of bPEI–Ag NCs was 430 nm at an excitation wavelength of 365 nm, which confirms the synthesis of silver nanoclusters (**Figure 4.1b**).<sup>224</sup> The hydrodynamic size of these nanoclusters was found to be ~3 nm (**Figure 4.1c**) with a  $\zeta$ -potential of +30 mV showing their decent stability. High-resolution transmission electron microscopy (HRTEM) analysis revealed isotropic and spherical morphology of Ag NCs with an average core diameter of ~2 nm (**Figure 4.1d**). The amount of elemental silver in the as-made clean bPEI–Ag NC solution was determined to be 8.95  $\mu\text{g}/\text{mL}$  using inductively coupled plasma mass spectrometry and TGA.<sup>286</sup> This estimation was helpful to prepare concentrations of controls to make the antibacterial assay more reproducible.

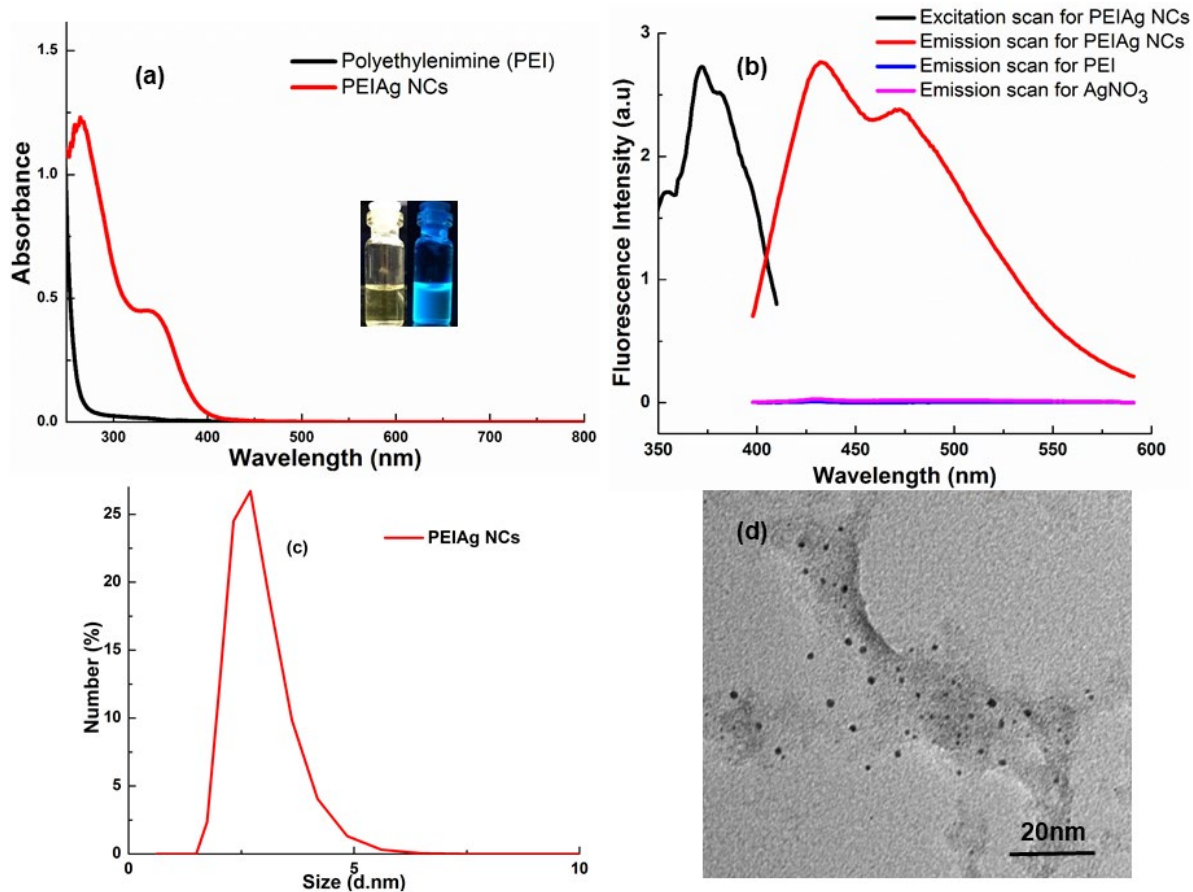


**Figure 4.1** (a) UV-visible absorption spectrum of polyethylenimine silver nanoclusters (bPEI-Ag NCs) and polyethylenimine (PEI) showing multiple absorption peaks for Ag nanoclusters compared to those for PEI, and the inset shows bPEI-Ag NCs in 4-(2-hydroxyethyl)piperazine-1ethanesulfonic acid (HEPES) buffer (pH 7.0–9.0) is yellow under visible and blue fluorescent under UV, (b) Photoluminescence spectrum of blue fluorescent bPEI-Ag NCs showing excitation at 375 nm and emission at 430 nm, (c) Dynamic light scattering (DLS) analysis showing an average hydrodynamic diameter of 3 nm, (d) TEM micrographs of bPEI-Ag NCs showing size of 2 nm.

#### 4.3.2. *In-vitro* Studies of bPEI-Ag NCs

The antibacterial activity of cationic bPEI-Ag NCs was explored against lab strains of *P. aeruginosa* (ATCC 19660, Gram-negative) and *A. azurea* (Gram-positive) and 12 uropathogenic clinical MDR isolates (**Table 4.1**). The minimum inhibitory concentration (MIC) of bPEI was 32 nM, whereas that of AgNO<sub>3</sub> was around 2–0.125 nM against different lab strains. The MIC of bPEI-coated Ag NCs was, however, found to be 2- to 3-fold better than that of AgNO<sub>3</sub> alone. bPEI-Ag NCs could selectively suppress the growth of these

pathogens, with MICs ranging from 0.25 to 0.015 nM. Functionalized bPEI–Ag NCs could inhibit the growth of resistant superbug methicillin-resistant *S. aureus* (MRSA) at a concentration as low as 0.015 nM. Similar MIC values for clinical MDR and lab strains suggested that bPEI–Ag NCs could possibly share the common mechanism of targeting bacterial resistance.<sup>287, 288</sup> The antibacterial activity of bPEI–Ag NCs can be attributed to the cationic nature of surface ligands composed of hydrophobic segments that facilitate the contact of bPEI–Ag NCs with bacterial cells that causes membrane damage, as well as the release of Ag<sup>+</sup> ions from the bPEI–Ag NCs. The increased surface area of the bPEI–Ag NCs could increase the sustained dissolution of the Ag<sup>+</sup>; a process distinctively different from a burst release of Ag<sup>+</sup> ions when directly used in the form of AgNO<sub>3</sub>.<sup>289</sup> The bactericidal activity of PEI due to its cationic nature adds to the bactericidal activity along with Ag<sup>+</sup>, resulting in the observed broad-spectrum antibacterial activity of bPEI–Ag NCs.<sup>290, 291</sup>

**Table 4.1** A table presenting MIC data of polyethylenimine silver nanoclusters (bPEI–Ag NCs)

| Sr. No. | Strain Name | Pathogenicity | Species                      | No. of resistant drugs | MIC of AgNCs (nM) | MIC of AgNO <sub>3</sub> (nM) | MIC of PEI (nM) | MDR |
|---------|-------------|---------------|------------------------------|------------------------|-------------------|-------------------------------|-----------------|-----|
| 1       | ATCC 19660  | Nonpathogenic | <i>P. aeruginosa</i>         | 0                      | 0.03              | 0.125                         | > 32            | No  |
| 2       | CD-549      | Uropathogenic | <i>E. coli</i>               | 16                     | 0.06              | 0.125                         | > 32            | Yes |
| 3       | CD-1006     | Uropathogenic | <i>P. aeruginosa</i>         | 1                      | 0.125             | 0.5                           | > 32            | No  |
| 4       | CD-2        | Uropathogenic | <i>E. coli</i>               | 1                      | 0.25              | 0.2                           | > 32            | No  |
| 5       | CD-489      | Uropathogenic | <i>S. aureus</i><br>MRSA     | 10                     | 0.015             | 0.03                          | > 32            | Yes |
| 6       | CD-23       | Uropathogenic | <i>P. aeruginosa</i>         | 13                     | 0.125             | 0.5                           | > 32            | Yes |
| 7       | N/A         | Nonpathogenic | <i>A. azurea</i>             |                        | 0.125             | 0.25                          | > 32            |     |
| 8       | CD-3        | Uropathogenic | <i>E. coli</i>               | 3                      | 0.06              | 0.25                          | > 32            | Yes |
| 9       | CD-1412     | Uropathogenic | <i>E. cloacae</i><br>complex | 4                      | 0.06              | 0.25                          | > 32            | Yes |
| 10      | CD-746      | Uropathogenic | <i>E. faecalis</i>           |                        | 0.25              | 0.5                           | > 32            | No  |
| 11      | CD-866      | Uropathogenic | <i>E. cloacae</i><br>complex | 2                      | 0.25              | 1                             | > 32            | Yes |
| 12      | CD-895      | Uropathogenic | <i>E. faecalis</i>           | 2                      | 0.06              | 0.125                         | > 32            | yes |
| 13      | CD-1578     | Uropathogenic | <i>S. aureus</i>             | 4                      | 0.06              | 0.5                           | > 32            | Yes |
| 14      | CD-14       | Uropathogenic | <i>P. aeruginosa</i>         | 7                      | 0.06              | 0.25                          | > 32            | Yes |

#### 4.3.3. Cell Viability and Haemolysis Assay

The selectivity of antimicrobial agents to bacteria as opposed to mammalian cells is essential for their therapeutic efficacy.<sup>292</sup> A total of 20000 NIH 3T3 (ATCC CRL-1658) fibroblasts were cultured in Dulbecco's modified Eagle medium (DMEM) with 10% bovine calf serum (BSA) and 1% antibiotics at 37 °C in a humidified atmosphere of 5% CO<sub>2</sub> for 48 h. Old media was removed, and cells were washed with phosphate-buffered saline (PBS) before the addition of bPEI–Ag NCs in pre-warmed 10% BSA in media. The silver nanoclusters and cells were then incubated for 24 h at 37 °C under a humidified atmosphere of 5% CO<sub>2</sub>. Cell viability was determined using the alamar blue assay following the manufacturer's protocol.<sup>293</sup> Briefly, cells washed with PBS were treated with 220 µL of 10% alamar blue in

BSA serum containing media and incubated at 37 °C under a humidified atmosphere of 5% CO<sub>2</sub> for 3 h. After incubation, 200 µL of solution from each well was transferred into a 96-well black microplate. Red epifluorescence intensity, resulting from the alamar blue solution, was measured (excitation/emission: 560/ 590 nm) using a Spectro Max M5 microplate reader (Molecular Devices) to determine the cellular viability. Cells without bPEI–Ag NCs were considered as 100% viable. Each experiment was performed in triplicate. bPEI–Ag NCs showed low dose-dependent cytotoxicity against fibroblasts. IC<sub>50</sub> for bPEI–Ag NCs against fibroblasts was 38 nM, indicating their safe therapeutic window. It can be seen from **Figure 4.2** that concentrations <25 nM are quite safe to use against these cells.

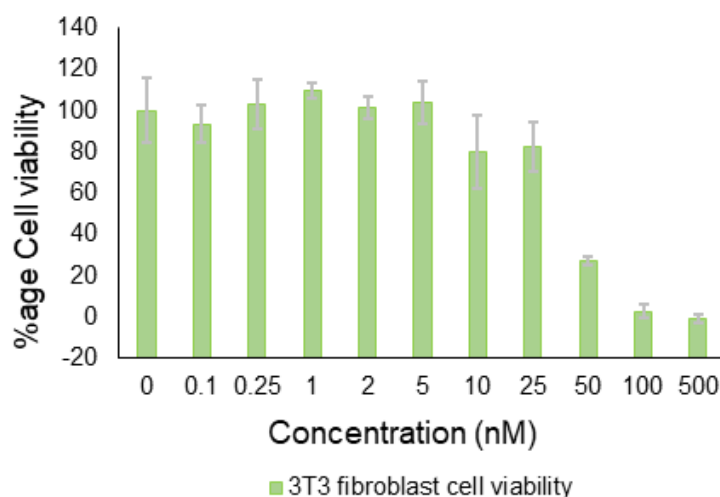


**Figure 4.2** Fibroblast cell viability test of polyethylenimine silver nanoclusters (bPEI–Ag NCs) to test their cytotoxicity against fibroblasts, which show their safe therapeutic window.

Haemolysis is a process of destruction of red blood cells, which results in escape of haemoglobin in the environment. The interaction of some materials with the erythrocyte membrane can cause its damage, which leads to the escape of haemoglobin from the cell. Consequently, when developing new pharmaceutical preparations, the test on the haemolytic activity is a necessary component, together with checking of their antibacterial activity. The wide use of a number of antibacterial preparations is limited as a result of their high haemolytic activity. Hemolysis assays were performed to examine the biocompatibility of bPEI–Ag NCs with human red blood cells, as RBCs are highly susceptible to lysis upon systemic administration of nanomedicine.<sup>286</sup> In the complete range of MIC concentrations of bPEI–Ag NCs against bacteria (0.25– 0.015 nM), silver nanoclusters showed minimal

hemolytic activity.  $HC_{50}$  i.e., the concentration of Ag NCs required to lyse 50% of RBCs, was much higher than  $\sim 500$  nM, with the resulting therapeutic index ( $HC_{50}/MIC$ )  $> 2000$  ( $500/0.25$ ). This indicates that these Ag NCs can be injected safely through blood without causing hemolysis of the RBCs. Previous studies on hemolysis by PEI and silver ions indicate that the polymer shows high hemolytic activity at therapeutically relevant concentrations, whereas bPEI–Ag NCs show minimal hemolytic activity, as shown in **Figure 4.3**, further corroborating the biocompatibility of Ag NCs.<sup>294</sup>

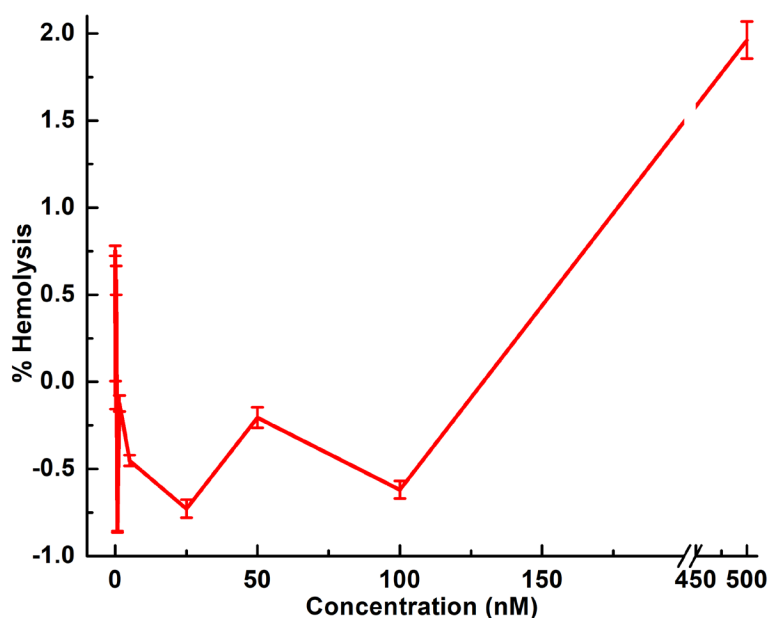


**Figure 4.3** Hemolysis study of polyethylenimine silver nanoclusters (bPEI–Ag NCs) to test their compatibility with red blood cells.

This observed high selectivity of bPEI–Ag NCs against bacterial cells may be attributed to the bacteria having more negatively charged surface than that of the mammalian cells. Moreover, mammalian cell membranes are highly stabilized because of the presence of cholesterol that makes them less vulnerable to antimicrobial metal NCs.<sup>249, 295</sup>

#### 4.3.4. Scanning Electron Micrographs

First and most readily noticeable effect on exposure of cells to any material is the change in cell shape or morphology. In order to see the interaction of bPEI–Ag NCs with the bacterial membrane; the morphology of Ag NC-treated bacteria was studied using TEM. Microscopic observation of *E. coli* cells treated with bPEI–Ag NCs clearly revealed their abnormal

morphology, whereas untreated bacterial cells as control appeared normal (**Figure 4.4a**). bPEI-Ag NC-treated cells appeared to be stressed, and membrane distortion was observed. The probable mechanism for the interaction/ penetration of bPEI-Ag NCs through the bacterial membrane is the formation of breaks called pits.<sup>282</sup> The pit formation has been observed for *E. coli* using scanning TEM (STEM) (**Figure 4.4b**).<sup>283, 289</sup> The morphology was completely changed with a total loss of integrity after 8 h (**Figure 4.4c**).<sup>293</sup> These Ag NCs act by forming a direct contact with the bacterial membrane, without penetrating deep into their cells, resulting in the failure of antibiotic resistance of bacteria, and are thus potential candidates to address serious global healthcare challenges like MDR because they might be less prone to resistance than antibiotics.<sup>296</sup>

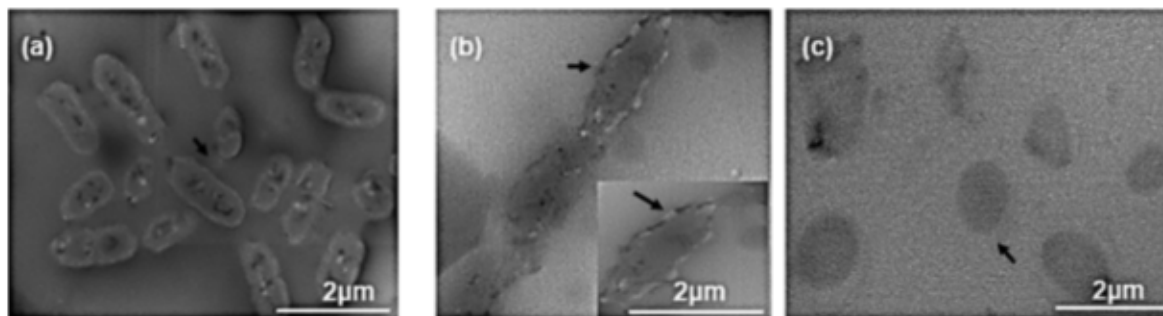


**Figure 4.4** SEM micrographs showing interaction of *E. coli* with bPEI-AgNCs at: (a) 0 h-control, (b) 4 h incubation, and (c) 8 h incubation.

#### 4.4. Conclusions

In summary, branched polyethylenimine silver nanoclusters were synthesized by a chemical reduction method and are found to be potential candidates to target MDR in various pathogenic and nonpathogenic strains of bacteria. They showed multiple-fold improved bactericidal effects compared to those of controls, which is attributed to their smaller size, surface chemistry, and cationic nature. The bPEI-Ag NCs act as broad-spectrum antibiotics by targeting bacteria using the membrane disruption mechanism with limited toxicity against mammalian and red blood cells. They have broader implications of developing nanocapsules to carry and deliver drugs against multidrug-resistant bacterial infections, in vivo, because of the combinatorial effect. These bioinorganic bPEI-Ag NCs, therefore, have the potential to provide therapeutics for antibiotic-resistant pathogens.

## Chapter 5.

# **Comparative Study of Design, Synthesis and Evaluation of Silver Nanoclusters and Nanoparticles against *P. aeruginosa* Resistant Biofilms**

## **5.1. Synopsis**

This chapter presents comparative study of polyethylenimine stabilized silver nanoclusters (bPEI-Ag NCs) and nanoparticles (bPEI-Ag NPs) as potential candidates to target *P. aeruginosa* amyloids involved in their resistant biofilm formation. The 1<sup>st</sup> part covers the introduction and background of this project. The 2<sup>nd</sup> part includes the discussion of results of the chemical and physical characterization, *in-vitro* study, *in-silico* study, antibiofilm study, cytotoxicity study against HEK cells, and the mechanistic study by TEM, HIM, HSI, fluorescence microscopy and ROS study of these nanoparticles.

## **5.2. Introduction**

Bacterial infections are a major source of human diseases and mortality, while the gut microbiota are a key constituent of the gut-brain axis implicated in the physio-pathogenesis of neurological disorders, type 2 diabetes, obesity, depression and cancer.<sup>297-301</sup> Current antibiotic strategies usually target bacterial cell wall as well as their translational and gene replication machineries, but some bacteria can evade virtually all antibiotics by enzymatic degradation, modifications to the cell wall and cellular organelles, as well as elevated expression of efflux pumps.<sup>302, 303</sup> As a result, multidrug resistance (MDR) of bacteria has become a major public health threat, and alternative strategies involving novel mechanisms are urgently needed.

### **5.2.1. Bacterial Amyloidosis**

Conventionally, amyloidosis refers to the aggregation of proteins and peptides into toxic oligomers, protofibrils and cross-beta amyloid fibrils, a hallmark of Alzheimer's disease, Parkinson's disease and type 2 diabetes.<sup>304</sup> Functional amyloidosis, in contrast, is a relatively

new concept, exemplified by melanin synthesis via Pmel-17 aggregation in the skin against UV exposure, as well as by the formation of bacterial amyloid network/biofilm.<sup>305, 306</sup> A biofilm is a multicellular community in which bacteria lives happily by releasing extracellular matrix (ECM).<sup>307</sup> Biofilms are highly stable communities of bacteria and their robustness is attributed to the encasing of an extracellular polymeric matrix.<sup>308</sup> Biofilms are responsible for 60% of healthcare associated and intensive care infections. The bacterial amyloid provides support for polysaccharides deposition to reinforce the encased community,enable cell adhesion, motility, cell-cell interaction and quorum sensing, and hinder penetration of antimicrobial agents.<sup>309-311</sup> This bacterial biofilm formation is one of the major cause of antimicrobial resistance.<sup>312-314</sup> FapC, in particular, is a main protein component of the extracellular amyloid network of *P. aeruginosa*, a Gram-negative opportunistic pathogen inhabiting plants and animals, including humans.<sup>305, 315</sup> *P. aeruginosa* has a particularly large armamentarium of resistance mechanisms and can become resistant against all currently available antibiotics (in monotherapy). Furthermore, *P. aeruginosa* strains commonly form biofilm, which makes infections by this pathogen even more challenging to treat. The aggregation of FapC into amyloid fibrils is similar to the assembly of CsgA of the curli system in the amyloid biogenesis of *E. coli*.<sup>315, 316</sup> Amyloid fibrils have many features that make them attractive targets for nanotechnology: they self-assemble from their component peptides/proteins, are incredibly strong and robust, and the physicochemical properties of the fibril core and surface can be controlled with relative ease by changing the amino acid sequence of the peptides.<sup>304</sup> FapC fibrils strengthen the bacterial biofilm mechanically, and small molecules which remodel or dissociate FapC fibrils weaken the biofilm against antibiotics and reduce biofilm formation to an extent which correlates with their ability to inhibit FapC fibrillization *in-vitro*.<sup>317-319</sup> Accordingly, controlling bacterial amyloids may entail new antimicrobial strategies.

### **5.2.2. Silver Nanoparticles: Efficient Candidates to Target Bacterial Biofilms**

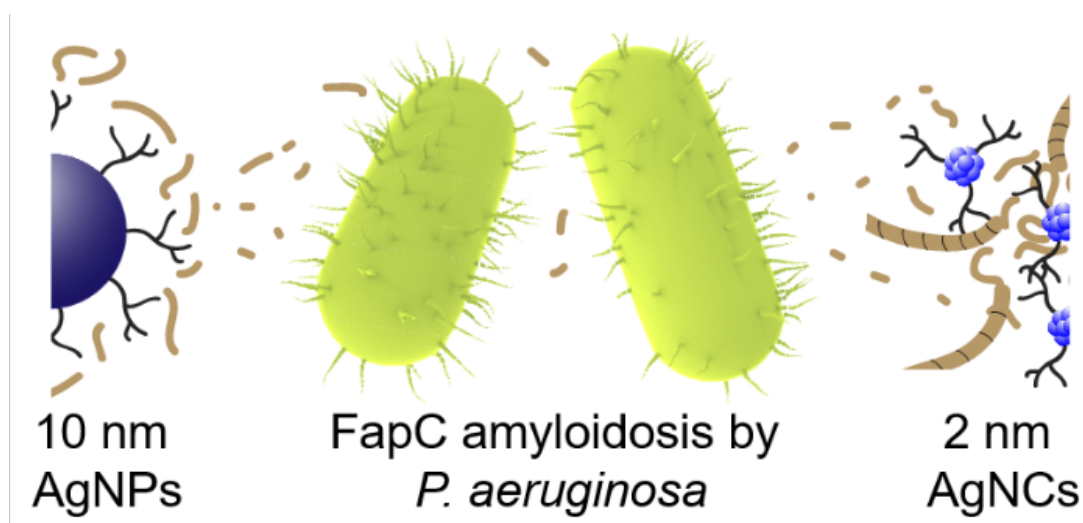
Nanotechnology offers unique advantages in bactericidal development, as the versatile and tunable physicochemical properties of nanomaterials facilitate their adsorption and penetration into bacterial membranes, biocatalysis, drug delivery and ion release. Indeed,

gold, silver and zinc oxide nanoparticles and nanoclusters are common antimicrobial agents utilizing their strong capacity in inducing membrane damage and toxic ion release.<sup>303, 320-323</sup> Recently, silver nanoclusters (AgNCs) packed with daptomycin have shown improved potency and synergy in compromising bacterial membrane integrity, eliciting DNA damage, and generating reactive oxygen species (ROS).<sup>273</sup> In another study, silver bromide nanoparticle-pyridinium polymeric composites adhered onto glass substrates and exhibited long-term biocidal properties against airborne and waterborne bacteria.<sup>324</sup> Furthermore, lanthanum hydroxide-graphene oxide nanocomposites (La@GO) conferred strong bactericidal effects on both wild-type and antibiotic-resistant *E. coli*, *L. crispatus*, *S. aureus* and *P. aeruginosa* strains.<sup>325</sup>

Within the context of amyloid inhibition, the catalytic or inhibitory effects of metal nanoparticles depend upon the surface functionalization, metal core, and size of the particles.<sup>326-328</sup> For example, gold nanoparticles (AuNPs) capped with citrate or polyethylene glycol (PEG) accelerated amyloidosis, while AuNPs coated with milk proteins inhibited the fibrillization of amyloid proteins.<sup>329-333</sup> Larger metal nanoparticles elicited a stronger inhibitory effect on amyloidosis than smaller nanoparticles of similar surface functionalization.<sup>327</sup> Silver nanoparticles (AgNPs) capped with citrate, chitosan, or natural products have also been reported to inhibit the aggregation of amyloid proteins.<sup>334-336</sup>

The surface charge and antimicrobial property of silver nanoparticles (AgNPs) often correlate. For example, cationic AgNPs are more toxic to the net negatively charged bacterial cells, as they promote membrane permeability and reduce bacterial drug efflux.<sup>337</sup> In comparison, ultra-small silver nanoclusters (AgNCs, <3 nm) can target MDR bacteria by a membrane disruption mechanism and act as a broad spectrum antimicrobial agent.<sup>338</sup> Motivated by the tremendous health implications of the gut microbiota as well as the urgent need to develop safe and potent nanobactericides against a range of human diseases, here we examined the interactions between *P. aeruginosa* biofilms and AgNPs/AgNCs from the unique perspective of FapC amyloidosis. In this study, we tried to compromise bacterial viability by weakening the bacterial biofilm through a reduction of functional amyloid formation by AgNPs/AgNCs.

While AgNPs/ AgNCs have been studied for their tremendous potential against wild-type and drug-resistant bacteria, the toxicity associated with AgNPs/AgNCs hinders their clinical implications.<sup>339-341</sup> Here, we exploited the anti-amyloid activities of AgNPs/ AgNCs at sub-bactericidal doses to inhibit biofilm formation. Our working hypothesis is that we can compromise bacterial viability by weakening the bacterial biofilm through a reduction of functional amyloid formation. AgNPs/AgNCs were synthesized via a chemical reduction method by adjusting the ligand to reductant ratio, and were functionalized with cationic branched polyethylenimine (bPEI) polymer.<sup>337</sup> bPEI coating enhances the interaction of nanoparticles with amyloid proteins and negatively charged *P. aeruginosa*,<sup>342, 343</sup> and is known for its interaction with bacterial surface and its associated bactericidal activities (TOC 5.1).<sup>344, 345</sup>



**TOC 5.1** Table of content illustrating the pictorial view of targeting *P. aeruginosa* biofilm using Ag NCs and AgNPs.

Herein, we synthesized silver nanoparticles of two different sizes, functionalized with cationic polymer branched polyethylenimine (bPEI) and interfaced them with FapC amyloidosis (Figure 5.1). Silver nanoparticles were synthesized via a chemical reduction method by adjusting the ligand to reductant ratio.<sup>339</sup> The nanoparticles of 2 nm size were designated as silver nanoclusters (AgNCs), and nanoparticles of 10 nm size were designated as silver nanoparticles (AgNPs). The interactions between AgNPs/AgNCs and FapC were studied via a thioflavin T (ThT) assay (for amyloidosis and inhibition), transmission electron

microscopy (TEM, for effect on aggregate morphology), high-angle annular darkfield (HAADF) imaging (for elemental imaging and analysis), energy-dispersive X-ray spectroscopy (EDAX, for elemental analysis), circular dichroism (CD) spectroscopy (for protein secondary structure), and cytotoxicity (for biocompatibility of bactericides), complemented by discrete molecular dynamics (DMD) simulations (for molecular details of FapC–AgNC binding). In addition, bacterial cell cultures of *P. aeruginosa* (PAO1) in the presence of AgNPs/AgNCs were examined with a biofilm assay (for viability), fluorescence microscopy (for biofilm architecture), TEM, and helium ion microscopy (HIM) (for more detailed biofilm architecture). Our results demonstrated a safe and facile new antimicrobial strategy through amyloidosis inhibition with nanomaterials.

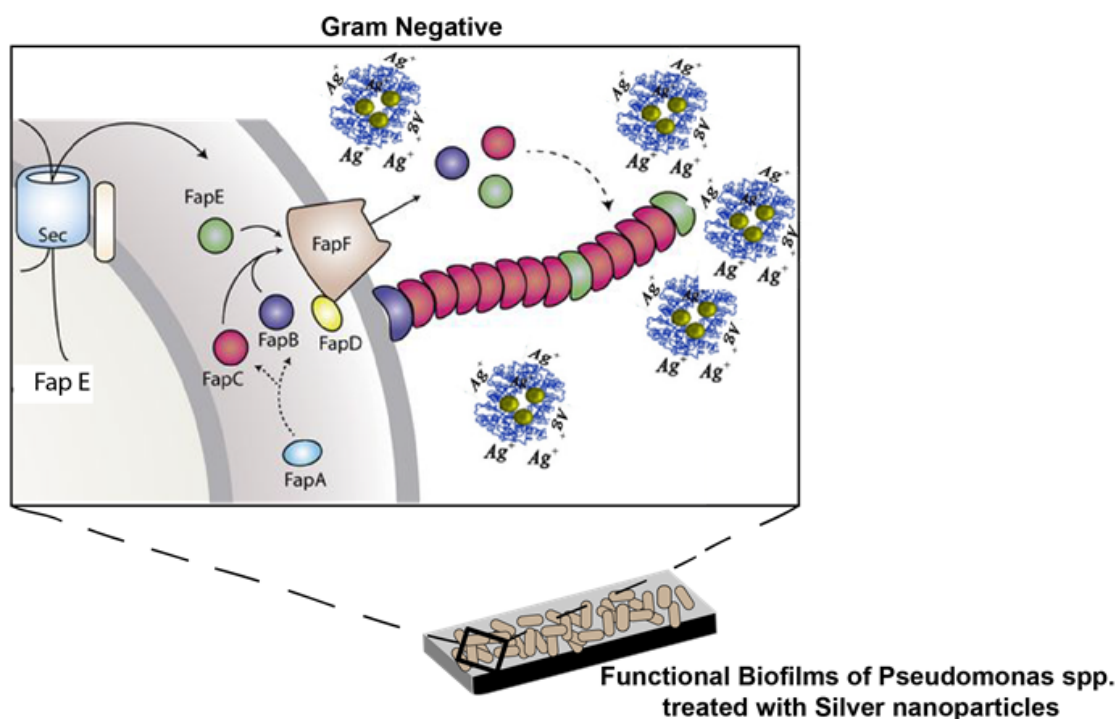


**Figure 5.1** A diagrammatic representation of Ag NPs. inhibiting *P. aeruginosa* biofilms by targeting bacterial amyloid proteins (FapC).

## 5.3. Results and Discussion

### 5.3.1. Synthesis and Characterizations of bPEI-Capped AgNPs and AgNCs

Cationic branched polyethyleneimine (bPEI)<sup>346</sup> was employed to graft two types of Ag nanostructures (**Figure 5.2A,B**) by chemical reduction.<sup>281, 347</sup> The size, morphology and zeta potential of the nanoparticles are summarized in **Figure 5.2C-H**. The nanoparticles of ~2 nm in size and exhibiting UV-Vis absorption peaks at 268 nm and 354 nm were designated as bPEI-capped AgNCs, while the nanoparticles of ~10 nm in size and possessing a definite surface plasmon peak at 420 nm were labelled as bPEI-capped AgNPs (**Figure 5.2C,D**). TEM micrographs revealed that both the AgNCs (2 nm) and AgNPs (10 nm) were well dispersed and near spherical (**Figure 5.2E,F**). Dynamic light scattering (DLS) measurements indicated the corresponding hydrodynamic diameter and zeta potential for the bPEI-capped AgNCs and AgNPs were 6.2 nm and +33 mV, and 18.6 nm and +15 mV, respectively, and the nanoparticles were relatively uniform with a polydispersity index (PDI) of < 0.4 (**Figure 5.2G,H**). ICP-OES was used to quantify the concentrations of Ag in AgNCs and AgNPs. The samples were digested in aqua regia and the Ag contents were quantified to be  $0.37 \times 10^{-3}$  and  $34 \times 10^{-3}$  M for AgNCs and AgNPs, respectively. The bPEI contents were quantified via thermogravimetric analysis (TGA), at  $0.95 \times 10^{-3}$  M for AgNCs and  $13.2 \times 10^{-3}$  M AgNPs, accordingly.

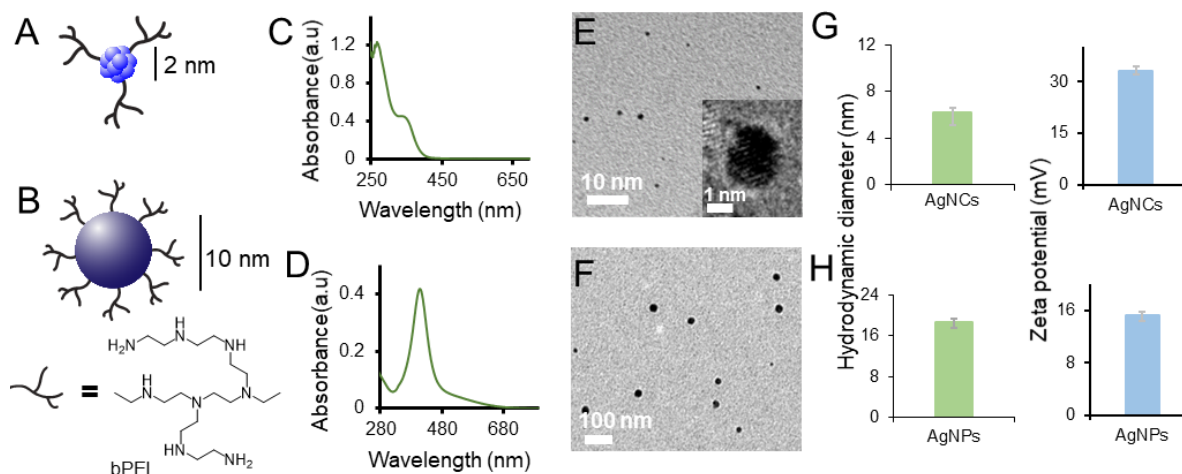


**Figure 5.2** Physical characteristics of bPEI-capped AgNCs and AgNPs. Graphical illustrations of bPEI-capped A. AgNCs and B. AgNPs. UV-vis absorption spectra of bPEI-capped C. AgNCs and D. AgNPs. TEM micrographs of bPEI-capped E. AgNCs and F. AgNPs. Zeta potentials and hydrodynamic diameters of bPEI-capped G. AgNCs and H. AgNPs were measured twice with three repeats and no significant difference was observed in them as per one-way ANOVA analysis.

### 5.3.2. *In-vitro* Interactions Between FapC and bPEI-Capped AgNPs and AgNCs

Amyloidosis inhibition with nanomaterials is an emerging frontier against amyloid diseases,<sup>328, 331, 348, 349</sup> but has rarely been attempted before for antimicrobial purposes.<sup>346</sup> Here the effects of bPEI-capped AgNPs or AgNCs on FapC fibrillization were systematically investigated to inhibit biofilm formation by *P. aeruginosa*. FapC monomers (50  $\mu$ M) were incubated alone or with bPEI-capped AgNPs or AgNCs (equivalent to 1  $\mu$ M Ag) for 5 days at 37  $^{\circ}$ C. In the absence of agitation, FapC fibrillization (monitored by the fluorescence of the amyloid-binding ThT) was slow and showed a lag time of 50 h, after which it reached a plateau within the next  $\sim$ 25 h (**Figure 5.3A**). When FapC was incubated with bPEI-capped AgNPs, FapC fibrillization was completely inhibited. In contrast, AgNCs shortened the lag phase to  $\sim$ 25 h but also reduced the end-level ThT fluorescence by 4-fold (**Figure 5.3A**). CD spectroscopy revealed changes in the secondary structure of FapC before and after fibrillization, in the presence and absence of AgNPs or AgNCs (**Figure 5.3B**). According to the deconvolution program DichroWeb, the  $\alpha$ -helical content of FapC was decreased from 28.4% (monomers) to 5.9% (fibrils), while the  $\beta$ -sheet content was increased from 15.6% (monomers) to 47.7% (fibrils). When incubated with AgNPs, the secondary structure of the

AgNPs + FapC complexes was similar to that of FapC monomers, at 25% for  $\alpha$ -helices and 18% for  $\beta$ -sheets. This suggests that the AgNPs inhibited FapC fibrillization by sequestering monomeric FapC (**Figure 5.3C**).<sup>334</sup> The secondary structure contents of the AgNCs + FapC complexes appeared to be between that for FapC monomers and fibrils, indicating limited formation of cross- $\beta$  amyloid fibrils (**Figure 5.3B,C**). Similarly, the zeta potential of the AgNCs + FapC complexes was -25 mV, compared to a zeta potential of -36 mV for FapC amyloid fibrils and +30 mV for AgNCs, indicating the presence of fibrils in the AgNCs + FapC complexes (**Figure 5.3D**). Also, the zeta potential of AgNPs dropped from +16 mV to +10 mV, after binding with FapC, confirming sequestration of FapC by AgNPs. The influence of AgNPs/AgNCs on FapC amyloidosis was further studied by TEM. No FapC amyloids were observed in the FapC + AgNPs sample, indicating full inhibition of FapC amyloidosis by AgNPs (**Figure 5.3E**), while AgNCs were clustered together with FapC monomers and supported the formation of short FapC fibrils (**Figure 5.3F**). The white signals from the HAADF images (**Figure 5.3G,H**) indicated the presence of Ag metal (EDAX mapping spectra in **Figure 5.3I,J**). The Cu signal was from the Cu grid. The presence of AgNCs in the core of clustered AgNCs + FapC complexes was further confirmed by HAADF imaging (**Figure 5.3H**). **Figure 5.3K,L** presents graphical illustrations of the binding between FapC and AgNPs or AgNCs. bPEI and AgNO<sub>3</sub> did not elicit any effect on FapC fibrillization, at a concentration equivalent to 1  $\mu$ M (with respect to Ag) of AgNPs/NCs. No toxicity of FapC was observed against HEK 293 cells, while AgNPs and AgNCs were biocompatible at 1  $\mu$ M Ag equivalent concentration.

The differences in the size and curvature of AgNPs and AgNCs can explain their differential behavior against FapC fibrillization. The large size of AgNPs (10 nm) matched the cross sections of single amyloid fibrils (~5-10 nm) and also provided a surface area large enough to physically interface with FapC monomers,<sup>304</sup> thereby enabling surface-assisted binding with the protein to prevent FapC from aggregation.<sup>330, 331</sup> In case of AgNCs, their small size (3 nm) resulted in the formation of hetero-aggregates with FapC that may act as nucleation sites for early FapC fibrillization, leading to a shortened lag phase. However, due to the heterogeneity of the AgNCs + FapC aggregates, elongation of FapC protofibrils into fibrils

could be entropically unfavorable, leading to a reduced yield of fibrils compared with FapC alone (**Figure 5.3A**).

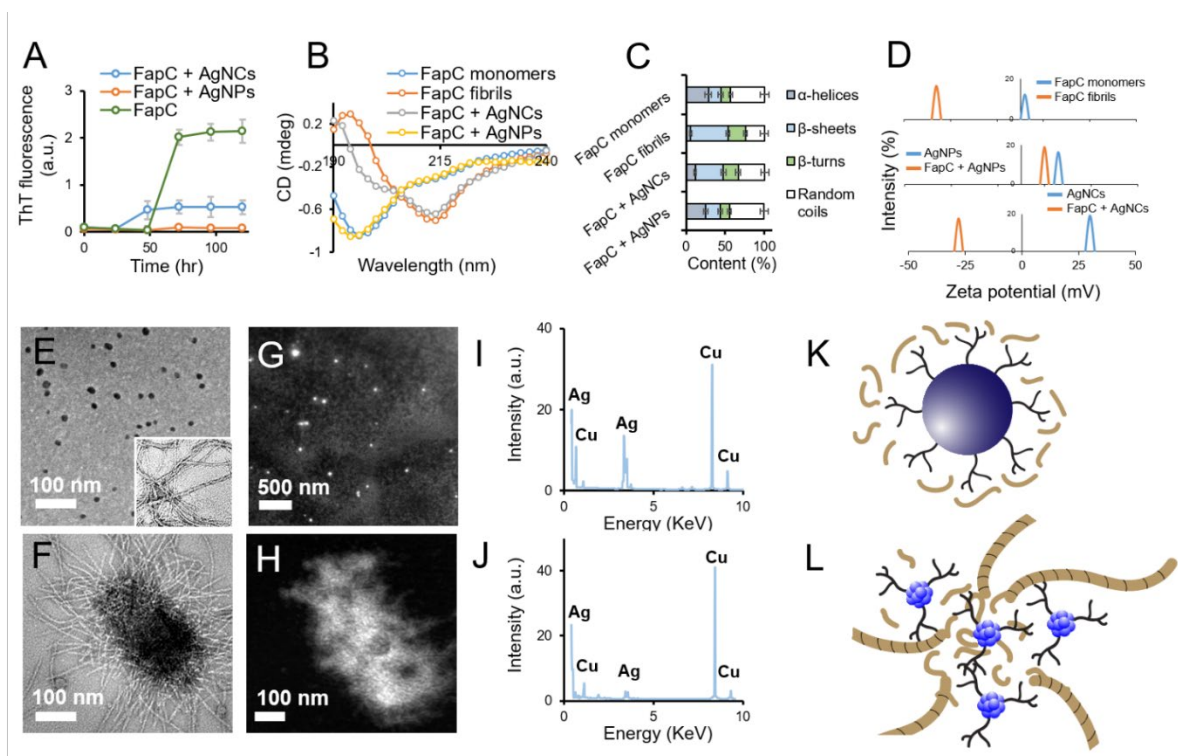


**Figure 5.3** Binding between FapC and bPEI-capped AgNPs or AgNCs. A. ThT kinetic assay of FapC mixed with AgNPs or AgNCs. B. CD spectra and C. percentage secondary structure of FapC monomers, fibrils, and FapC monomers after incubation with bPEI-capped AgNPs or AgNCs, calculated using DichroWeb. D. Changes in the zeta potential of FapC monomers before and after incubation with bPEI-capped AgNPs and AgNCs. TEM micrographs of E. FapC + AgNPs and F. FapC + AgNCs. The inset shows control FapC fibers. Panels, G-H. and I-J. present the respective HAADF images and EDAX spectra of FapC + AgNPs and FapC + AgNCs. Panels K. and L. represent graphical illustrations of bPEI-capped AgNPs and AgNCs interacting with FapC.

### 5.3.3. *In-silico* Interactions of bPEI-Capped AgNC with FapC Monomer and FapC Fragment Dimer

In an early study,<sup>255</sup> the effect of large AgNPs was modelled by a nano-sized (111) silver surface with five atom layers, where each layer comprised of 648 atoms occupying a dimension of  $\approx 7.0 \times 6.8 \text{ nm}^2$ . In contrast to the 38-atom AgNC coated with three bPEIs, only 9 bPEIs with strong electrostatic repulsion with each other were able to bind the nano-AgNP surface due to differences in radii and thus surface curvatures of the two types of

nanostructures (Experimental Section). Compared to AgNC, the lower bPEI coating density of the simulated AgNP was consistent with its smaller zeta potential observed experimentally (**Figure 5.2**).

In the dimer simulations of both L1R2 (**Figure 5D–F**) and L2R3, the bPEI-capped AgNC preferred to bind the linker regions as also observed in the monomer simulations. Compared to the full-length FapC (**Figure 5.4A**), fragments had a lower overall  $\beta$ -sheet content. Nevertheless, with the addition of a bPEI-capped AgNC, significant inhibition of  $\beta$  sheets and promotion of  $\alpha$  helices were observed for fragment L1R2 (**Figure 5.4D–F**). Similarly, the bPEI-capped AgNC also significantly inhibited the formation of  $\beta$  sheets by the L2R3 dimer. In the presence of bPEI-capped AgNP, stronger inhibition of  $\beta$  sheets and promotion of coil were observed for both L1R2 (**Figure 5.4D–F**) and L2R3. Compared to bPEI-capped AgNC, the low coating density of bPEI molecules in AgNP resulted in more surface silver atoms exposed to interact with the peptides. As a result, bPEI-capped AgNP could bind more FapC regions than bPEI-capped AgNC (**Figure 5.4E**), leading to the observed stronger inhibition of  $\beta$  sheets and promotion of coils. Overall, the dimer simulation results were consistent with the CD measurement showing increased  $\alpha$ -helices and decreased  $\beta$ -sheets upon addition of bPEI-capped AgNCs or AgNPs (**Figure 5.3B,C**), and also consistent with the experimental observation that bPEI-capped AgNPs rendered stronger inhibition against the formation of  $\beta$ -rich aggregates. The analysis of interpeptide contact frequencies indicated that the linker regions (especially L1) played an important role in dimerization by forming interpeptide  $\beta$  sheets in the absence of the AgNC or AgNP. By binding to the linker regions multivalently (e.g., typical snapshots in **Figure 5.4F**), the bPEI-capped AgNC disrupted  $\beta$ -sheet formation with a long-range order to mitigate FapC fibrillization. In the case of bPEI-capped AgNP, the binding with additional regions than the linkers in FapC resulted in stronger disruption of intermolecular  $\beta$ -sheet formation and subsequent FapC fibrillization.

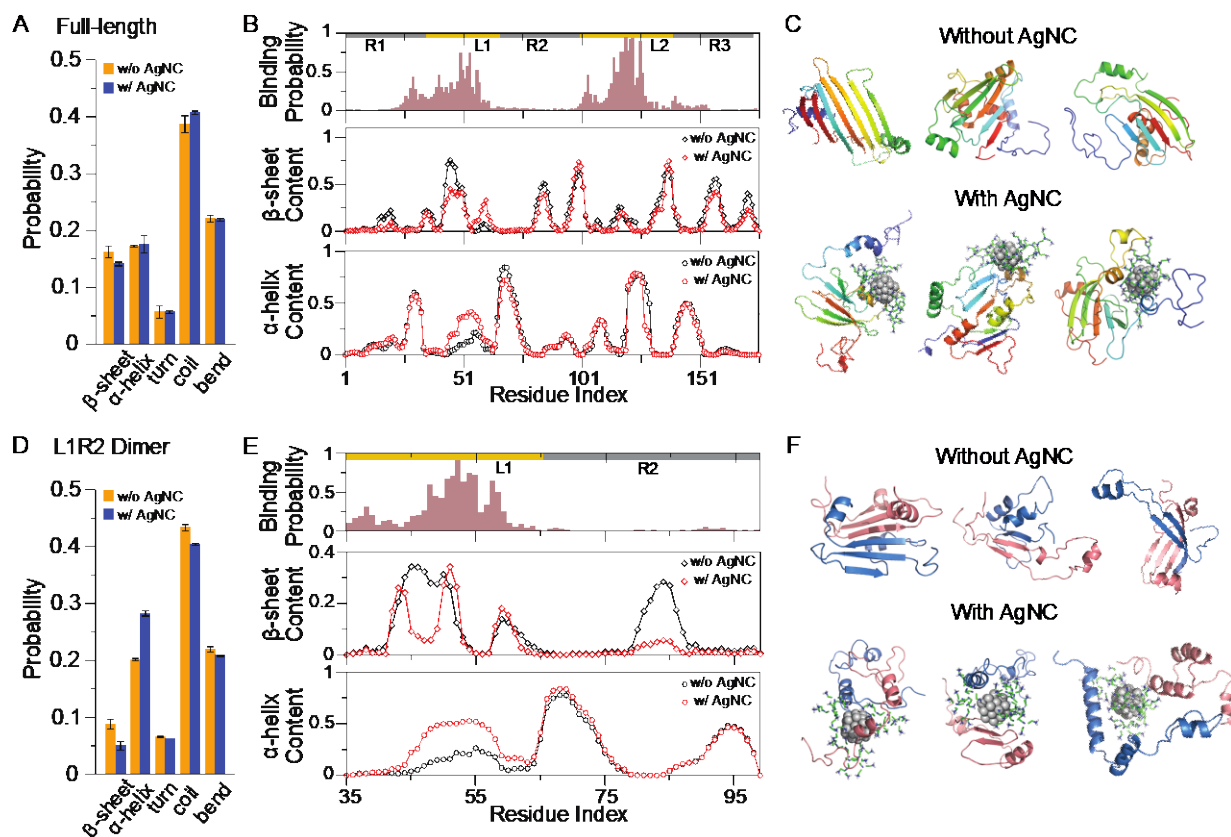


**Figure 5.4** DMD simulations of a bPEI-capped AgNC interacting with a FapC monomer and a FapC fragment dimer. A–C. Full-length FapC monomer (R1L1R2L2R3) with and without the presence of the bPEI-capped AgNC. A. Overall secondary structure contents of the full-length FapC monomer. B. The bPEI-capped AgNC-binding probability, and the  $\beta$ -sheet and  $\alpha$ -helix propensities of each residue. C. Three representative structures of FapC in the absence (upper) and presence (lower) of the AgNC. The peptide shown as cartoon is colored rainbow from blue (N-terminus) to red (C-terminus). The core of the AgNC is shown as spheres and bPEIs as sticks. D,E. A L1R2 dimer with and without the presence of the bPEI-capped AgNC. D. Overall secondary structure contents of the dimer. E. The binding probability with bPEI-capped AgNC or AgNP, and the  $\beta$ -sheet and  $\alpha$ -helix propensities of each residue. F. Representative structures of the L1R2 dimer in the absence (upper) and presence of the bPEI-capped AgNC (lower left) and AgNP (lower right). The two peptides are colored differently.

### 5.3.4. Effect of bPEI-Capped AgNPs and AgNCs on Biofilm Formation

Following the *in-vitro* characterizations of FapC interactions with AgNPs or AgNCs, the effect of such interactions on *P. aeruginosa* biofilm formation was studied by incubating the nanoparticles with the bacteria in microtiter plate wells as triplicates for 24 h in duplicate experiments. The statistical analysis was done to confirm reproducibility of experiments by

one-way ANOVA (Bonferroni test) using Prism 5 software. First, the effects of AgNPs and AgNCs on biofilm formation and planktonic bacterial viability were studied. AgNCs completely suppressed biofilm formation  $\geq 500 \times 10^{-9}$  M (**Figure 5.5A**), but below  $500 \times 10^{-9}$  M AgNCs, the bactericidal effect diminished (**Figure 5.5B**). At all concentrations, biofilm formation correlated with bacterial viability (**Figure 5.5C**). In contrast,  $250 \times 10^{-9}$  M to  $1 \times 10^{-6}$  M AgNPs suppressed biofilm formation (**Figure 5.5A'**) while displaying an insignificant bactericidal effect (**Figure 5.5B'**). Below  $250 \times 10^{-9}$  M, the antibiofilm activity of AgNPs became less prominent while the bacteria remained intact. At concentrations higher than  $1 \mu\text{M}$ , the bactericidal activity of AgNPs eliminated the availability of viable bacteria from establishing biofilm (**Figure 5.5C'**).<sup>338</sup> The *in-vitro* anti-FapC activities of AgNPs/AgNCs were correlated with their antibiofilm activity. The relative bactericidal and antiFapC activity of AgNCs and AgNPs can be explained based on their sizes and surface areas per particle. The larger AgNPs (10 nm) have more contact area per particle, which enabled them to sequester more FapC molecules per AgNP to mitigate FapC fibrillization. This is consistent with the literature where larger nanoparticles were more efficient amyloid inhibitors than their smaller counterparts.<sup>351, 352</sup> However, in terms of antibacterial efficacy, smaller AgNPs have been shown to be more efficient, as they possess a greater affinity for bacterial cell wall and can be efficiently internalized by bacteria.<sup>353, 354</sup>

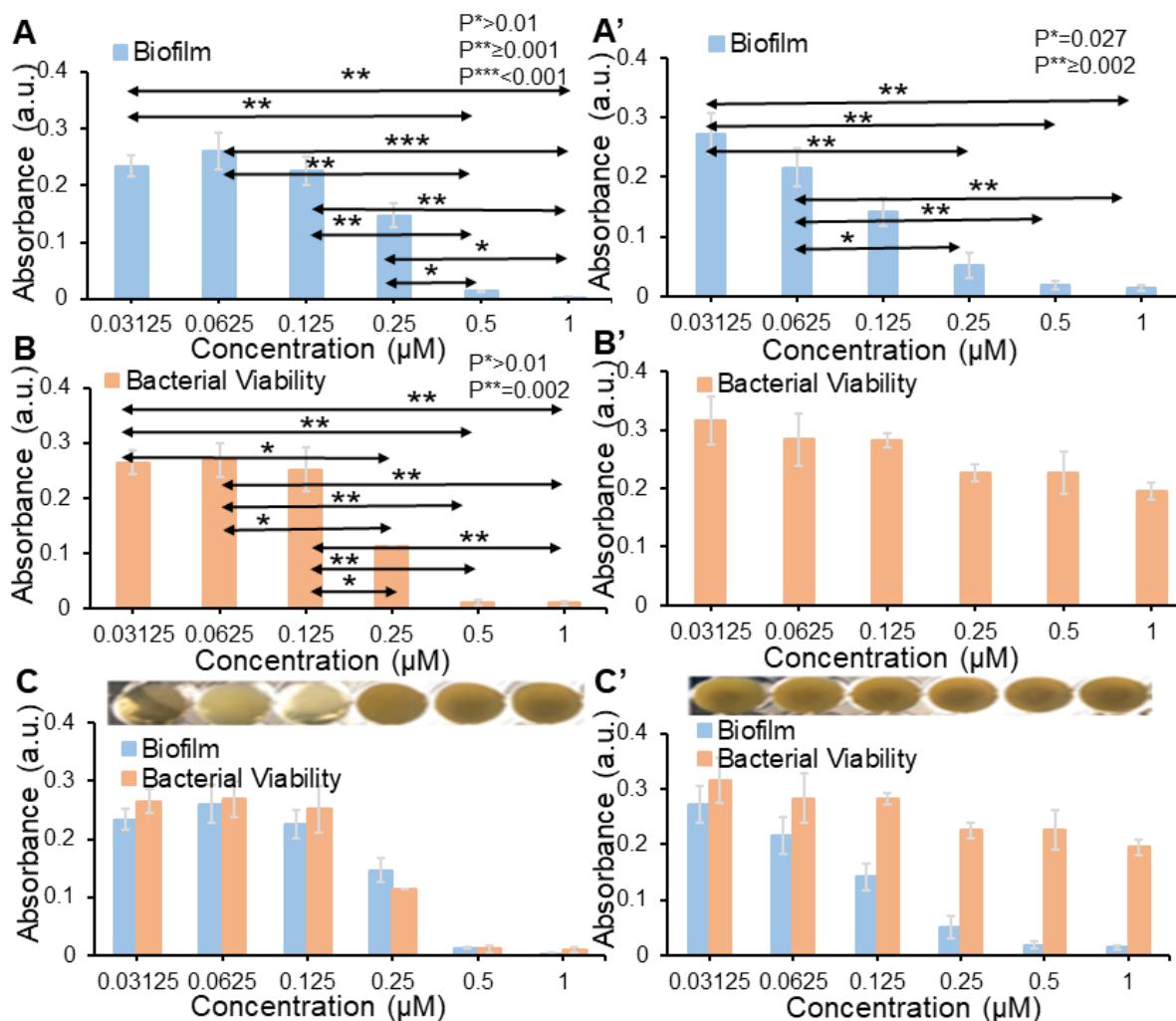


**Figure 5.5** The effects of bPEI-capped AgNCs and AgNPs on the biofilm formation of *P. aeruginosa*. Relative biofilm formation and bacterial viability of *P. aeruginosa* PAO1 in the presence of different concentrations of bPEI-capped A,B. AgNCs and A',B'. AgNPs. C is the overlapped A & B to see the comparative response of AgNCs and C' is the overlapped A' & B' to see the comparative response of AgNPs. All of these experiments were done in triplicates in two repeats and the P values were assigned by one-way ANOVA (Bonferroni test). The statistically significant viability is indicated by P values (\*,  $P > 0.01$ ; \*\*,  $P \geq 0.001$ ; \*\*\*,  $P < 0.001$ ). Each error bar represents standard errors of means.

To image the interactions of the nanoparticles with *P. aeruginosa*, a fluorescent strain of *P. aeruginosa* (AH298-GFP) was incubated with AgNPs or AgNCs while ThT dye was used to stain the biofilm. Consistent with **Figure 5.5C,C'**, individually dispersed bacterial cells and no biofilm mass were observed with AgNPs (**Figure 5.6A**), while debris of dead bacteria was evident in the AgNC-associated sample (**Figure 5.6B**). Intact bacteria embedded in biofilm mass were present in the untreated control (**Figure 5.6C**). HSI spectra derived from the SPR

of AgNPs, bacterial cells + AgNPs and untreated control are presented in **Figure 5.6D-F**. The SPR spectra of AgNPs were observed in the sample of bacterial cells + AgNPs with no traces of biofilms.

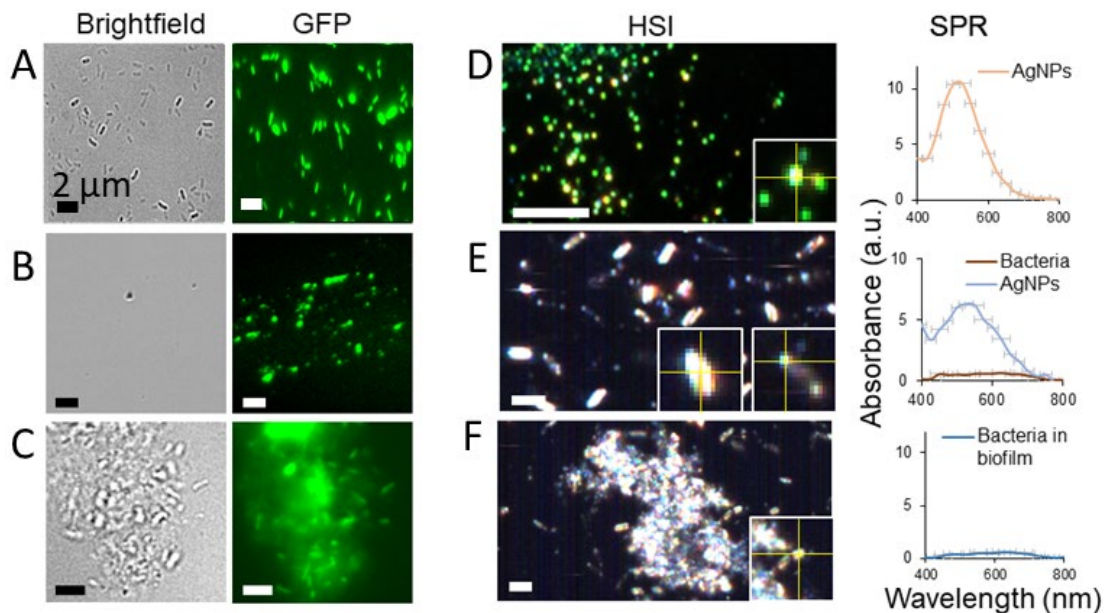


**Figure 5.6** Fluorescence microscopy images of *P. aeruginosa* AH298-GFP incubated with  $1 \times 10^{-6}$  M of A. AgNPs and B. AgNCs and C. untreated control that formed biofilms. A fluorescent strain of *P. aeruginosa* was used for fluorescence microscopy and ThT dye was used to stain the biofilms. Panels D–F. represent the hyperspectral images (HSI) along with the SPR spectra of AgNPs, *P. aeruginosa* incubated with  $1 \times 10^{-6}$  M AgNPs, and *P. aeruginosa* control, respectively.

The morphologies of control bacterial cells as well as cells exposed to AgNPs or AgNCs were also imaged via HIM and TEM. Intact bacterial cells with no biofilm or fibrillary aggregates were observed with AgNPs (**Figure 5.7A,B**), while dead bacterial cells displaying flattened, blebbing, dents and protrusions in the outer membranes were found for the AgNCs-treated sample (**Figure 5.7C,D**). In untreated control, fibrillar aggregates of FapC biofilms were evident between the cells (**Figure 5.7E,F**). Furthermore, to determine the oxidative effect conferred by AgNPs or AgNCs to bacterial cells, ROS production in the cells was quantified. AgNPs and AgNCs induced ROS generation in a concentration dependent manner (**Figure 5.7G**) but to very different extents, consistent with their respective bactericidal activities (**Figure 5.5C,C'**). This further indicates that biofilm inhibition by AgNPs was based on the inhibition of FapC fibrillization and not by their bactericidal activity as was

the case with AgNCs. AgNO<sub>3</sub> and bPEI alone were used as controls at concentrations equivalent to their concentration in AgNCs/NPs. At 1 μM concentration, specifically, soluble Ag<sup>+</sup> released by AgNO<sub>3</sub> did not induce any bactericidal or antibiofilm effect. This is quite as expected, as the minimum inhibition concentration (MIC) of AgNO<sub>3</sub> reported against *P. aeruginosa* is 17.6 μM.<sup>355</sup> This indicates that the bactericidal effect of AgNCs and the antibiofilm effect of AgNPs were associated with their nano-sized architectures and not with ion release at this given silver concentration. The enhanced bactericidal activity of AgNCs can be attributed to their ultrastructural disruption of the outer membranes followed by ROS generation, a mechanism that is shared with Ag<sup>+</sup> released from AgNPs.<sup>273, 355, 356</sup>

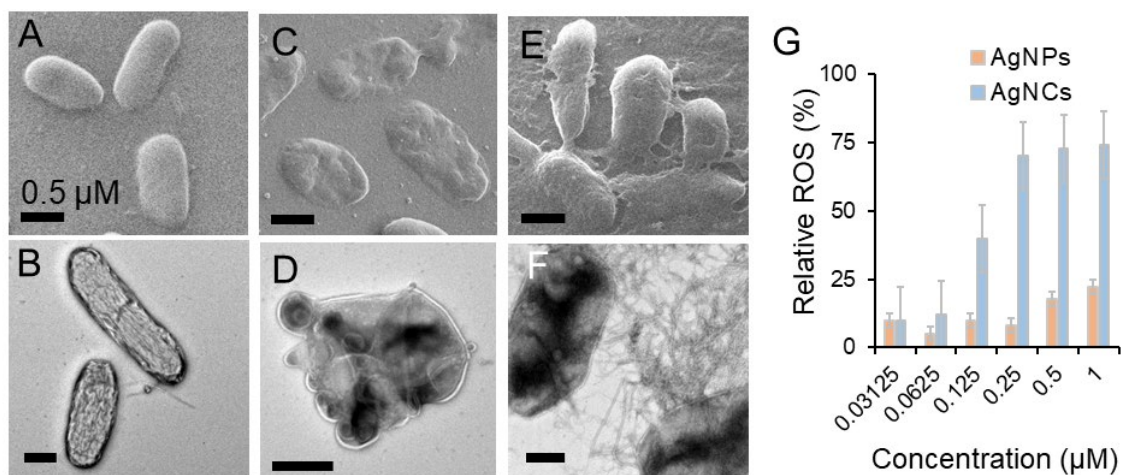


**Figure 5.7** Helium ion microscopy (HIM) and TEM micrographs of *P. aeruginosa* incubated with AgNPs (HIM: panel (A), TEM: panel (B)), *P. aeruginosa* incubated with AgNCs (HIM: panel (C), TEM: panel (D)), and *P. aeruginosa* control (HIM: panel (E), TEM: panel (F)). ROS generation by *P. aeruginosa*, relative to positive control (H<sub>2</sub>O<sub>2</sub>), upon incubation with AgNPs and AgNCs (panel (G)).

#### 5.4. Conclusion

We have examined the antibiofilm and antimicrobial potentials of bPEI-capped AgNPs and AgNCs, at concentrations below their toxicity thresholds for mammalian HEK 293 cells. As revealed by the ThT kinetic assay, both types of nanoparticles inhibited the amyloid aggregation of FapC, the protein constituent of the extracellular amyloid network of *P. aeruginosa*, through electrostatic interaction as well as H-bonding and hydrophobic interaction between the bPEI polymer and the protein. AgNPs sequestered FapC monomers

while the much smaller AgNCs clustered with FapC monomers to render short amyloid fibrils, as revealed by TEM, HAADF and EDAX experiments. These biophysical phenomena entailed contrasting consequences in the antibiofilm application of the nanoparticles. Specifically, with increased nanoparticle concentrations, AgNPs inhibited *P. aeruginosa* biofilm formation without killing the bacteria, through suppression of FapC amyloidosis and their associated extracellular amyloid network. In comparison, AgNCs impaired biofilm formation and were rendered bactericidal through structural-based disruption of cell membranes as well as elevated ROS production. Previously, AgNPs of biogenic origin were supposed to inhibit the bacterial biofilm formation by interfering with exopolysaccharides synthesis.<sup>286</sup> Here, we demonstrated that AgNPs at low concentrations directly sequestered FapC to inhibit the bacterial biofilm activity. In agreement with previous work targeting functional amyloid to compromise biofilm,<sup>318, 319</sup> this study demonstrated the potential of exploiting functional amyloidosis inhibition with nanomaterials as a safe and facile antimicrobial strategy.

## Chapter 6.

### **Design, Synthesis and Evaluation of Silver Nanocluster Based Levofloxacin Loaded Nanocapsules Against *S. pneumoniae*.**

#### **6.1. Synopsis**

This chapter presents antibacterial role of polyethylenimine stabilized silver nanoclusters (bPEI-Ag NCs) based nanocapsules loaded with levofloxacin (L-Ag NCps) as potential candidates to target various strains of *S. pneumoniae*. The 1<sup>st</sup> part covers the introduction and background of this project. The 2<sup>nd</sup> part includes the discussion of results related to the physical and chemical characterization of nanoclusters/nanocapsules, *in-vitro* study, and the mechanistic study supported by SEM and ROS study of these nanocapsules.

#### **6.2. Introduction**

Pneumococcal pneumoniae is the most prevalent childhood and community-acquired pneumonia.<sup>357</sup> It kills nearly 1 million children annually, and over 80% of these losses are kids of age under 2 years.<sup>5</sup> The reported ratio of *S. pneumoniae* with compromised susceptibility to fluoroquinolones among infants is almost 24-34 % in even developed countries like United States (**Figure 6.1**).<sup>358</sup> It will be unfortunate, and terrible indeed, if the increase in drug-resistant microbial cells leave us as susceptible to germs as we were 130 years back due to the dominance of these infectious diseases, and the variation in the liability of commonly used drugs.<sup>359</sup>

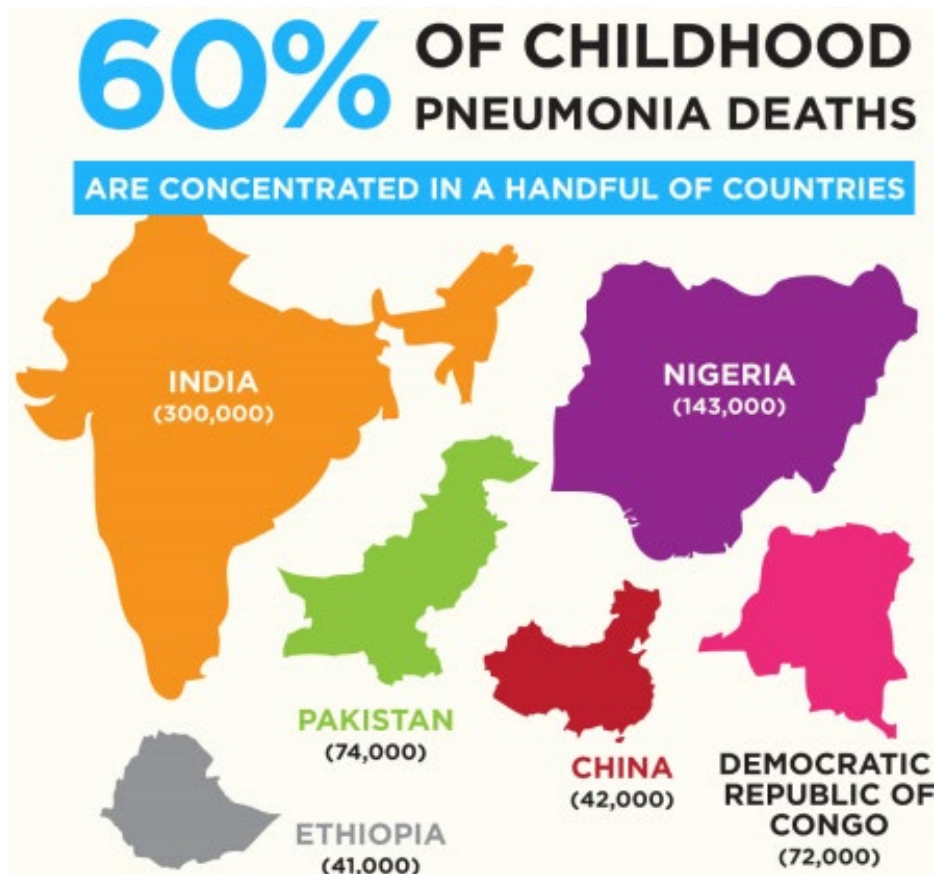


**Figure 6.1** Occurrence of pneumonia in different areas of the world.<sup>360</sup>

In 1881, Louis Pasteur and George Sternberg first discovered *S. pneumonia* from saliva. Later in 1800s, Christian Gram recognised it as Gram-positive bacterium using gram staining. During early 1900s, bacterial structure and communication with immune system was revealed. In 1913, anti-pneumococcal serum therapy decreased the mortality rate from 25% to 7.5%. In 1923, Heidelberger and Avery reported the production of antibodies by B cells in immune system to abolish bacteria. The first line antibacterial agent, sulfapyridine, was used to control pneumonia in 1930, which was substituted by penicillin. The prevailing situation of resistance against almost all major antibiotics further aggravated the problem. The mechanism behind the resistance to cephalosporins and penicillin in pneumococcal cells involves changes in their molecular targets in cell wall and penicillin-binding proteins (PBPs) (**Figure 6.2**).<sup>361</sup> The first vaccine introduced in 1977 was pneumococcal polysaccharide vaccine (PPV) followed by pneumococcal conjugate vaccine (PCV) in 2000. These vaccines took almost 3 years until licensure of an *S. pneumoniae* vaccine that costed \$240 million at

that time.<sup>362, 363</sup> The recurring infections from escaped microbes is responsible for appearance of MDR. Aside from bouncing chemotherapy, prompt metabolic clearance of drugs, reduced oral availability and incapability to penetrate deep into target site all this leads to advancement in MDR. It is, therefore, highly desired to develop smart and effective strategies to treat infections by deceiving all resistant mechanisms.<sup>364</sup>

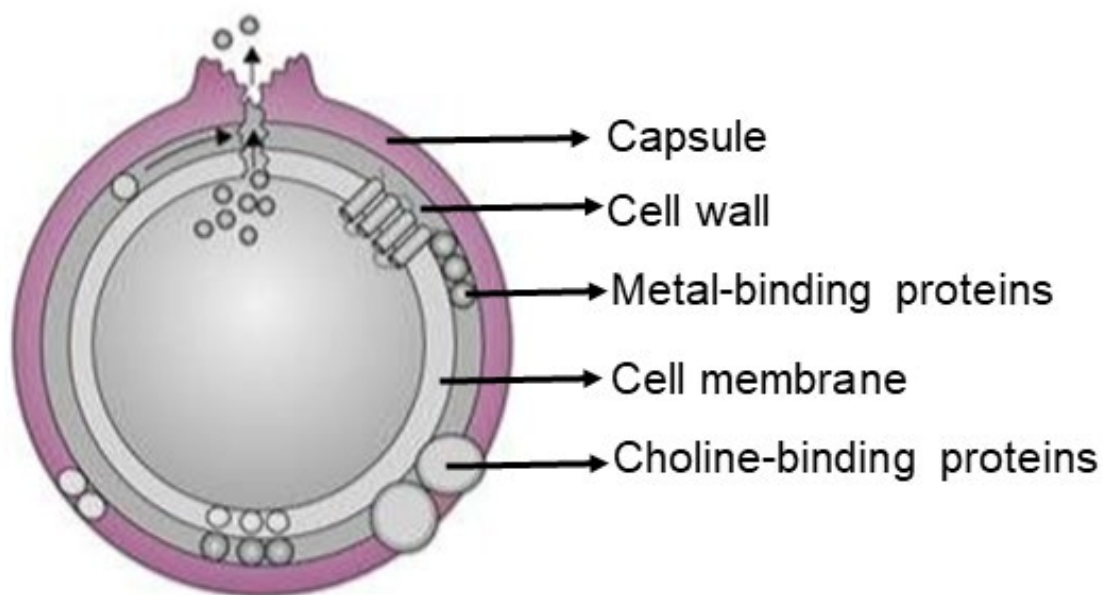


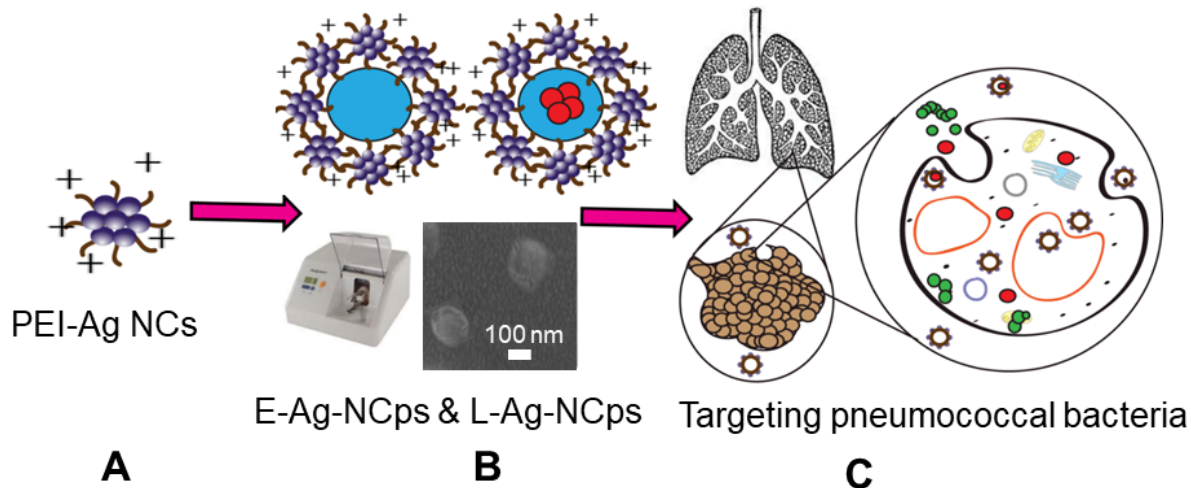
**Figure 6.2** Pneumococcal structure showing its various important components which was used by antimicrobials to target them.

Several ‘nanodrugs’, especially liposomal nanoformulations have been permitted by FDA and are in clinical use against many diseases. Correspondingly, various therapeutics can be used to encapsulate inside the nanomaterials, which increases their therapeutic efficiency resulting in reduced dosage requirements and decreased host toxicity. The levofloxacin loaded in silver core mesoporous silica nanovehicles (Ag@MSNs@LEVO) showed good synergistic response against *E. coli* MDR isolates.<sup>365</sup> Similarly, nanocapsules are a type of vesicular systems exhibiting core-shell type structure and have ability to load different cargo inside their core. They are important vectors for many active substances i.e., hormones, DNA, siRNA, vitamins, drugs.<sup>366</sup> In order for payload to play its role, it needs to be available in cytosol of bacterial cells by endosomal escape and breaking resistance. In this chapter, we present very simple materials to address the emerging health issues related to MDR in

*S. pneumoniae* by the design/development of nanocapsules comprising of Ag NCs conjugated with PEI and an antibiotic. These cationic nanocapsules with decent amphiphilic balance can manifest effective antibacterial effects with reduced cytotoxicity. This medicinal chemistry approach to address MDR is very cost-effective and therapeutically superior alternative strategy.

### 6.3. Results and Discussion

The silver nanoclusters (**Scheme 6.1A**) were successfully synthesized by chemical reduction method as mentioned in chapter 4. Nanocapsules (NCps) of Ag were synthesized via emulsification method by the stabilization of NCs at the interface of water and oil phase as shown in **Scheme 6.1B**.<sup>367</sup> Peppermint oil was used as an oily phase due to its biocompatible nature. These NCps were stabilized due to electrostatic interactions with the help of surfactant (SDS). A hydrophobic drug (levofloxacin) was loaded inside NCps by co-dissolving it in hydrophobic phase (oil), to form Levofloxacin loaded silver nanocapsules (L-Ag-NCps), whereas, the unloaded NCps i.e. empty silver nanocapsules (E-Ag-NCps) were used as control. Ultra-sonication and amalgamation was employed to control the size and emulsification behaviour of NCs to form Nanocapsules as shown in **Figure 3.3**. These nanocapsules after basic characterization using UV-visible spectroscopy, DLS measurements and scanning electron microscopy were employed to target different pneumococcal strains as shown in **Scheme 6.1B,C**.



**Scheme 6.1** Schematic illustration includes A. synthesis of bPEI-Ag NCs, B. emulsification to form nanocapsules (E-Ag-NCps and L-Ag-NCps), C. targeting of pneumococcal strains by nanocapsules (E-Ag-NCps and L-Ag-NCps).

The UV-visible absorption spectrum of L-Ag-NCps along with controls (drug, E-Ag-NCps, AgNCs) confirmed the loading of Levofloxacin with  $\lambda$ -max at 283 nm in common with the drug, whereas E-Ag-NCps and AgNCs shows no such peak (**Figure 6.3A**). The effective synthesis of NCps was confirmed by DLS size measurement and TEM (**Figure 6.3B,C**). The hydrodynamic size of E-Ag-NCps and L-Ag-NCps checked by zetasizer was 180 and 193 nm as shown in **Figure 6.3B**. The polydispersity Index, measured by Zetasizer, for all samples was  $< 0.5$ . The stability of nanocapsules was checked for 48 h by DLS-size analysis and were found quite stable. The TEM size measurements of Ag NCs, E-Ag-NCps and L-Ag-NCps was 2, 160 and 185 nm as shown in **Figure 6.3C(a,b,c)**, respectively. Surface morphology was spherical and smooth as observed in all of the STEM images (**Figure 6.3C**). The size of L-Ag-NCps was greater than E-Ag-NCps and were even more stable.<sup>341</sup> This size of NCps was based on their intrinsic ability to encapsulate drug. It is the most stable size obtained for L-Ag-NCps, and their stability decreases with further increase in the amount of loaded drug. It was observed that E-Ag-NCps are smaller than L-Ag-NCps, which may be attributed to the loading of drug, which also makes them more stable due to strong electrostatic interactions, by the nanoclusters.

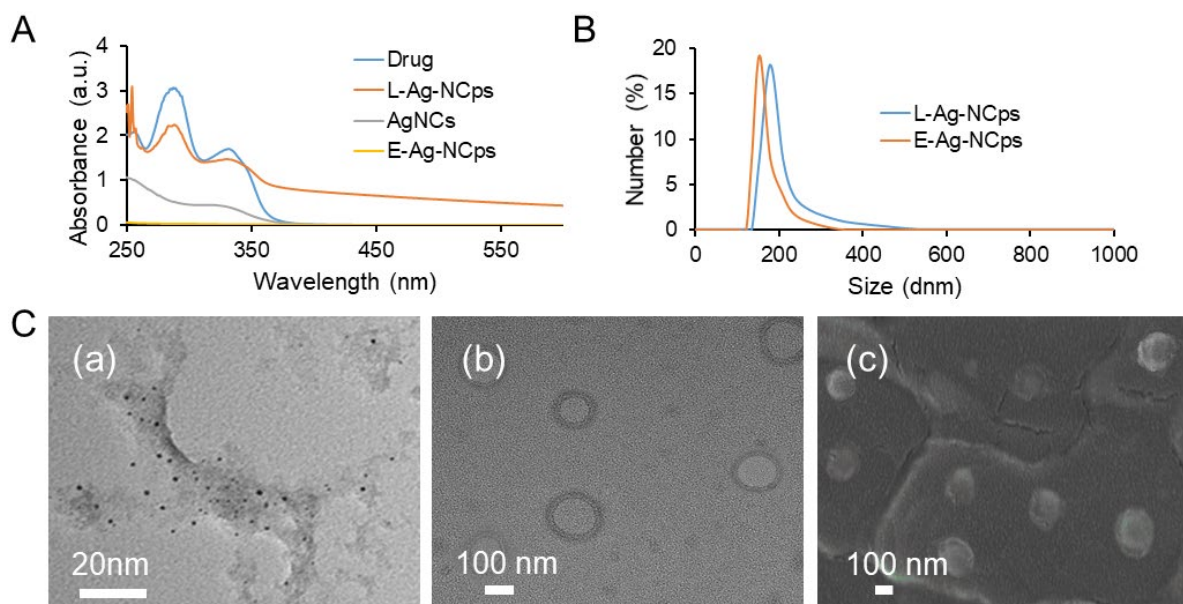


**Figure 6.3** The characterization of PEI-Ag NCs, E-Ag-NCps and L-Ag-NCps using A. UV-vis spectroscopy showing  $\lambda$ -max at 283 nm for the drug and the corresponding peak for L-Ag-NCps, B. DLS- Zetasizer displaying size of 180 and 193 nm for L-Ag-NCps and E-Ag-NCps, C. Transmission electron micrograph showing (a) PEI-Ag NCs with 2 nm, Scanning electron micrographs showing (b) E-Ag-NCps with 160 nm and (c) L-Ag-NCps with 185 nm size, respectively.

### 6.3.1. Drug Loading Efficiency of L-Ag NCps

Drug loading was estimated by UV-visible spectroscopy (**Figure 6.3A**). It is expected that drug loading efficiency of L-Ag-NCps depend on the quantity of adsorbed drug together with the adsorbed/tangled drug in the strands of PEI. The drug carrying efficiency was estimated by removing the free/loosely bound drug on L-Ag-NCps by centrifuging the NCps formulation for 10 min at 5000 g at 4 °C. Hydrophobic untrapped drug pelleted down and the quantity of encapsulated drug in L-Ag-NCps was measured by determining the absorbance of levofloxacin at 283 nm respectively (**Figure 6.3A**). For this reason, L-Ag-NCps were mixed in chloroform:methanol (1:4) mixture and quickly sonicated for 1 min to break the NCps and release the entrapped levofloxacin in solvent system. Drug loading efficiency was estimated to be 20 % by following expression:

$$\text{Encapsulation efficiency (\%)} = \frac{\text{Levofloxacin in supernatant after breaking L-Ag-NCps /}}{\text{[total levofloxacin added to formulation]} \times 100}$$

### 6.3.2. Anti-Pneumococcal Activity of Nanocapsules

The frozen stocks of *S. pneumoniae* were maintained at 80°C in Todd-Hewitt Broth with 5% yeast extract (THY) and glycerol (10%). A small portion of these frozen stocks was inoculated on blood agar plates and set for overnight incubation in a candle jar at 37°C. A loopful of pneumococci were scraped from the plate, resuspended into THY broth and incubated at 37°C to attain an optical density (OD<sub>600</sub>) of 0.2 (early exponential phase). The final pellet of bacteria were harvested via centrifugation and washed thrice with PBS before resuspending into THY. The different strains of bacteria were first incubated with drug and AgNCs to determine their respective MIC by plating. Pneumococcal strains demonstrated variability in killing by AgNCs and drug, where the MIC for AgNCs and drug ranged from 8.19 µM and 512 µM for type 2 strain, 16.4 µM and 204.8 µM for type 13 strain, 8.19 µM and 32 µM for type 16F strain, and 16.4 µM and 102.4µM for type 19F strain respectively, as shown in **Table 6.1A**. After this drug-loaded nanocapsules (L-Ag-NCps) and empty nanocapsules (E-Ag-NCps) with drug/AgNC concentrations quite lower compared to their MIC (**Table 6.1B**), along with drug (Levofloxacin) as control were incubated with actively growing cultures of *S. pneumoniae*. The three of the tested serotypes 16F, 2 and 19F were susceptible to fluoroquinolones, whereas type 13 is a resistant strain. The 2 h incubation at 37°C was followed by serial dilution of bacteria and their plating on blood agar to estimate viable CFU counts. These CFU counts were converted into log<sub>10</sub> values to normalize the comparison. The Log<sub>10</sub> CFU killed was determined by subtracting log<sub>10</sub> CFU value of samples from log<sub>10</sub> CFU value of control pneumococci. All of the experiments were done as triplicates in two repeats to ensure reproducibility. The statistical analysis was done by comparing average of these triplicates for two independent experiments of all three samples (L-Ag-NCps, E-Ag-NCps, Drug). P values were assigned using one-way ANOVA (Bonferroni test). This analysis was done using Prism 5 analytical software.

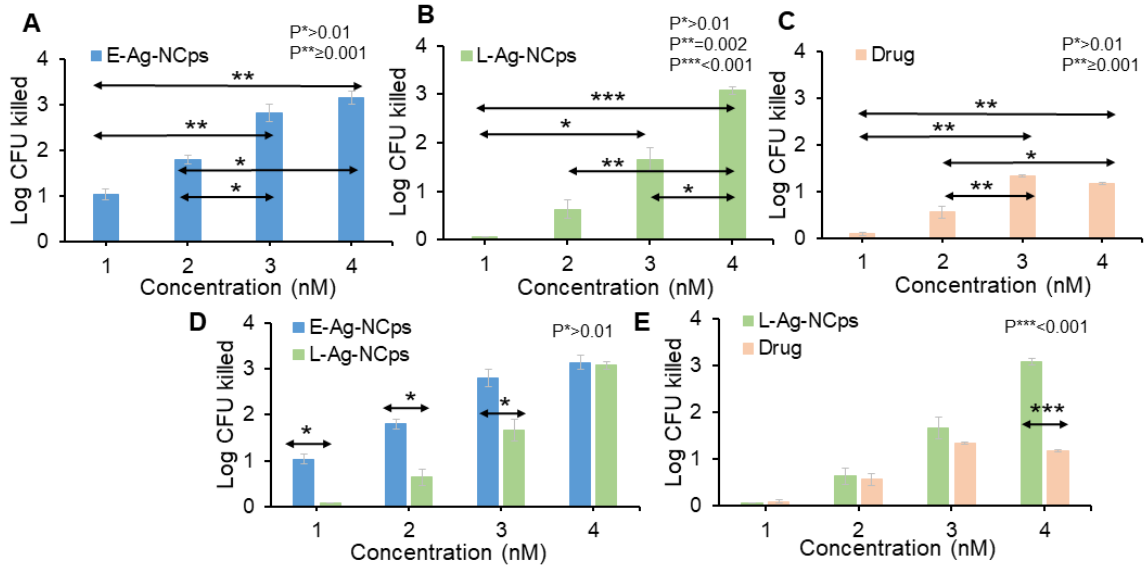
**Table 6.1** A. MIC of AgPEI NCs and drug against four different pneumococcal serotypes B. The concentration of AgPEI NCs and drug loaded into E-Ag-NCps/L-Ag-NCps used for anti-pneumococcal activity.

| <b>A</b>               |                                    |                                       |
|------------------------|------------------------------------|---------------------------------------|
| Pneumococcal serotypes | MIC of AgPEI NCs ( $\mu\text{M}$ ) | MIC of Levofloxacin ( $\mu\text{M}$ ) |
| Type 16F               | 8.19                               | 32                                    |
| Type 19F               | 16.4                               | 102.4                                 |
| Type 13                | 16.4                               | 204.8                                 |
| Type 2                 | 8.19                               | 512                                   |

| <b>B</b> |  |  |
|----------|--|--|
| Codes    | Conc. of AgPEI NCs in E-Ag-NCps/L-Ag-NCps (nM) | Conc. of Levofloxacin in L-Ag-NCps ( $\mu\text{M}$ ) |
| 1        | 13   | 0.62   |
| 2        | 26   | 1.24   |
| 3        | 64   | 3  |
| 4        | 128  | 6  |

In case of type 16F, at higher concentrations both E-Ag-NCps and L-Ag-NCps showed comparable killing and almost 2 Log times increased killing compared to drug control (**Figure 6.4**). This increased targeting of E-Ag-NCps at lower concentrations in this strain is attributed to more sensitivity of this strain towards Ag NCs as indicated by their lower MIC compared to other strains in **Table 6.1A**.



**Figure 6.4** Anti-pneumococcal activity of A. empty nanocapsules (E-Ag-NCps), B. levofloxacin loaded nanocapsules (L-Ag-NCps), C. drug against serotype 16F, D. Represents overlapped A & B to see the comparative effect of E-Ag-NCps and L-Ag-NCps on type 16F, while E. represents overlapped B & C to see the comparative effect of L-Ag-NCps and drug on type 16F. Each error bar represents standard errors of means. The statistically significant Log CFU killing was represented by P values (\*, > 0.01; \*\*, ≥ 0.001).

In case of type 13, which is also levofloxacin resistant, L-Ag-NCps showed best response of 1 Log times increased killing compared to E-Ag-NCps and 2.5 Log times increased killing compared to drug control (**Figure 6.5**). This might be because of resistance of type 13 strain against drug, whereas L-Ag-NCps showed increase response by crossing the resistive barrier and release drug inside the bacterial cell due to their smaller size and biocompatible shell. In **Figure 6.5F**, pneumococcal colonies can be seen growing visibly on blood agar plates in control and E-Ag-NCps compared to L-Ag-NCps against type 13 strain.

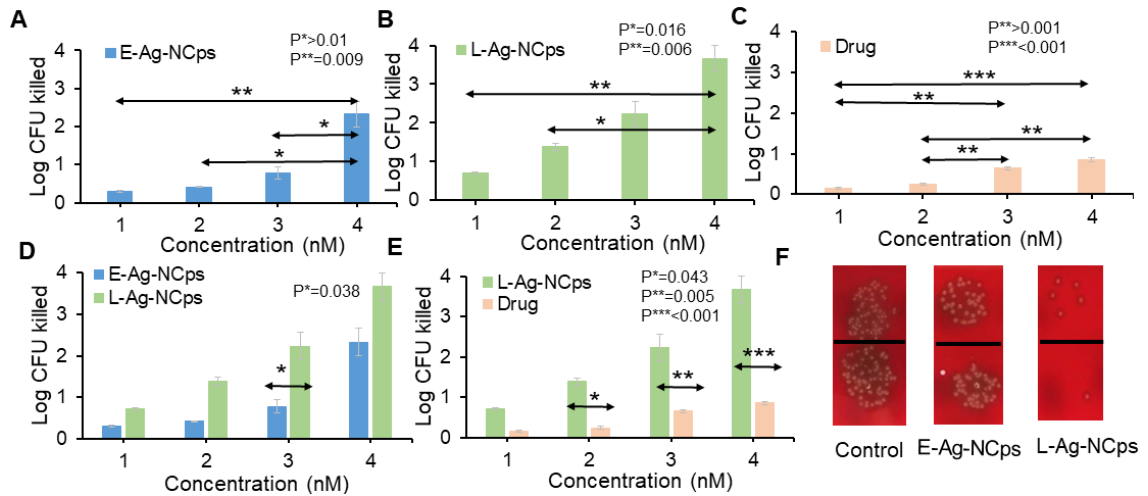


**Figure 6.5** Anti-pneumococcal activity of A. empty nanocapsules (E-Ag-NCps), B. levofloxacin loaded nanocapsules (L-Ag-NCps), C. drug against serotype 13, D. Represents overlapped A & B to see the comparative effect of E-Ag-NCps and L-Ag-NCps on type 13, while E. represents overlapped B & C to see the comparative effect of L-Ag-NCps and drug on type 13. Each error bar represents standard errors of means. The statistically significant Log CFU killed was represented by P values (\*, > 0.01; \*\*,  $\geq 0.001$ ; \*\*\*, < 0.001). F. Pictorial view of colonies grown on blood agar plates after 2 h incubation of treatments with type 13 showing increased death of colonies in L-Ag-NCps compared to controls.

In case of type 19F, L-Ag-NCps showed 0.5 Log increased killing compared to E-Ag-NCps in lower concentrations and 0.5 Log increased killing compared to drug at all concentrations. This might be attributed to increased internalization of drug into the bacteria by L-Ag-NCps. However, at higher concentrations both E-Ag-NCps and L-Ag-NCps showed comparable killing due to complete lysis of bacterial cells because of high Ag NCs concentration in these nanocapsules (**Figure 6.6**).

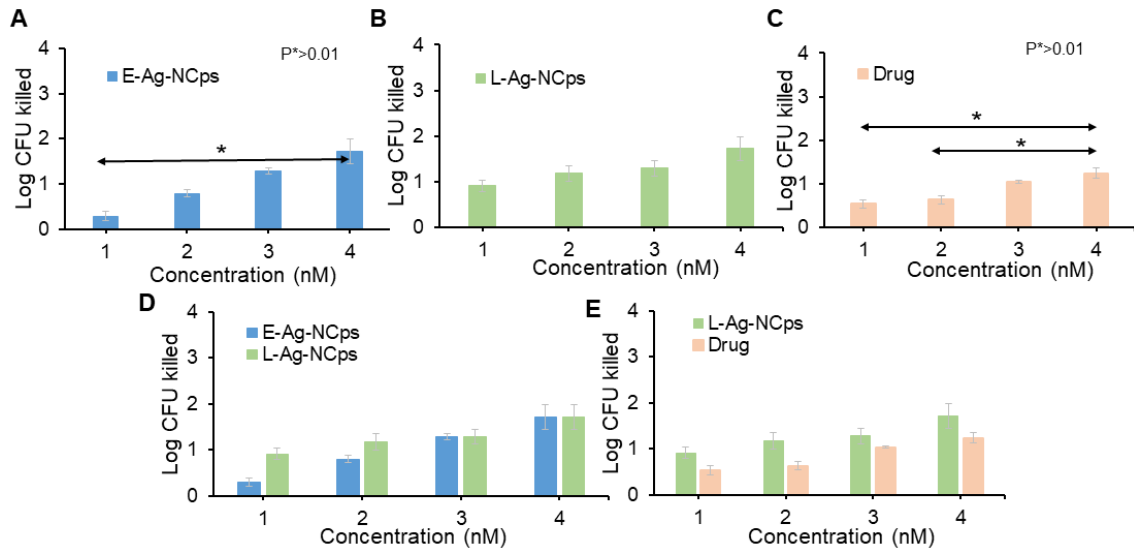


**Figure 6.6** Anti-pneumococcal activity of A. empty nanocapsules (E-Ag-NCps), B. levofloxacin loaded nanocapsules (L-Ag-NCps), C. drug against serotype 19F, D. Represents overlapped A & B to see the comparative effect of E-Ag-NCps and L-Ag-NCps on type 19F, while E. represents overlapped B & C to see the comparative effect of L-Ag-NCps and drug on type 19F. Each error bar represents standard errors of means. The statistically significant Log CFU killed was represented by P values (\*, > 0.01).

An increase of two-log killing was observed in case of type 2 by L-Ag-NCps compared to E-Ag-NCps and drug. This can be linked to the controlled drug discharge inside the bacterial cell by L-Ag-NCps (**Figure 6.7**). In **Figure 6.7F**, pneumococcal colonies can also be seen growing visibly on blood agar plates in control and E-Ag-NCps compared to L-Ag-NCps against type 2 strain.

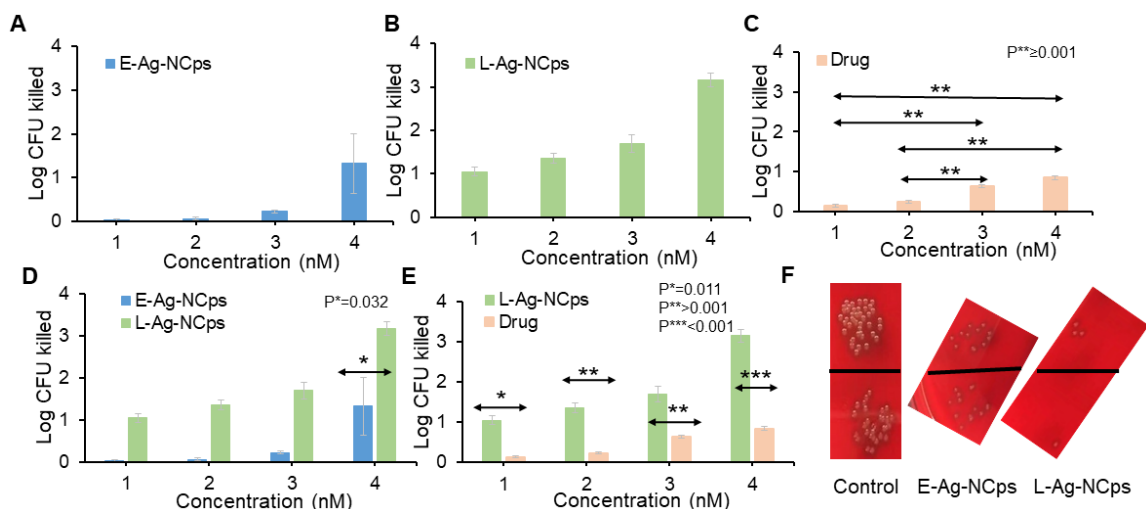


**Figure 6.7** Anti-pneumococcal activity of A. empty nanocapsules (E-Ag-NCps), B. levofloxacin loaded nanocapsules (L-Ag-NCps), C. drug against serotype 2. D. Represents overlapped A & B to see the comparative effect of E-Ag-NCps and L-Ag-NCps on type 2, while E. represents overlapped B & C to see the comparative effect of L-Ag-NCps and drug on type 2. Each error bar represents standard errors of means. The statistically significant Log CFU killed was represented by P values (\*, > 0.01; \*\*,  $\geq 0.001$ ; \*\*\*, < 0.001). F. Pictorial view of colonies grown on blood agar plates after 2 h incubation of treatments (L-Ag-NCps, E-Ag-NCps, drug) with type 2 showing increased death of colonies compared to controls.

The antibacterial activity results demonstrated that the nanocapsules showed good pneumococcal inhibition, which increases with an increase in amount of nanocapsules similar to control drug (Levofloxacin). It was observed that E-Ag-NCps was quite effective carrier utilizing killing properties of Ag NCs but with loading of levofloxacin in L-Ag-NCps, we observed a good combined response in few pneumococcal strains (type 13, type 2 and type 16F), so this drug releasing property/ anti-pneumococcal response is dose and strain dependent. This enhanced activity is credited to antimicrobial potential of silver along with enhanced loading and drug releasing properties of NCps inside pneumococcal cells.<sup>368</sup>

### 6.3.3. Mechanistic Study by Scanning Electron Microscopy and Reactive Oxygen Species generation

The initial contact of L-Ag-NCps with surface lipids, which built cell wall portions of bacteria, is the basis for their extensive non-specific action even for the drug resistant strains. *S. pneumoniae* possess six layers thick lipid built outside the casing of peptidoglycan with negatively charged teichoic and lipoteichoic acid, thus major contact of NCps with

pathogen can be expected (**Figure 6.2**). This was in fact evidenced by SEM analysis. It was observed that pneumococcal serotype 2 cells were living initially in the form of chains **Figure 6.8A(a)**. After 2 h of incubation, bacterial cells were having nanocapsules stucked on their surface creating pits **Figure 6.8A(b,b')** and after 5h, complete lysis of pneumococcal cells can be seen with debris everywhere **Figure 6.8A(c)**. According to the literature, cationic nanocapsules show electrostatic interaction with negatively charged groups like teichoic acid and lipoteichoic acid on the bacterial cell wall, which is accountable for nasopharyngeal colonisation of host and after getting into the cell they kill bacteria by ROS generation (**Figure 6.8B**).<sup>369</sup> The ROS estimation was done using resazurin assay and is done as duplicates in two repeats. These measurements were further analysed statistically using one-way Anova. This extent of reactive oxygen species (ROS) supports that the antimicrobial potential of nanocapsules (L-Ag-NCps) at concentration (13 nM) against serotype 2 was attributed to the Ag content of nanocapsules. The combined release of Ag NCs, Ag ions and drug from the nanocapsules also result in significant parallel pharmacological processes with intracellular biomolecules accordingly limiting the bacteria capacity to develop resistance to fight with them, as it normally does for other drugs. The expected mechanism is likely to involve the initial contact of Ag content in nanocapsules with –SH containing proteins and carboxyl groups of teichoic and lipoteichoic acid at the exterior of pneumococcal cells. This resulted in direct entry of NCps through membrane fusion into the bacterial cytosol by bypassing endosomal entrapment. The successful entry of NCps lead to successive reactive oxygen species (ROS) production and drug discharge that can trigger membrane rupture and various other processes deactivating the functioning of cellular machinery.<sup>370</sup> In addition, all the materials used in nanocapsule synthesis were biocompatible and the nanoclusters were also biocompatible in such lower concentrations as previously reported.

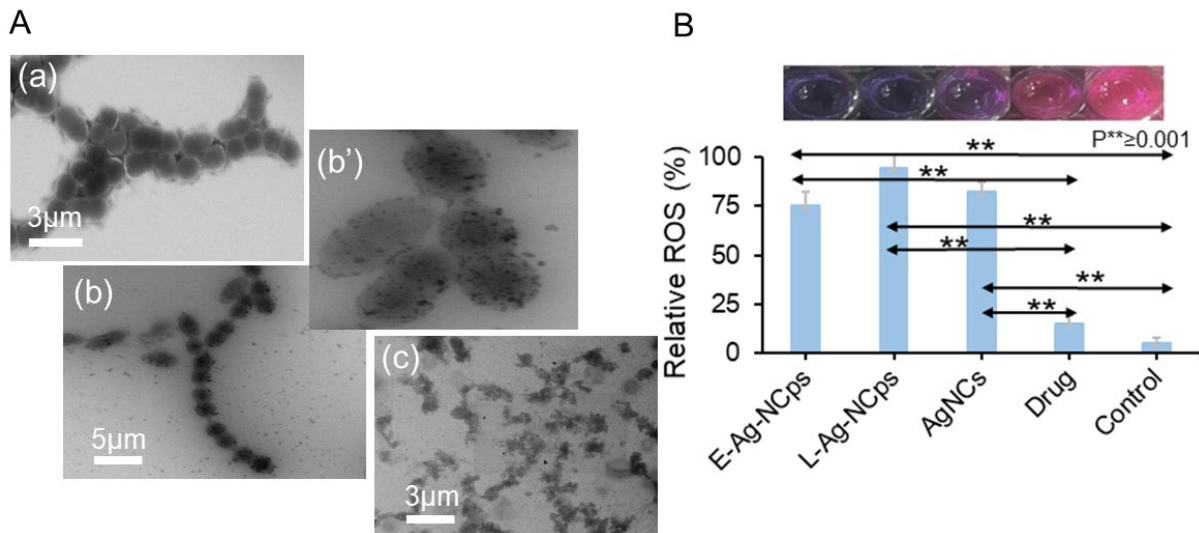


**Figure 6.8** The possible mechanism involved in killing of bacterial cells was studied by (A) SEM images of (a) Pneumococcal serotype 2 control cells, (b) pneumococcal cells showing stress response in the form of long chains, (b') pneumococcal cells with pits on their surface due to L-Ag-NCps targeting, (c) the complete lysis of pneumococcal serotype 2 cells with designed nanocapsules (L-Ag-NCps), (B) and ROS generation playing effective role in pneumococcal serotype 2 targeting, which is truly attributed to silver content of nanocapsules (L-Ag-NCps). Each error bar represents standard errors of means. The statistically significant killing by ROS production was indicated by P values (\*\*,  $\geq 0.001$ ).

#### 6.4. Conclusion

In this study we explored the usage of drug loaded nanocapsules by comparing it with controls and observe the capacity of bacterial cells to uptake and respond to them. The levofloxacin loaded silver nanocapsules (L-Ag-NCps) proved as good alternative anti-bacterial agent to address MDR in pneumococcal cells by membrane disruption and ROS generation, by utilizing combined potential of silver and drug (Levofloxacin). These nanocapsules found to be potential antibacterial candidates, which act by endosomal escaping and break resistance in bacterial cells. Such nanomaterials based solutions, though still in infancy, are highly desired to address MDR and will be highly appreciated globally, especially in the third-world/developing countries, which are currently at the brink of resistant microbe's dominance.

## Chapter 7.

### Summary and Future Perspectives

Ag based nanoclusters were quite unexplored until 2009 despite of their wonderful therapeutic efficiency. We, therefore, set out to explore the applications of silver nanoclusters to address a serious global healthcare challenge i.e., multidrug resistance. The findings of this study offer the fundamental knowledge and a potential use to address MDR using silver-based nanoclusters coated with cationic ligands such as polyethylenimine. These nanoclusters have provided remarkable therapeutic applications at concentrations safe to mammalian cells, which aided in understanding the mechanistic profile and demonstrating the cellular interactions of such nanomaterials with normal and resistant bacterial cells. The small size (2 nm), stable nature (more than a month), organic capping (PEI), compact coating, selective targeting (electrostatically), sustained discharge of Ag<sup>+</sup> ions and the positive surface potential (+30mV) are the key attributes of these nanoclusters to demonstrate their ability to kill different MDR bacterial strains. These Ag NCs were found very effective to kill 12 MDR clinical bacterial strains (uropathogenic) at minimal concentration of ~1 nM.

In another related application, the silver-based nanoclusters (3 nm) were used in comparison with silver nanoparticles (10 nm) to target *P. aeruginosa* biofilms via their network of extracellular amyloids. Both of these nanoparticles were prepared by chemical reduction method. Their anti-bacterial and antibiofilm study was done against *P. aeruginosa*. The mechanistic analysis was done with the help of TEM, SEM, HIM, fluorescence microscopy, ROS study, HSI. The comparative study of these nanomaterials revealed that with the change in surface charge and size of nanoparticles, their bactericidal and antibiofilm properties can be tuned. It was further observed that at concentrations of 1 μM or lower, both the bactericidal and antibiofilm potential of nanomaterials was linked with their structure based bionano communications but not with the discharge of silver ions. This study demonstrated the biocidal ability of safe nanotechnology through the unique direction of amyloidosis inhibition.

In another study, the emerging health issue related to MDR in pneumococcal cells was addressed by the design/development of smart and effective nanocapsules encapsulating antibiotic and silver NCs coated with organic ligands to guide the nanocapsules to the desired target. These NCps were synthesized using emulsion stabilization method and were quite stable with 20% of drug loading efficiency. The designed/developed nanocapsules have shown their potential of efficient targeting, delivering and retaining hydrophobic drug in the desired pneumococcal strains by breaking resistant barriers at concentrations safe to mammalian cells. This method is quite simple and easy to modify according to specific application.

The study of relationship of size, structure, drug loading, metal and type of the surface coated organic ligands, and the ability of bacterial cells to uptake such nanomaterials and respond to them in regard of anti-bacterial activity have generated a considerable knowledge. Moreover, these silver-based nanomaterials have great potential for additional structure-activity investigations by controlling their size, shape and surface chemistry and identifying the best possible materials with enhanced antibacterial activity. Such studies may also bring basic insights regarding the response of MDR bacterial strains against nanomaterials, and potentially viruses. At economical scale, cost involved in medicinal chemistry approaches to address MDR may be reduced by exploring such cost-effective and therapeutically superior alternative strategies.

One of the most important concern for the use of AgNPs in targeting bacteria is their effect on gut microbiota, out of which 99% are beneficial for us. In Chapter 5, for the first time we explored the effect of AgNPs on FapC amyloidosis, which is an important component of *P. aeruginosa* matrix. Similar proteins are also present in various other gut microbes so, they are also very likely to be affected. For this purpose, there is still a need for more selective approach design materials that can only target the pathogenic bacteria without affecting the useful bacteria. This study also prompted the need to explore gut-brain axis with reference to the influence of gut microbiota on various neurological disorders and vice versa. It has been observed that the various bacterial endotoxins plays a vital role in progression of neurological disorders.<sup>371</sup> For the future design of Nanomedicine, it is essential to consider

their effect in relation to gut microbes and the resulting implications on brain.<sup>372</sup> In this regard, Javed et al. has recently beautifully demonstrated an increase in A $\beta$  and IAPP amyloidosis by bacteria endotoxins and successive mitigation of amyloidosis by amphiphilic carbon quantum dots via H-bonding and hydrophobic interactions with amyloid peptides.<sup>373</sup> Additionally for future work, *in-vivo* and cytotoxicity studies of these nanomaterials need to be done on mouse models as well.

Another aspect that needs further attention for the use of AgNPs for any such applications is their specific targeting. The design and synthesis of Ag NPs with controlled surface chemistry and high bacterial selectivity might be an attractive strategy to address these problems. The coupling of nanocapsules with CRISPRs, a comparatively new technology, is very likely to offer the desired activity required to combat multidrug-resistant bacteria with enhanced selectivity.<sup>374</sup>

## References

1. Marlieke, E. A. K; Andrew, J. S.; Stephan, H., Will 10 Million People Die a Year due to Antimicrobial Resistance by 2050?. *PLoS Med* **2016**, 13, 1-6.
2. WHO GAP AMR Newsletter No.32, **2017**, 1-4.(<https://www.who.int/antimicrobial-resistance/news/WHO-GAP-AMR-Newsletter-No-32-Nov-2017.pdf?ua=1>).
3. WHO Antimicrobial resistance, **2018**.(<https://www.who.int/news-room/fact-sheets/detail/antimicrobial-resistance>).
4. Sean, R. N.; John, W. S.; Anand, G.; Catherine, J. M.; Tara, L. S., Targeted Photothermal Lysis of the Pathogenic Bacteria, *Pseudomonas aeruginosa*, with Gold Nanorods. *Nano Lett.* **2008**, 8, 1, 302–306.
5. Editorial, The case for action on childhood pneumonia, *The Lancet* **2017**, 390, 2122.
6. Orihuela, C. J.; Gao, G.; Francis, K. P.; Yu, J.; Tuomanen, E. I., Tissue-specific contributions of pneumococcal virulence factors to pathogenesis. *Journal of Infectious Diseases* **2004**, 190, 1661-1669.
7. Yuyun, Z.; Zeliang, C.; Yanfen, C.; Jie, X.; Jinghong, L.; Xingyu, J., Synergy of Non-antibiotic Drugs and Pyrimidinethiol on Gold Nanoparticles against Superbugs. *J. Am. Chem. Soc* **2013**, 135, 12940–12943.
8. Xinglong, Y.; Junchuan, Y.; Le, W.; Bei, R.; Yuexiao, J.; Lingmin, Z.; Guang, Y.; Huawu, S.; Xingyu, J., Pharmaceutical Intermediate-Modified Gold Nanoparticles: Against Multidrug-Resistant Bacteria and Wound-Healing Application via an Electrospun Scaffold. *ACS Nano* **2017**, 11, 5737-5745.
9. Extensively Drug-Resistant Typhoid Fever in Pakistan, *Centre for Disease Control and Prevention* **2019**.
10. Anton, Y.; Peleg, M. B.; David, C.; Hooper, M.D., Hospital-Acquired Infections Due to Gram-Negative Bacteria. *N Engl J Med.* **2010**, 362, 1804-1813.

11. Dini, C.; Fabbri, A.; Geraci, A., The potential role of garlic (*Allium sativum*) against the multi-drug resistant tuberculosis pandemic: a review. *Annali dell'Istituto superiore di sanità* **2011**, *47*, 465-473.
12. Kibria, G.; Hatakeyama, H.; Harashima, H., Cancer multidrug resistance: mechanisms involved and strategies for circumvention using a drug delivery system. *Archives of pharmacal research* **2014**, *37*, 4-15.
13. Vinayak, A.; Satish, K. N., Antibiotics for Emerging Pathogens. *Infectious Diseases*, Springer **2012**, 7-26.
14. Walsh, C., Molecular mechanisms that confer antibacterial drug resistance. *Nature* **2000**, *406*, 775-781.
15. Appelbaum, P.; Hunter, P., The fluoroquinolone antibacterials: past, present and future perspectives. *International journal of antimicrobial agents* **2000**, *16*, 5-15.
16. Hiroshi, N., Multidrug Resistance in Bacteria. *Annu Rev Biochem* **2009**, *78*, 119–146.
17. Michael A. F.; Christopher, T. W., Antibiotics for emerging pathogens. *Science* **2009**, *325*, 1089-1093.
18. Dini, C.; Fabbri, A.; Geraci, A., The potential role of garlic (*Allium sativum*) against the multi-drug resistant tuberculosis pandemic: a review. *Annali dell'Istituto superiore di sanità* **2011**, *47*, 465-473.
19. Catia, D.; Alessia, F.; Andrea, G., The functions and structure of ABC transporters: implications for the design of new inhibitors of Pgp and MRP1 to control multidrug resistance (MDR). *Current drug targets* **2006**, *7*, 893-909.
20. Akash, G.; Neveen, M S.; Riddha, D.; Ryan, F. L.; Arafah, B.; Khatereh, M.; Alexandre, R. C.; Kenneth, P.; Morteza, M.; Vincent, M. R., Synergistic antimicrobial therapy using nanoparticles and antibiotics for the treatment of multidrug-resistant bacterial infection, *Nano Futures* **2017**, *1*, 1-10.
21. Donald, M. N. S., The Multi-target drug design era is here, consider it, *Drug designing* **2012**, *1*, 1-2.
22. Ramanan, L.; Thomas, V. B.; Isabel, F.; Samuel, K.; Ejaz, A. K.; Direk, L.; D. G. Joakim, L.; Gabriel, L.; Marc, M.; Kevin, O.; Sharon, J. P.; Yong-Guan, Z., *The Lancet Infectious Diseases*

- Commission on antimicrobial resistance: 6 years later. *Lancet Infect Dis* **2020**, 20, 30003-30007.
23. Brooks, B. D.; Brooks, A. E., *Advanced drug delivery reviews* **2014**, 78, 14.
24. Wenzel, R. P.; Edmond, M. B., Managing antibiotic resistance. *New England Journal of Medicine* **2000**, 26, 1961-1963.
25. Federico, P.; David, V. D., Carbapenem-resistant Enterobacteriaceae: a menace to our most vulnerable patients. *Cleveland Clinic journal of medicine* **2013**, 4, 225-33.
26. Carolus, A. C., Society must seize control of the antibiotics crisis. *Nature* **2016**, 533, 439.
27. Thomas A. S.; Joan B., Resistance to Nalidixic Acid. *JAMA* **1976**, 236, 1857-1860.
28. César, A. M.; Leonardo, J. M.; Eugene, J. G.; Guillermo, G., Epidemic Shiga-Bacillus dysentery in Central America derivation of the epidemic and its progression in Guatemala, 1968–68. *The American Journal of Tropical Medicine and Hygiene* **1971**, 20, 927-933.
29. Ana, S., Drug resistance: Does antibiotic use in animals affect human health? *Medical News Today* **2018**.
30. Charles, W. S., Linking TB and the environment: An overlooked mitigation strategy. *Environ Health Perspect* **2008**, 116, A478–A485.
31. Kohanski, M., Dwyer, D. & Collins, J. How antibiotics kill bacteria: from targets to networks. *Nat Rev Microbiol* **2010**, 8, 423–435
32. Zeinab, B.; Buthaina, J.; Rafik, K., Action and resistance mechanisms of antibiotics: A guide for clinicians. *Molecules* **2020**, 25, 1340.
33. Juillerat-Jeanneret, L.; Schmitt, F., Chemical Modification of Therapeutic Drugs or Drug Vector Systems to Achieve Targeted Therapy: Looking for the Grail. *Medicinal Research Reviews* **2007**, 27, 574-590.
34. Nicole, A. L.; Andrew, D. S. C., Horizontal transfer of antibiotic resistance genes in clinical environments. *Can J Microbiol* **2019**, 65, 34-44.
35. Martin, E.; Sanjay, B.; Bärbel, C.; Jürgen, G.; Peter, G.; Philippe, H.; Peter, H.; Carola, I.; Axel, K.; Elaine, L.; Wolfgang, M.; Martin, M.; Peter, O.; Birgit, R.; Manfred, R.; Ricarda, M. S.; Hans-Günther, S.; Matthias, T., Antibiotic resistance: What is so special about Multidrug-resistant Gram-negative bacteria? *GMS Hyg Infect Control* **2017**, 12, 1-24

36. Silpak, B.; Jean-Michel, B.; Jean-Christophe, D.; Martine, R.; Jean-Marc, R., Colistin: an update on the antibiotic of the 21st century. *Expert Rev Anti Infect Ther* **2012**, *8*, 917-934.
37. Angela, H. D.; Alex, S.; Paul, H.; Jonathan, S. W., A critical role for amino-terminal glutamine/asparagine repeats in the formation and propagation of a yeast prion. *Cell* **1998**, *93*, 1241–1252.
38. Rodney, M. D., Biofilm elimination on intravascular catheters: Important considerations for the infectious disease practitioner. *CID* **2011**, *52*, 1038-1045.
39. Meng-Hua, X.; Yan, B.; Xian-Zhu, Y.; Yan-Hua, Z.; Jun, W., Delivery of antibiotic with polymeric particles. *Adv Drug Deliv Rev* **2014**, *78*, 63-76.
40. Cherie, R. K.; Laura, E. F.; Yury, G.; Paula, T. H.; Mark, C. H.; Andre, E. N.; Reginald, M. P.; Paul, S. W., Nano day: Celebrating the next decade of nanoscience and nanotechnology. *ACS.Nano* **2016**, *10*, 1021-1031.
41. Aastha, C.; Ziad, S.; David, C.; Helen, H., Global contributors to antibiotic resistance. *J Glob Infect Dis* **2019**, *11*, 36–42.
42. Ping, H.; Junping, A.; Linzhu, Z.; Yue, S.; Wei, H.; Xinyuan, Z.; Deyue, Y., A facile approach to construct ternary cocktail nanoparticles for cancer combination therapy. *Bioconjugate chemistry* **2016**, *27*, 1564-1568.
43. Aaron, G.; Biswanath, M.; Andrew, D.; Sudharshan, R.; David, G.; Mohammad, K.; Pradip, K. M.; Shiladitya, S., Temporally sequenced anticancer drugs overcome adaptive resistance by targeting a vulnerable chemotherapy-induced phenotypic transition. *Nat. Commun.* **2015**, *6*, 6139.
44. O'Brien, M. E. R., Reduced cardiotoxicity and comparable efficacy in a phase III trial of PEGylated liposomal doxorubicin HCl (CAELYXTM/Doxil™) versus conventional doxorubicin for first-line treatment of metastatic breast cancer. *Ann. Oncol* **2004**, *15*, 440–449.
45. Erika, C. H., *Nature* **2015**, 7510, 620.
46. Benjamin, D. B.; Amanda, E. B., Therapeutic strategies to combat antibiotic resistance. *Advanced drug delivery reviews* **2014**, *78*, 14.
47. Joseph, A. D.; Henry, G. G., The cost of biopharmaceutical R&D: Is biotech different? *Managerial and Decision Economics* **2007**, *28*, 469–479.

48. Thomas, J. D.; Danielle, B.; John, F. B., New quinolones and the impact on resistance. *DDT* **2001**, 6, 529-536.
49. Gan, L.; Peng, M.; Chengchao, C.; Jun, Z.; Gang, L., Inorganic nanocarriers overcoming multidrug resistance for cancer theranostics. *Advanced Science* **2016**, 10, 1600120-1600134
50. Caitriona, H.; Sandra, V. S.; Daniel, B. L.; Patrick, G. J., Cancer drug resistance: an evolving paradigm. *Nature Reviews Cancer* **2013**, 13, 714-726
51. National institute of biomedical imaging and bioengineering. Overcoming multidrug-resistant cancer with smart nanoparticles. *Science Daily* **2016**.
52. Qingmei, Y.; Kai, L.; Qun, S.; Qingyue, L.; Jinghui, H.; Fangxuan, Han.; Ren-Wang, J., Reversal of multidrug resistance in cancer by multi-functional flavonoids. *Front. Oncol* **2019**, 9, 1-16.
53. Assaf, G.; Keren, C. M.; Dan, P., Overcoming multidrug resistance with nanomedicines. *Expert Opin. Drug Delivery* **2015**, 12, 223–238.
54. Vladimir, P. T., Multifunctional, stimuli-sensitive nanoparticulate systems for drug delivery. *Nat. Rev. Drug Discovery* **2014**, 13, 813–827.
55. Hasan, M., Breast cancer kills 40,000 women in Pakistan every year: experts. Dawn NEWS **2015**, <http://www.dawn.com/news/1215772>.
56. Baran, S.; Jinming, G., Theranostic nanomedicine for cancer. *Nanomedicine (Lond)* **2008**, 3, 137-140.
57. Fabienne, D.; Olivier, F.; Véronique, P., To exploit the tumor microenvironment: passive and active tumor targeting of nanocarriers for anti-cancer drug delivery. *Journal of Controlled Release* **2010**, 148, 135-146.
58. Emiliano, R. M., Alarming surge in drug-resistant HIV uncovered. *Nature* **2019**.
59. Kasturi, H., From cell and organismal biology to drugs. *PLoS Pathogens* **2015**, 11, 1-2.
60. Helen, W. B.; George, H. T.; Daniel, K. B.; John, B.; Robert, J. G.; Ronald, N. Jones.; Barbara, E. M.; Robert, A. B.; David, G., 10x'20 Progress—Development of new drugs active against Gram-Negative Bacilli: An update from the infectious diseases society of America. *IDSA* **2013**, 56, 1685–94.
61. Gonçalo, D.; João, C.; Bruno, V.; Leticia, G.; C, A.; Maria, A.; João, R.; Pedro, V. B., Noble metal nanoparticles for biosensing applications. *Sensors* **2012**, 12, 1657-1687.

62. Estefânia, V. R. C.; Anderson, E. S. P.; Jhones, L. O.; Lucas, B. C.; Mariana, G.; Renata, L.; Leonardo, F. F., How can nanotechnology help to combat COVID-19? Opportunities and urgent need. *Journal of Nanobiotechnology* **2020**, *18*, 125.
63. Matthew, D. E.; Nicole, M. S.; Karen, E. F.; Saber, M. H.; Glenn, R. J., Lysozyme catalyzes the formation of antimicrobial silver nanoparticles. *ACS Nano* **2009**, *3*, 984–994.
64. Yuyun, Z.; Yue, T.; Yan, C.; Wenwen, L.; Wanshun, M.; Xingyu, J., Small molecule-capped gold nanoparticles as potent antibacterial agents that target Gram-Negative bacteria. *J. Am. Chem. Soc* **2010**, *132*, 12349–12356.
65. Tianmeng, S.; Yu, S. Z.; Bo, P.; Dong, C. H.; Miaoxin, Y.; Younan, X.; Engineered nanoparticles for drug delivery in cancer therapy. *Angew. Chem. Int. Ed.* **2014**, *53*, 2 – 47.
66. Zhentao, L.; Vairavan, N.; Bin, Z.; Ning, Y.; David, T. L.; De-en, J.; Jianping, X., Toward understanding the growth mechanism: tracing all stable intermediate species from reduction of Au (I)–thiolate complexes to evolution of Au<sub>25</sub> nanoclusters. *Journal of the American Chemical Society* **2014**, *136*, 10577-10580.
67. Yong-Siou, C.; Prashant, V. K., Glutathione-capped gold nanoclusters as photosensitizers. Visible light-induced hydrogen generation in neutral water. *Journal of the American Chemical Society* **2014**, *136*, 6075-6082.
68. Bootharaju, M.; Pradeep, T., Investigation into the reactivity of unsupported and supported Ag<sub>7</sub> and Ag<sub>8</sub> clusters with toxic metal ions. *Langmuir* **2011**, *27*, 8134-8143.
69. Bootharaju, M.; Deepesh, G.; Udayabhaskararao, T.; Pradeep, T., Atomically precise silver clusters for efficient chlorocarbon degradation. *Journal of Materials Chemistry A* **2013**, *1*, 611-620.
70. Wang, S.; Jin, S.; Yang, S.; Chen, S.; Song, Y.; Zhang, J.; Zhu, M., Total structure determination of surface doping [Ag<sub>46</sub>Au<sub>24</sub> (SR)<sub>32</sub>](BPh<sub>4</sub>)<sub>2</sub> nanocluster and its structure-related catalytic property. *Science advances* **2015**, *1*, e1500441.
71. Zheng, K.; Yuan, X.; Goswami, N.; Zhang, Q.; Xie, J., Recent advances in the synthesis, characterization, and biomedical applications of ultrasmall thiolated silver nanoclusters. *RSC Advances* **2014**, *4*, 60581-60596.

72. Mathew, A.; Pradeep, T., Noble metal clusters: applications in energy, environment, and biology. *Particle & Particle Systems Characterization* **2014**, *31*, 1017-1053.
73. Abdul, Halim, L. G.; Ashraf, S.; Katsiev, K.; Kirmani, A. R.; Kothalawala, N.; Anjum, D. H.; Abbas, S.; Amassian, A.; Stellacci, F.; Dass, A., A scalable synthesis of highly stable and water dispersible Ag 44 (SR) 30 nanoclusters. *Journal of Materials Chemistry A* **2013**, *1*, 10148-10154.
74. Abdul, Halim, L. G.; Kothalawala, N.; Sinatra, L.; Dass, A.; Bakr, O. M., Neat and complete: Thiolate-ligand exchange on a silver molecular nanoparticle. *Journal of the American Chemical Society* **2014**, *136*, 15865-15868.
75. Bootharaju, M. S.; Joshi, C. P.; Alhilaly, M. J Bakr, O. M., Switching a nanocluster core from hollow to nonhollow. *Chemistry of Materials* **2016**, *28*, 3292-3297.
76. Jayanta, K. P.; Kwang-Hyun, B., Antibacterial activity and synergistic antibacterial potential of biosynthesized silver nanoparticles against foodborne pathogenic bacteria along with its anticandidal and antioxidant effects. *Front. Microbiol* **2017**, *8*, 1-14.
77. Jie, Y.; Nan, X.; Xinan, W.; Xianhu, L.; An, X.; Zhikun, W.; Zhixun, L., One-pot one-cluster synthesis of fluorescent and bio-compatible Ag 14 nanoclusters for cancer cell imaging. *Nanoscale* **2015**, *7*, 18464-18470.
78. Naoki, N.; Hiroshi, Y.; Tomoyasu, U.; Akito, S.; Keisaku, K., Synthesis and chiroptical study of d/lPenicillamine-capped silver nanoclusters. *Chemistry of materials* **2007**, *19*, 2831-2841.
79. Shahed, B.; Vahid, S.; Wei, T.; Majd, A. H.; Mahmoud, Y. A.; Erik, C. D.; Dennis, B.; Alaaldin, M. A.; Omid, C. F.; Morteza, M., Cellular uptake of nanoparticles: Journey inside the cell. *Chem Soc Rev.* **2017**, *46*, 4218–4244.
80. Linda, C. S.; Edgar, G.; Andreas, S.; Eudald, C.; Albert, D.; Victor, P.; Gertie, J. O., Shape matters: effects of silver nanospheres and wires on human alveolar epithelial cells. *Particle and Fibre Toxicology* **2011**, *8*, 1-15.
81. Min, L.; Shao, S.; Yao, H.; Qing, H.; Wenbing, H.; Di, L.; Chunhai, F.; Shuit-Tong, L., Long-term antimicrobial effect of silicon nanowires decorated with silver nanoparticles. *Adv. Mater* **2010**, *22*, 5463–5467.

82. Youngmin, S.; Jangsun, H.; Jieun, K.; Yoon, J.; Mintai, P. H.; Jonghoon, C., Antibacterial activity and cytotoxicity of multi-walled carbon nanotubes decorated with silver nanoparticles. *International Journal of Nanomedicine* **2014**, *9* 4621–4629.
83. Essam, N. S.; Maged, S. A.; Manal, M. Y.; Noor, E., Anti-microbiological activities of bio-synthesized silver Nano-stars by *Saccharopolyspora hirsute*. *Saudi Journal of Biological Sciences* **2019**, *26*, 195–200.
84. Babak, S.; Farshid S. G.; M. Hashemi; H. R. Nezhad; A. Nasrollahi; Sima, A.; Sahar, A., comparison of the anti-bacterial activity on the nanosilver shapes: Nanoparticles, nanorods and nanoplates. *Advanced Powder Technology* **2012**, *23*, 22–26.
85. Fouzia, T.; Atif, Y.; Shazia, T.; William, A. A., Poly-L-arginine coated silver nanoprisms and their anti-bacterial properties. *Nanomaterials* **2017**, *7*, 296-311.
86. Nien-Chu, F.; Fong-Yu, C.; Ja-an Annie, H.; Chen-Sheng, Y., Photocontrolled targeted drug delivery: Photocaged biologically active folic acid as a light-responsive tumor-targeting molecule. *Angewandte Chemie International Edition* **2012**, *51*, 8806-8810.
87. Akash, G.; Shazia, M.; Cheng-Hsuan, L.; Irshad, H.; Vincent, M. R., Combatting antibiotic-resistant bacteria using nanomaterials. *Chem. Soc. Rev* **2019**, *48*, 415-442.
88. Giuseppina, B.; Agnese, M., Liposomes as nanomedical devices. *Int J Nanomedicine* **2015**, *10*, 975-999.
89. Nadia, A.; Patrick, C., Nanocarriers for antibiotics: A promising solution to treat intracellular bacterial infections. *International journal of antimicrobial agents* **2014**, *43*, 485-496.
90. Xiaoning, L.; Sandra, M. R.; Akash, G.; Krishnendu ,S.; Ziwen, J.; Daniel, F. M.; Ali, S.; Margaret, A. R.; Vincent, M. R., Functional gold nanoparticles as potent antimicrobial Aagents against multi-drug resistant bacteria. *ACS Nano* **2014**, *8*, 10682–10686.
91. Hongwei, G.; P. L. Ho; Edmond, T.; Ling, W.; Bing, X., Presenting vancomycin on nanoparticles to enhance antimicrobial activities. *Nano Letters* **2003**, *3*, 1261-1263.
92. Muhammad, R.; Saba, M.; Bhatti, T. M.; Akhter, J. I.; Abdul, H.; Wasim, Y.; Ul-Hasan, M. M., Investigations into the antibacterial behavior of copper nanoparticles against *Escherichia coli*. *Annals of microbiology* **2010**, *60*, 75-80.

93. Guogang, R.; Dawei, H.; Eileen, W.C.; Miguel, A. V.; Paul, R.; Robert, P. A., Characterisation of copper oxide nanoparticles for antimicrobial applications. *International journal of antimicrobial agents* **2009**, *33*, 587-590.
94. Nathaniel, C. C.; Jason, L. B.; Aaron, D. S., Copper-based nanostructured coatings on natural cellulose: Nanocomposites exhibiting rapid and efficient inhibition of a multi-drug resistant wound pathogen, *A. baumannii*, and mammalian cell biocompatibility *in-vitro*. *Advanced Functional Materials* **2011**, *21*, 2506-2514.
95. Wang, Y.; Yang, F.; Zhang, H.; Zi, X.; Pan, X.; Chen, F.; Luo, W.; Li, J.; Zhu, H.; Hu, Y., Cuprous oxide nanoparticles inhibit the growth and metastasis of melanoma by targeting mitochondria. *Cell death & disease* **2013**, *4*, e783.
96. Ruchira, C.; Tarakdas, B., Metallic copper nanoparticle induces apoptosis in human skin melanoma, A-375 cell line. *Nanotechnology, at press*: **2017**, *25*, 135101-135134.
97. Ye, W.; Xiao-Yuan, Z.; Juan, S.; Hong-Xia, Z.; Xin-Rong, Z.; Hai-Ying, Z.; Jian-Xiu, L.; Meng, Y.; Feng, Y.; Yi-Ping, H., Cuprous oxide nanoparticles selectively induce apoptosis of tumor cells. *International journal of nanomedicine* **2012**, *7*, 2641-2652.
98. Ae, J. H.; Young, J. K., "Nanoantibiotics": a new paradigm for treating infectious diseases using nanomaterials in the antibiotics resistant era. *Journal of Controlled Release* **2011**, *156*, 128-145.
99. Qiang, Y.; Jeremy, B. F., Sulfhydryl binding sites within bacterial extracellular polymeric substances. *Environmental science & technology* **2016**, *50*, 5498–5505.
100. Rai, M.; Deshmukh, S.; Ingle, A.; Gade, A., Silver nanoparticles: the powerful nanoweapon against multidrug-resistant bacteria. *Journal of applied microbiology* **2012**, *112*, 841-852.
101. Zong-ming, X.; Qing-bo, Z.; Hema, L. P.; Vicki, L. C.; Pedro, J. J. A., Negligible particle-specific antibacterial activity of silver nanoparticles. *Nano Lett.* **2012**, *12*, 4271–4275.
102. Drinking Water and Health: Volume 2. <https://www.ncbi.nlm.nih.gov/books/NBK234590/>
103. Elvio, A.; Yuri, A. D.; Angelo, T.; Piersandro, P.; Luca, P.; Lucia, C.; Chiara, M.; Pietro, G.; Cesare, D.; Jose, M. F. H.; Vittorio, N., Synthesis, Characterization and antibacterial activity against Gram Positive and Gram Negative bacteria of biomimetically coated silver nanoparticles. *Langmuir* **2011**, *15*, 9165-73.

104. Kaiyuan, Z.; Magdiel, I. S.; Tze-Peng, L.; David, T. L.; Jianping, X., Antimicrobial cluster bombs: Silver nanoclusters packed with daptomycin. *ACS Nano* **2016**, *10*, 8, 7934–7942.
105. Samuel, N. N.; Lucy, O.; Eric, M.; Margaret, N., One-pot microwave-assisted synthesis of size-dependent L-glutathione-capped spherical silver nanoparticles suitable for materials with antibacterial properties. *ISSN* **2019**, *4*, 86-94.
106. Doria, G.; Conde, J.; Veigas, B.; Giestas, L.; Almeida, C.; Assunção, M.; Rosa, J.; Baptista, P. V., Noble metal nanoparticles for biosensing applications. *Sensors* **2012**, *12*, 1657-1687.
107. Meng, X.; Liu, Z.; Zhu, M.; Jin, R., Controlled reduction for size selective synthesis of thiolate protected gold nanoclusters Aun (n= 20, 24, 39, 40). *Nanoscale research letters* **2012**, *7*, 277-284.
108. Basiruddin, S.; Chakraborty, A., One step synthesis of maltose functionalized red fluorescent Ag cluster for specific glycoprotein detection and cellular imaging probe. *RSC Advances* **2014**, *4*, 43098-43104.
109. Yang, H.; Wang, Y.; Huang, H.; Gell, L.; Lehtovaara, L.; Malola, S.; Häkkinen, H.; Zheng, N., Allthiol-stabilized Ag<sub>44</sub> and Au<sub>12</sub>Ag<sub>32</sub> nanoparticles with single-crystal structures. *Nature communications* **2013**, *4*, 1-8.
110. Ruiyi, L.; Huiying, W.; Xiaoyan, Z.; Xiaoqing, L.; Xiulan, S.; Zaijun, L., d-Penicillamine and bovine serum albumin co-stabilized copper nanoclusters with remarkably enhanced fluorescence intensity and photostability for ultrasensitive detection of Ag<sup>+</sup>. *New Journal of Chemistry* **2016**, *40*, 732-739.
111. Aaron, G.; Ashish, K.; Mohammad, K.; Prithvi, P.; Poornima, R.; Siva, K. N.; Venkata, S.; Shiladitya, S., Rationally designed 2-in-1 nanoparticles can overcome adaptive resistance in cancer. *ACS nano* **2016**, *10*, 5823-5834
112. Mandeep, S. B.; Harpreet, K.; Tarlok, S. B.; Narpinder, S.; Gurinder, K., Biomineralization of gold nanoparticles by lysozyme and cytochrome C and their applications in protein film formation, *Langmuir* **2010**, *26*, 13535–13544.
113. Chen, Z.; Lu, D.; Cai, Z.; Dong, C.; Shuang, S., Bovine serum albumin-confined silver nanoclusters as fluorometric probe for detection of biothiols. *Luminescence* **2014**, *29*, 722-727.

114. Daniel, M. C.; Amares, C.; Peng, Z., Properties and applications of protein stabilized fluorescent gold nanoclusters: short review, *Journal of Nanophotonics* **2012**, 6, 1-16.
115. Jie, Y.; Nan, X.; Xinan, W.; Xianhu, L.; An, X.; Zhikun, W.; Zhixun, L., One-pot one-cluster synthesis of fluorescent and bio-compatible Ag 14 nanoclusters for cancer cell imaging. *Nanoscale* **2015**, 7, 18464-18470.
116. Zong-ming, X.; Qing-bo, Z.; Hema, L. P.; Vicki, L. C.; Pedro, J. J. A., Negligible particle-specific antibacterial activity of silver nanoparticles. *Nano letters* **2012**, 12, 4271-4275.
117. Xiaoming, Y.; Yuanjiao, F.; Shanshan, Z.; Yawen, L.; Yan, Z.; Yao, D., One-step synthesis and applications of fluorescent Cu nanoclusters stabilized by L-cysteine in aqueous solution. *Analytica chimica acta* **2014**, 847, 49-54.
118. Poovathinthodiyil, R.; Jie, F.; Scott, L. W., A simple and “green” method for the synthesis of Au, Ag, and Au–Ag alloy nanoparticles. *Green Chemistry* **2006**, 8, 34-38.
119. Xin, Z.; Meinan, Y.; Muhua, C.; Liqiang, L.; Chengyan, D.; Yi, H.; Huiyun, Z.; Bing, Jia.; Fan, W., Hyaluronic acid-coated silver nanoparticles as a nanoplatform for *in-vivo* imaging applications. *ACS Applied Materials & Interfaces* **2016**, 8, 25650-25653.
120. Zheng, H.; Yogesh, V. S.; Yang, L.; Feiqing, D.; Jothy, L. S.; Vikashini, R.; Rubí, Z.; Damien, K.; Huiwen, L.; Moon, Y. F. T.; Surajit, B.; Scott, A. R.; Jian, S.; Hongwei, D.; Xue-Wei, L.; Yuguang, M.; Nguan, S. T.; Kam, C. T.; Kevin, P.; Mary, B. C., Nanoparticles of short cationic peptidopolysaccharide self-assembled by hydrogen bonding with antibacterial effect against multidrug resistant bacteria. *ACS Appl. Mater. Interfaces* **2017**, 9, 38288–38303.
121. Daniel, J.; Robert, P.; Donald, F. W.; Peng, Z., Structure of tiopronin-protected silver nanoclusters in a one-dimensional assembly. *J. Phys. Chem. C* **2015**, 119, 43, 24627–24635.
122. Linlin, W.; Chen, H.; Longquan, S., The antimicrobial activity of nanoparticles: Present situation and prospects for the future. *Int. J. Nanomed.* **2017**, 12, 1227–1249.
123. Urawadee, R.; Vijayalekshmi, S., Recent developments in antimicrobial-peptide-conjugated gold nanoparticles. *Bioconjug Chem* **2017**, 28, 2673-2686.
124. Muhammad, R.; F. Hussain.; Tariq, M. B.; J. I. Akhter; Abdul, H.; Masood, M. H., Antibacterial characterization of silver nanoparticles against *E. Coli* ATCC-15224. *Journal of Materials Science and Technology* **2007**, 24,192-196.

125. Sonja, E.; Priscilla, S. B.; Jacinthe, G.; Magdalena, P.; Bernd, G.; Katharina, M. F., Nanobio silver: Its interactions with peptides and bacteria, and its uses in medicine. *Chem. Rev.* **2013**, *113*, 4708–4754.
126. Reiko, S.; Kenichi, N.; Pamela, S. S.; Haitian, L.; Chi-Huey, W.; Akarat, S.; Fusao, T.; Kenji, M.; Shin-Ichiro, N.; Cell-wall engineering of living bacteria. *J Am Chem Soc* **2002**, *124*, 9018-9029.
127. Yun'an, Q.; Lin, C.; Ruiyan, L.; Guancong, L.; Yanbo, Z.; Xiongfeng, T.; Jincheng, W.; He, L.; Yanguo, Q., Potential antibacterial mechanism of silver nanoparticles and the optimization of orthopedic implants by advanced modification technologies. *Int J Nanomedicine* **2018**, *13*, 3311–3327.
128. Tikam, C. D.; Anu, K.; Rita, S. M.; Vinod, Y., Mechanistic basis of antimicrobial actions of silver nanoparticles. *Front Microbiol* **2016**, *7*, 1-17.
129. Xi-Feng, Z.; Wei, S.; Sangiliyandi, G., Silver nanoparticle-mediated cellular responses in various cell lines: An *in-vitro* model. *Int J Mol Sci* **2016**, *17*, 1603-1629.
130. Carmen, L.; Simone, B.; Veronica, C.; Paola, Z.; Ivan, M.; Federica, G.; Michela, Z.; Lisa, B.; Giancarlo, B.; Antonia, R., Antibacterial activity of silver nanoparticles: sensitivity of different *Salmonella serovars*. *Front. Microbiol.* **2014**, *5*, 1-9.
131. Angelo, F.; Johannes, Z.; Alysha, G. E.; Murray, B.; Stefan, B.; Christopher, B.; Feng, C.; Christopher, D.; Gilles, D.; Nicole, J.; A. Paden, K.; Ahmed, M. M.; Massimiliano, M.; John, M.; Heba, A. M.; Anna, K. R.; Peter, J. R.; Peter, J. S.; Matthew, H. T.; Charlotte, E. W.; Justin, J. W.; Matthew, A. C.; Mark, A. T. B., Metal complexes as a promising source for new antibiotics. *Chem. Sci.* **2020**, 1-23.
132. Russell, A. D.; Hugo, W. B., Antimicrobial activity and action of silver. *Prog Med Chem* **1994**, *31*, 351–370.
133. Moyer, C. A.; Brentano, L.; Gravens, D. L.; Margraf, H. W.; Monafo, W., Treatment of large human burns with 0.5 per cent silver nitrate solution. *Arch Surg* **1965**, *90*, 812–867
134. Cason, J. S.; Lowbury, E. J., Mortality and infection in extensively burned patients treated with silver-nitrate compresses. *Lancet* **1968**, *1*, 651–654.

135. Modak, S. M.; Sampath, L.; Fox, C. L., Combined topical use of silver sulfadiazine and antibiotics as a possible solution to bacterial resistance in burn wounds. *J Burn Care Rehabil* **1988**, 9, 359–363.
136. Klasen, H. J., A historical review of the use of silver in the treatment of burns. II. Renewed interest for silver. *Burns* **2000**, 26, 131–138.
137. British National Formulary. *Oxford: Pharmaceutical Press* **2011**, Issue 58.
138. Nermin, E. E.; Ayat, A.; Sahar, B. H.; Mahmoud, M. O., Nanomedicine fight against antibacterial resistance: An overview of the recent pharmaceutical innovations. *Pharmaceutics* **2020**, 12, 142-191.
139. Harold, C. N., The crisis in antibiotic resistance. *Science* **1992**, 257, 1064–1073.
140. Linlin, W.; Chen, H.; Longquan, S., The antimicrobial activity of nanoparticles: present situation and prospects for the future. *Int. J. Nanomed.* **2017**, 12, 1227–1249.
141. Ventola, C. L., The antibiotic resistance crisis: part 1: causes and threats. *P T A peer-reviewed J. Formul. Manag.* **2015**, 40, 277–283.
142. Hajipour, M. J.; Fromm, K. M.; Akbar, A.; Jimenez de Aberasturi, D.; de Larramendi, I. R.; Rojo, T.; Serpooshan, V.; Parak, W. J.; Mahmoudi, M., Antibacterial properties of nanoparticles. *Trends Biotechnol.* **2012**, 30, 499–511.
143. Choi, O.; Deng, K. K.; Kim, N. J.; Ross, L. J.; Surampalli, R. Y.; Hu, Z., The inhibitory effects of silver nanoparticles, silver ions, and silver chloride colloids on microbial growth. *Water Res.* **2008**, 42, 3066–3074.
144. Yuan-Chieh, Y.; Tse-Hung, H.; Shih-Chun, Y.; Chin-Chang, C.; Jia-You, F., Nano-based drug delivery or targeting to eradicate bacteria for infection mitigation: A review of recent advances. *Front. Chem.* **2020**, 8, 286-308.
145. Fatemeh, F.; Amir, G.; Omid, G.; Amir, R.; Mahdi, K.; Michael, R. H., Nanopharmaceuticals and nanomedicines currently on the market: challenges and opportunities. *Nanomedicine (Lond.)* **2019**, 10, 2217-2250.
146. Schacht, V. J.; Neumann, L. V.; Sandhi, S. K.; Chen, L.; Henning, T.; Klar, P. J.; Theophel, K.; Schnell, S.; Bunge, M.; Effects of silver nanoparticles on microbial growth dynamics. *J Appl Microbiol* **2012**, 114, 25–35.

147. Prasher, P.; Singh, M.; Mudila, H., Green synthesis of silver nanoparticles and their antifungal properties. *BioNanoScience* **2018**, *8*, 254–263.
148. Bajaj, M.; Pandey, S. K.; Nain, T.; Brar, S. K.; Singh, P.; Singh, S., Stabilized cationic dipeptide capped gold/silver nanohybrids: Towards enhanced antibacterial and antifungal efficacy. *Colloids Surf. B Biointerfaces* **2017**, *158*, 397–407.
149. Haibo, W.; Aixin, Y.; Zhigang, L.; Xinming, Y.; Zeling, X.; Yuchuan, W.; Runming, W.; Mohamad, K.; Ligang, H.; Wei, X.; Huiru, T.; Yulan, W.; Hongyan, L.; Hongzhe, S., Deciphering molecular mechanism of silver by integrated omic approaches enables enhancing its antimicrobial efficacy in *E. coli*. *PLoS Biol* **2019**, *17*, 1-31.
150. Haibo, W.; Minji, W.; Xinming, Y.; Xiaohan, X.; Quan, H.; Aixin, Y.; Menglong, H.; Ryszard, L.; Hongyan, L.; Hongzhe, S., Antimicrobial silver targets glyceraldehyde-3- phosphate dehydrogenase in glycolysis of *E. coli*. *Chem. Sci.*, **2019**, *10*, 7193-7199.
151. Marambio-Jones, C.; Hoek, E. M. V., A review of the antibacterial effects of silver nanomaterials and potential applications for human health and the environment. *J Nanopart Res* **2010**, *12*, 1531–1551.
152. Choi, O.; Hu, Z., Size dependent and reactive oxygen species related nanosilver toxicity to nitrifying bacteria. *Environ. Sci. Technol.* **2008**, *42*, 4583–4588.
153. Zong-ming, X.; Qing-bo, Z.; Hema, L. P.; Vicki, L. C.; Pedro, J. A., Negligible particle-specific antibacterial activity of silver nanoparticles. *Nano Lett* **2012**, *12*, 4271-4275.
154. Rosaria, C.; Yael, A.; Mario, P., New antivirals and antibacterials based on silver nanoparticles. *Chem Med Chem* **2020**, 1-4.
155. Xiu, Z. M.; Zhang, Q. B.; Puppala, H. L., Negligible particle-specific antibacterial activity of silver nanoparticles. *Nano Lett* **2012**, *12*, 4271–4275.
156. Natalie, G.; Joe, L.; Kate, C.; Ying, Y.; Gordon, C.; Raymond, J. T. Using a chemical genetic screen to enhance our understanding of the antibacterial properties of silver. *Genes* **2018**, *9*, 344.
157. Zong-Ming, X.; Jie, M.; Pedro, J. J. A., Differential effect of common ligands and molecular oxygen on antimicrobial activity of silver nanoparticles versus silver ions. *Environ. Sci. Technol.* **2011**, *45*, 9003- 9008.

158. Sheng, Z.; Liu, Y., Potential impacts of silver nanoparticles on bacteria in the aquatic environment. *J Environ Manage* **2017**, 191, 290–296.
159. Xiao, C.; Hermann, J. S., Nanosilver: A nanoproduct in medical application. *Toxicology Letters* **2008**, 176, 1-12.
160. Steven, L. P.; Phillip, G. B.; Jayne, D., Antimicrobial activity of silver-containing dressings on wound microorganisms using an in vitro biofilm model. *Int. Wound J.* **2007**, 4, 186-91.
161. Gianluigi, F.; Annarita, F.; Stefania, G.; Luciana, P.; Mahendra, R.; Giancarlo, M.; Massimiliano, G., Silver nanoparticles as potential antibacterial agents. *Molecules* **2015**, 20, 8856-8874.
162. Le Ouay, B.; Stellacci, F., Antibacterial activity of silver nanoparticles: A surface science insight. *Nano Today* **2015**, 10, 339–354.
163. Gogoi, S. K.; Gopinath, P.; Paul, A.; Ramesh, A.; Ghosh, S. S.; Chattopadhyay, A., Green fluorescent protein-expressing *Escherichia coli* as a model system for investigating the antimicrobial activities of silver nanoparticles. *Langmuir* **2006**, 22, 9322–9328.
164. Maillard, J.; Hartemann, P., Silver as an antimicrobial: facts and gaps in knowledge. *Crit. Rev. Microbiol.* **2012**, 39, 373–383.
165. Pal, S.; Tak, Y. K.; Song, J. M., Does the antibacterial activity of silver nanoparticles depend on the shape of the nanoparticles? A study of the Gram negative bacterium *Escherichia coli*. *Appl. Environ. Microbiol.* **2007**, 73, 1712–1720.
166. Qin, Y.; Ji, X.; Jing, J.; Liu, H.; Wu, H.; Yang, W., Size control over spherical silver nanoparticles by ascorbic acid reduction. *Colloids Surf A Physicochem Eng Asp* **2010**, 372, 172–176.
167. Pillai, Z. S.; Kamat, P. V., What factors control the size and shape of silver nanoparticles in the citrate ion reduction method? *J Phys Chem B* **2004**, 108, 945–951.
168. Van, H. D. L.; Zukoski, C. F., Formation mechanisms and aggregation behavior of borohydride reduced silver particles. *Langmuir* **1998**, 14, 7034–7040.
169. Merga, G.; Wilson, R.; Lynn, G.; Milosavljevic, B.; Meisel, D., Redox catalysis on “naked” silver nanoparticles. *J Phys Chem C* **2007**, 111, 12220–12226.

170. Sambalova, O.; Thorwarth, K.; Heeb, N. V.; Bleiner, D.; Zhang, Y.; Borgschulte, A.; Kroll, A., Carboxylate functional groups mediate interaction with silver nanoparticles in biofilm matrix. *ACS Omega* **2018**, 3, 724–733.
171. Liu, Y-S.; Chang, Y-C.; Chen, H-H., Silver nanoparticle biosynthesis by using phenolic acids in rice husk extract as reducing agents and dispersants. *J Food Drug Anal* **2018**, 26, 649–656.
172. Battocchio, C.; Meneghini, C.; Fratoddi, L.; Venditti, L.; Russo, M. V.; Aquilanti, G.; Maurizio, C.; Bondino, F.; Matassa, R.; Rossi, M.; Mobilio, S.; Polzonetti, C., Silver nanoparticles stabilized with thiols: a close look at the local chemistry and chemical structure. *J Phys Chem C* **2012**, 116, 19571–19578.
173. Oliveira, M.; Ugarte, D.; Zanchet, D.; Zarbin, A.; Influence of synthetic parameters on the size, structure, and stability of dodecane thiol-stabilized silver nanoparticles. *J Colloid Interface Sci* **2005**, 292:429–435.
174. Dondi, R.; Su, W.; Griffith, G. A.; Clark, G.; Burley, G. A., Highly size and shape-controlled synthesis of silver nanoparticles via a templated tollens reaction. *Small* **2012**, 8, 770–776.
175. Zeinab, B.; Buthaina, J.; Rafik, K., Resistance of Gram-Negative bacteria to current antibacterial agents and approaches to resolve it. *Molecules* **2020**, 25, 1340-1363.
176. Zazo, H.; Colino, C. I.; Lanao, J. M., Current applications of nanoparticles in infectious diseases. *J. Control. Release* **2016**, 224, 86–102.
177. Veerapandian, M.; Lim, S.K.; Nam, H.M.; Kuppannan, G.; Yun, K.S., Glucosamine-functionalized silver glyconanoparticles: Characterization and antibacterial activity. *Anal. Bioanal. Chem.* **2010**, 398, 867–876.
178. Aymonier, C.; Schlotterbeck, U.; Antonietti, L.; Zacharias, P.; Thomann, R.; Tiller, J.C.; Mecking, S., Hybrids of silver nanoparticles with amphiphilic hyperbranched macromolecules exhibiting antimicrobial properties. *Chem. Commun.* **2002**, 24 3018–3019.
179. Wei, D.; Sun, W.; Qian, W.; Ye, Y.; Ma, X., The synthesis of chitosan-based silver nanoparticles and their antibacterial activity. *Carbohydr. Res.* **2009**, 344, 2375–2382.
180. Ngoc, D. T. T.; Nam, V. N.; Nhan, T. T.; Bich, N. T. T.; Minh, L. Q.; To, N. B. T.; Le, V. P.; Quang, D. V., *Mater. Res. Express* **2019**, 6, 1250 g9.

181. Banerjee, M.; Mallick, S.; Paul, A.; Chattopadhyay, A.; Ghosh, S. S., Heightened reactive oxygen species generation in the antimicrobial activity of a three component iodinated chitosan silver nanoparticle composite. *Langmuir* **2010**, *26*, 5901–5908.
182. Mei, L.; Lu, Z.; Zhnag, X.; Li, C.; Jia, Y., ACS Appl. Mater. Polymer-Ag nanocomposites with enhanced antimicrobial activity against bacterial infection. *Interfaces*, **2014**, *6*, 15813–15821.
183. Aleksandra, I.; Kristina, I.; Javier, H.; Thomas, H.; Susana, S.; Tzanko, T., Layer-by-layer decorated nanoparticles with tunable antibacterial and antibiofilm properties against both Gram-Positive and Gram-Negative bacteria. *ACS Appl. Mater. Interfaces* **2018**, *10*, 3314-3323.
184. Akash, G.; Ryan, F. L.; Cheng-Hsuan, L.; Martin, S.; Riddha, D.; Yi-Wei, L.; Mahdieh, Y.; Yuanchang, L.; Anastasia, K.; Vincent, M. R., Engineered polymer nanoparticles with unprecedented antimicrobial efficacy and therapeutic indices against multidrug-resistant bacteria and biofilms. *J. Am. Chem. Soc.* **2018**, *140*, 12137-12143.
185. Kvitek, L.; Panacek, A.; Soukupova, J.; Kolar, M.; Vecerova, R.; Pucek, R.; Holecova, M.; Zboril, R., Effect of surfactants and polymers on stability and antibacterial activity of silver nanoparticles (NPs). *J Phys Chem C* **2008**, *112*, 5825–5834.
186. Shrivastava, S.; Bera, T.; Roy, A.; Singh, G.; Ramachandrarao, P.; Dash, D., Characterization of enhanced antibacterial effects of novel silver nanoparticles. *Nanotechnology* **2007**, *18*, 2251-2303.
187. Gnanadhas, D. P.; Thomas, M. B.; Thomas, R.; Raichur, A. M.; Chakravorty, D.; Interaction of silver nanoparticles with serum proteins affects their antimicrobial activity in vivo. *Antimicrob Agents Chemother* **2013**, *57*, 4945–4955.
188. Smetana, A.; Klabunde, K.; Marchin, G.; Sorensen, C., Biocidal activity of nanocrystalline silver powders and particles. *Langmuir* **2008**, *24*, 7457–7464.
189. Kooti, M.; Sedeh, A. N.; Motamedi, H.; Rezatofghi, S. E., Magnetic graphene oxide inlaid with silver nanoparticles as antibacterial and drug delivery composite. *Appl. Microbiol. Biotechnol.* **2018**, *102*, 3607–3621.

190. Morones, J. R.; Elechiguerra, J. L.; Camacho, A.; Ramirez, J. T., The bactericidal effect of silver nanoparticles. *Nanotechnology* **2005**, *16*, 2346–2353.
191. Kavya, S.; Das, S.; Moti, H. S.; Jyoti, A.; Kaushik, S., Antibacterial synergy of silver nanoparticles with gentamicin and chloramphenicol against *Enterococcus faecalis*. *Pharmacogn Mag* **2018**, *13*, S828–S833.
192. Hwang, I.; Hwang, J. H.; Choi, H.; Kim, K.; Lee, D. G., Synergistic effects between silver nanoparticles and antibiotics and the mechanisms involved. *J Med Microbiol* **2012**, *61*, 1719–1726.
193. Ping, L.; Li, J.; Wu, C.; Wu, Q.; Li, J, Synergistic antibacterial effects of  $\beta$ -lactam antibiotic combined with silver nanoparticles. *Nanotechnology* **2005**, *16*, 1912–1917.
194. Deng, H.; McShan, D.; Zhang, Y.; Sinha, S. S.; Arslan, Z.; Ray, P. C.; Yu, H., Mechanistic study of the synergistic antibacterial activity of combined silver nanoparticles and common antibiotics. *Environ Sci Technol* **2016**, *50*, 8840–8848.
195. Wallock-Richards, D.; Doherty, C. J.; Doherty, L.; Clarke, D. J.; Place, M.; Govan, J. R., Garlic revisited: antimicrobial activity of allicin-containing garlic extracts against *Burkholderia cepacia* complex. *PLoS ONE* **2014**, *9*, e112726.
196. Sharifi-Rad, J.; Hoseini Alfatemi, S.; Sharifi Rad, M.; Iriti, M., Antimicrobial synergic effect of allicin and silver nanoparticles on skin infection caused by methicillin-resistant *Staphylococcus aureus* spp. *Ann. Med. Health. Sci. Res.* **2014**, *4*, 863–868.
197. Malanovik, N.; Lohner, K., Gram-positive bacterial cell envelopes: the impact on the activity of antimicrobial peptides. *Biochim Biophys Acta Biomembr* **2016**, *1858*, 936–946.
198. Acharya, D.; Singha, M.; Pandey, P.; Mohanta, B.; Rajkumari, J.; Singha, L. P., Shape dependent physical mutilation and lethal effects of silver nanoparticles on bacteria. *Sci Rep* **2018**, *8*, 201-212.
199. Yuan, G.; Peng, Q.; Gurunathan, S., Effects of silver nanoparticles on multiple drug-resistant strains of *Staphylococcus aureus* and *Pseudomonas aeruginosa* from mastitis-infected goats: an alternative approach for antimicrobial therapy. *Int J Mol Sci* **2017**, *18*, 569-591.

200. Radzig, M. A.; Nadtochenko, V. A.; Koksharova, O. A.; Kiwi, J.; Lipasova, V. A.; Khmel, I. A., Antibacterial effects of silver nanoparticles on gram-negative bacteria: influence on the growth and biofilms formation, mechanisms of action. *Colloid Surf B Biointerfaces* **2013**, *102*, 300–306.
201. Akash, G.; Ryan, F. L.; Vincent, M. R., Nanoparticle-based antimicrobials: Surface functionality is critical. *F1000Research* **2016**, *5*, 364-374.
202. de Campos, P. A.; Royer, S.; Batistão, D. W.; Araújo, B. F.; Queiroz, L. L.; de Brito, C. S.; Gontijo-Filho, P. P.; Ribas, R. M., Multidrug resistance related to biofilm formation in *Acinetobacter baumannii* and *Klebsiella pneumoniae* clinical strains from different pulsotypes. *Curr Microbiol* **2016**, *72*, 617-628.
203. Singh, S.; Singh, S. K.; Chowdhury, I.; Singh, R.; Understanding the mechanism of bacterial biofilms resistance to antimicrobial agents. *Open Microbiol J* **2017**, *11*, 53-62.
204. Mohanty, S.; Mishra, S.; Jena, P.; Jacob, B.; Sarkar, B.; Sonawane, A., An investigation on the antibacterial, cytotoxic, and antibiofilm efficacy of starch-stabilized silver nanoparticles. *Nanomedicine* **2012**, *8*, 916–924.
205. Habash, M.B.; Park, A.J.; Vis, E.C.; Harris, R.J.; Khursigara, C.M., Synergy of silver nanoparticles and aztreonam against *Pseudomonas aeruginosa* PAO1 biofilms. *Antimicrob. Agents Chemother.* **2014**, *58*, 5818–5830.
206. Bryaskova, R.; Pencheva, D.; Nikolov, S.; Kantardjiev, T., Synthesis and comparative study on the antimicrobial activity of hybrid materials based on silver nanoparticles (AgNPs) stabilized by polyvinylpyrrolidone (PVP). *J. Chem. Biol.* **2011**, *4*, 185–191.
207. Jaiswal, S.; Bhattacharya, K.; McHale, P.; Duffy, B., Dual effects of beta-cyclodextrin-stabilised silver nanoparticles: Enhanced biofilm inhibition and reduced cytotoxicity. *J. Mater. Sci. Mater. Med.* **2015**, *26*, 52-62.
208. Li, Y.; Leung, P.; Yao, L.; Song, Q.W.; Newton, E., Antimicrobial effect of surgical masks coated with nanoparticles. *J. Hosp. Infect.* **2006**, *62*, 58–63.
209. Stevens, K.N.; Croes, S.; Boersma, R.S.; Stobberingh, E.E.; van der Marel, C.; van der Veen, F.H.; Knetsch, M.L.; Koole, L.H., Hydrophilic surface coatings with embedded biocidal silver

- nanoparticles and sodium heparin for central venous catheters. *Biomaterials* **2011**, 32, 1264–1269.
210. Gravante, G.; Montone, A., A retrospective analysis of ambulatory burn patients: Focus on wound dressings and healing times. *Ann. R. Coll. Surg. Engl.* **2010**, 92, 118–123.
211. Duran, N.; Duran, M.; de Jesus, M.B.; Seabra, A.B.; Favaro, W.J.; Nakazato, G., Silver nanoparticles: A new view on mechanistic aspects on antimicrobial activity. *Nanomed. Nanotechnol.* **2016**, 12, 789–799.
212. Li, J.; Tang, M.; Xue, Y., Review of the effects of silver nanoparticle exposure on gut bacteria. *J. Appl. Toxicol.* **2019**, 39, 27–37.
213. Vila, L.; García-Rodríguez, A.; Cortés, C.; Marcos, R.; Hernández, A., Assessing the effects of silver nanoparticles on monolayers of differentiated Caco-2 cells, as a model of intestinal barrier. *Food Chem. Toxicol.* **2018**, 116, 1–10.
214. Gil-Sánchez, I.; Monge, M.; Miralles, B.; Armentia, G.; Cueva, C.; Crespo, J.; de Luzuriaga, J.M.L.; Olmos, M.E.; Bartolomé, B.; de Llano, D.G., Some new findings on the potential use of biocompatible silver nanoparticles in winemaking. *Innov. Food Sci. Emerg.* **2019**, 51, 64–72.
215. Liu, H.; Wang, X.; Wu, Y.; Hou, J.; Zhang, S.; Zhou, N.; Wang, X., Toxicity responses of different organs of zebrafish (*Danio rerio*) to silver nanoparticles with different particle sizes and surface coatings. *Environ. Pollut.* **2019**, 246, 414–422.
216. Wilding, L.A.; Bassis, C.M.; Walacavage, K.; Hashway, S.; Leroueil, P.R.; Morishita, M.; Maynard, A.D.; Philbert, M.A.; Bergin, I.L., Repeated dose (28-day) administration of silver nanoparticles of varied size and coating does not significantly alter the indigenous murine gut microbiome. *Nanotoxicology* **2016**, 10, 513–520.
217. Vladimir, P. T., Multifunctional, stimuli-sensitive nanoparticulate systems for drug delivery. *Nat. Rev. Drug Discovery* **2014**, 13, 813–827.
218. Dissaya, P.; Li, Z.; Sage, O.; Santosh, A.; Marygorret, O.; Kenneth, V.; Chun-Ming, H.; Liangfang, Z., Bacterial toxin-triggered drug release from gold nanoparticle-stabilized liposomes for the treatment of bacterial infection. *J. Am. Chem. Soc.* **2011**, 133, 4132–4139.

219. Li-Li, L.; Jun-Hua, X.; Guo-Bin, Q.; Xingzhong, Z.; Faquan, Y.; Hao, W., Core-shell su./pramolecular gelatin nanoparticles for adaptive and "on-demand" antibiotic delivery. *ACS Nano*, **2014**, *8*, 4975–4983.
220. Begona, S.; Elias, F.; Roblot-Treupel, L.; Patrick, C., Design of nanoparticles of less than 50 nm diameter: preparation, characterization and drug loading. *Int. J. Pharm.* **1990**, *62*, 1–7.
221. Marchioni, M.; Jouneau, P.H.; Chevallet, M.; Michaud-Soret, I.; Deniaud, A., Silver nanoparticle fate in mammals: Bridging *in-vitro* and *in-vivo* studies. *Coord. Chem. Rev.* **2018**, *364*, 118–136.
222. Cueva, C.; Gil-Sánchez, I.; Ayuda-Durán, B.; González-Manzano, S.; González-Paramás, A.M.; Santos-Buelga, C.; Moreno-Arribas, M., An integrated view of the effects of wine polyphenols and their relevant metabolites on gut and host health. *Molecules* **2017**, *22*, 99.
223. Kaiyuan, Z.; Magdiel, I. S.; Tze-Peng, L.; David, T. L.; Jianping, X., Antimicrobial cluster bombs: Silver nanoclusters packed with daptomycin. *ACS Nano* **2016**, *10*, 7934–7942.
224. Kalishwaralal, K.; BarathManiKanth, S.; Pandian, S.R.; Deepak, V.; Gurunathan, S., Silver nanoparticles impede the biofilm formation by *Pseudomonas aeruginosa* and *Staphylococcus epidermidis*. *Colloids Surf. B Biointerfaces* **2010**, *79*, 340–344.
225. Yuan, Z.; Cai, N.; Du, Y.; He, Y.; Yeung, E. S. Sensitive and selective detection of copper ions with highly stable polyethyleneimine-protected silver nanoclusters. *Anal. Chem.* **2014**, *86*, 419–426.
226. Qu, F.; Li, N. B.; Luo, H. Q. Transition from nanoparticles to nanoclusters: microscopic and spectroscopic investigation of sizedependent physicochemical properties of polyamine-functionalized silver nanoclusters. *J. Phys. Chem. C* **2013**, *117*, 3548–3555.
227. Manoth, M.; Manzoor, K.; Patra, M.; Pandey, P.; Vadera, S.; Kumar, N. Dendrigrft polymer-based synthesis of silver nanoparticles showing bright blue fluorescence. *Mater. Res. Bull.* **2009**, *44*, 714–717.
228. Desai, R.; Mankad, V.; Gupta, S. K.; Jha, P. K., Size distribution of silver nanoparticles: UV-visible spectroscopic assessment. *Nanosci. Nanotechnol. Lett.* **2012**, *4*, 30-34.

229. Benjamin, B.; Mohamed, C.; Kunqiang, H.; Franck, R., Absorption spectra of aryl thiol-coated silver nanoclusters: A time dependent density-functional study. *J. Phys. Chem* **2015**, *119*, 8, 4268–4277.
230. Indranath, C.; Jayanthi, E.; Anuradha, G.; Sugi, K. S.; Thumu, U.; Atanu, G.; Thalappil, P., Emergence of metallicity in silver clusters in the 150 atom regime: a study of differently sized silver clusters. *Nanoscale* **2014**, *6*, 8024–8031.
231. Sami, A. M.; Lauri, L.; Jussi, E.; Hannu, J. H., Birth of the localized surface plasmon resonance in monolayer protected gold nanoclusters. *ACS Nano* **2013**, *7*, 11, 10263–10270.
232. Ciarán, M. M.; Matthias, R.; Peter, W.; Adriele, P., Characterisation of particles in solution –a perspective on light scattering and comparative technologies. *Science and Technology of Advanced Materials* **2018**, *19*, 732–745.
233. Chee, Y. Y., Enhanced molecular level dispersion and interface bonding at low loading of modified graphene oxide to fabricate super nylon 12 composites. *ACS Appl. Mater. Interfaces* **2015**, *7*, 5, 3142–3151.
234. Kim, K.; Lee, H. B.; Lee, J. W.; Park, H. K.; Shin, K. S. Self assembly of poly(ethylenimine)-capped Au nanoparticles at a toluene–water interface for efficient surface-enhanced raman scattering. *Langmuir* **2008**, *24*, 7178–7183.
235. Kumari, J.; Mamta, B.; Ajeet, S., Characterization of silver nanoparticles synthesized using *Urtica dioica* Linn. leaves and their synergistic effects with antibiotics. *Journal of Radiation Research and Applied Sciences* **2016**, *9*, 217-227.
236. Ibrahim, J.; Gutao, P.; Xing, Y. Yu, T.; Zhao, M.; Alexander, K.; Ava, F.; Parish, C. L.; Feng, D.; Thomas, P. D.; Pu, C. K.; Lin, S., Inhibition of amyloid beta toxicity in zebrafish with a chaperone-gold nanoparticle dual strategy. *Nat. Commun.* **2019**, *10*, 3780.
237. Cabaleiro-Lago, C.; Quinlan-Pluck, F.; Lynch, I.; Lindman, S.; Minogue, A. M.; Thulin, E.; Walsh, D. M.; Dawson, K. A.; Linse, S., Inhibition of amyloid  $\beta$  protein fibrillation by polymeric nanoparticles. *J. Am. Chem. Soc.* **2008**, *130*, 15437-15443.
238. Whitmore, L.; Wallace, B. A., Protein secondary structure analyses from circular dichroism spectroscopy: Methods and reference databases. *Biopolymers: Original Research on Biomolecules* **2008**, *89*, 392-400.

239. Rongtao, Z.; Wen, K.; Mingxuan, S.; Yi, Y.; Wanying, L.; Min, Lv.; Shiping, S.; Lihua, W.; Hongbin, S.; Rongzhang, H., Highly stable graphene-based nanocomposite (GO-PEI-Ag) with broad-spectrum, long-term antimicrobial activity and antibiofilm effects. *ACS Appl. Mater. Interfaces* **2018**, *10*, 17617–17629.
240. Yuan-Chieh, Y.; Tse-Hung, H.; Shih-Chun, Y.; Chin-Chang, C.; Jia-You, F., Nano-based drug delivery or targeting to eradicate bacteria for infection mitigation: A review of recent advances. *Front. Chem.* **2020**, *8*, 286-308.
241. Mounyr, B.; Moulay, S.; Saad, K. I., Methods for *in-vitro* evaluating antimicrobial activity: A review. *Journal of Pharmaceutical Analysis* **2016**, *6*, 71-79.
242. Akash, G.; Riddha, D.; Yesilbag Tonga, G.; Mizuhara, T.; Vincent, M. R., Charge-switchable nanozymes for bioorthogonal imaging of biofilm-associated infections. *ACS Nano* **2018**, *12*, 89–94.
243. Alakomi, H.-L.; Skyttä, E.; Saarela, M.; Mattila-Sandholm, T.; Latva-Kala, K.; Helander, I., Lactic acid permeabilizes gram-negative bacteria by disrupting the outer membrane. *Appl. Environ. Microbiol.* **2000**, *66*, 2001-2005.
244. Zannatul, F.; Abderrahim, N., Health impact of silver nanoparticles: A review of the biodistribution and toxicity following various routes of exposure. *Int. J. Mol. Sci.* **2020**, *21*, 2375-2406.
245. Mahmuda, A.; M. Tajuddin, S.; M. Mostafizur, R.; A.K.M. Atique, U.; Kaniz, F.; Binte, H.; Subrata, B.; Toshiyuki, H.; Takeshi, S.; Masaaki, K., A systematic review on silver nanoparticles-induced cytotoxicity: Physicochemical properties and perspectives. *Journal of Advanced Research* **2018**, *9*, 1-16.
246. Tianlu, Z.; Liming, W.; Qiang, C.; Chunying, C., Cytotoxic potential of silver nanoparticles. *Yonsei Med J* **2014**, *55*, 283-291.
247. Huo, S.; Jiang, Y.; Gupta, A.; Jiang, Z.; Landis, R. F.; Hou, S.; Liang, X. J.; Rotello, V. M. Fully zwitterionic nanoparticle antimicrobial agents through tuning of core size and ligand structure. *ACS Nano* **2016**, *10*, 8732–8737.

248. Yasemin, B.; Rabia, C.; Tolga, Z.; Burak, O.; Zeynep, K.; Abdurrahim, C. E.; Serda, K., Chapter-10 Assessment of nano-toxicity and safety profiles of silver nanoparticles. *Silver nanoparticles - Fabrication, characterization and applications* **2018**, 185-208.
249. Khan, Z.; Rehman, A.; Nisar, M. A.; Zafar, S., Molecular basis of Cd<sup>2+</sup> stress response in *Candida tropicalis*. *Appl. Microbiol. Biotechnol.* **2017**, 101, 7715–7728.
250. Catalina, M.; Eric, M. V. H., A review of the antibacterial effects of silver nanomaterials and potential implications for human health and the environment. *J Nanopart Res* **2010**, 12, 1531–1551.
251. Sun, Y.; Alexander, K.; Xing, Y.; Faridi, P.; Aparna, N.; Purcell, A. W.; Thomas, P. D.; Pu, C. K.; Feng, D., Amyloid self-assembly of hIAPP8-20 via the accumulation of helical oligomers,  $\alpha$ -helix to  $\beta$ -sheet transition, and formation of  $\beta$ -barrel intermediates. *Small* **2019**, 15, 1805166.
252. Shirvanyants, D.; Ding, F.; Tsao, D.; Ramachandran, S.; Dokholyan, N. V., DMD: An efficient and versatile simulation method for fine protein characterization. *J Phys. Chem. B* **2012**, 116, 8375-8382.
253. Proctor, E. A.; Dokholyan, N. V., Applications of discrete molecular dynamics in biology and medicine. *Curr. Opin. Str. Biol.* **2016**, 37, 9-13.
254. Ding, F.; Dokholyan, N. V., Discrete molecular dynamics simulation of biomolecules. *In Computational Modeling of Biological Systems, Springer: 2012*, 55-73.
255. Wang, B.; Seabrook, S. A.; Nedumpully-Govindan, P.; Chen, P.; Yin, H.; Waddington, L.; Epa, V. C.; Winkler, D. A.; Kirby, J. K.; Ding, F., Thermostability and reversibility of silver nanoparticle-protein binding. *Phys. Chem. Chem. Phys.* **2015**, 17, 1728-1739.
256. Levy, S. B.; Marshall, B. Antibacterial resistance worldwide: causes, challenges and responses. *Nat. Med.* **2004**, 10, S122–S129.
257. Agarwal, V.; Nair, S. K. Infectious disease diagnosis; *Springer*, **2013**, 7–26.
258. Christena, L. R.; Mangalagowri, V.; Pradheeba, P.; Ahmed, K. B. A.; Shalini, B. I. S.; Vidyalakshmi, M.; Anbazhagan, V.; Subramanian, N. S. Copper nanoparticles as an efflux pump inhibitor to tackle drug resistant bacteria. *RSC Adv.* **2015**, 5, 12899–12909.

259. Lin, G.; Mi, P.; Chu, C.; Zhang, J.; Liu, G. Inorganic nanocarriers overcoming multidrug resistance for cancer theranostics. *Adv. Sci.* **2016**, *3*, 1600134.
260. Wenzel, R. P.; Edmond, M. B. Managing antibiotic resistance. *N. Engl. J. Med.* **2000**, *343*, 1961–1963.
261. Norman, R. S.; Stone, J. W.; Gole, A.; Murphy, C. J.; SaboAttwood, T. L. Targeted photothermal lysis of the pathogenic bacteria, *Pseudomonas aeruginosa*, with gold nanorods. *Nano Lett.* **2008**, *8*, 302–306.
262. Ayala-Núñez, N. V.; Villegas, H. H. L.; et al. Silver nanoparticles toxicity and bactericidal effect against methicillin-resistant *Staphylococcus aureus*: nanoscale does matter. *Nanobiotechnology* **2009**, *5*, 2–9.
263. Fischbach, M. A. Combination therapies for combating antimicrobial resistance. *Curr. Opin. Microbiol.* **2011**, *14*, 519–23.
264. Eby, D. M.; Schaeublin, N. M.; Farrington, K. E.; Hussain, S. M.; Johnson, G. R. Lysozyme catalyzes the formation of antimicrobial silver nanoparticles. *ACS Nano* **2009**, *3*, 984–994.
265. Zhao, Y.; Tian, Y.; Cui, Y.; Liu, W.; Ma, W.; Jiang, X. Small molecule-capped gold nanoparticles as potent antibacterial agents that target Gram-negative bacteria. *J. Am. Chem. Soc.* **2010**, *132*, 12349–12356.
266. Rayan, F. L.; Li, C. H.; Akash, G.; Lee, Y. W.; Yazdani, M.; Ngernyuang, N.; Altinbasak, I.; Mansoor, S.; Khichi, M. A. S.; Sanyal, A.; Vincent, M. R., Biodegradable nanocomposite antimicrobials for the eradication of multidrug resistant bacterial biofilms without accumulated resistance. *J. Am. Chem. Soc.* **2018**, *140*, 6176–6182.
267. Zhao, Y.; Chen, Z.; Chen, Y.; Xu, J.; Li, J.; Jiang, X. Synergy of non-antibiotic drugs and pyrimidine thiol on gold nanoparticles against superbugs. *J. Am. Chem. Soc.* **2013**, *135*, 12940–12943.
268. Yang, X.; Yang, J.; Wang, L.; Ran, B.; Jia, Y.; Zhang, L.; Yang, G.; Shao, H.; Jiang, X. Pharmaceutical intermediate-modified gold nanoparticles: against multidrug resistant bacteria and wound-healing application via an electrospun scaffold. *ACS Nano* **2017**, *11*, 5737–5745.

269. Moyano, D. F.; Saha, K.; Prakash, G.; Yan, B.; Kong, H.; Yazdani, M.; Rotello, V. M. Fabrication of corona-free nanoparticles with tunable hydrophobicity. *ACS Nano* **2014**, *8*, 6748–6755.
270. Raffi, M.; Mehrwan, S.; Bhatti, T. M.; Akhter, J. I.; Hameed, A.; Yawar, W.; ul Hasan, M. M., Investigations into the antibacterial behavior of copper nanoparticles against *Escherichia coli*. *Annals of Microbiology* **2010**, *60*, 75-80.
271. Rai, M. K.; Deshmukh, S.; Ingle, A.; Gade, A. Silver nanoparticles: the powerful nanoweapon against multidrug-resistant bacteria. *J. Appl. Microbiol.* **2012**, *112*, 841–852.
272. Baker, C.; Pradhan, A.; Pakstis, L.; Pochan, D. J.; Shah, S. I. Synthesis and antibacterial properties of silver nanoparticles. *J. Nanosci. Nanotechnol.* **2005**, *5*, 244–249.
273. Zheng, K.; Setyawati, M. I.; Lim, T.; Leong, D. T.; Xie, J. Antimicrobial cluster bombs: silver nanoclusters packed with daptomycin. *ACS Nano* **2016**, *10*, 7934–7942.
274. Lemire, J. A.; Harrison, J. J.; Turner, R. J. Antimicrobial activity of metals: mechanisms, molecular targets and applications. *Nat. Rev. Microbiol.* **2013**, *11*, 371–384.
275. Goodman, C. M.; McCusker, C. D.; Yilmaz, T.; Rotello, V. M. Toxicity of gold nanoparticles functionalized with cationic and anionic side chains. *Bioconjugate Chem.* **2004**, *15*, 897–900.
276. Hayden, S. C.; Zhao, G.; Saha, K.; Phillips, R. L.; Li, X.; Miranda, O. R.; Rotello, V. M.; El-Sayed, M. A.; Schmidt-Krey, I.; Bunz, U. H. F. Aggregation and interaction of cationic nanoparticles on bacterial surfaces. *J. Am. Chem. Soc.* **2012**, *134*, 6920–6923.
277. Arbab, A. S.; Wilson, L. B.; Ashari, P.; Jordan, E. K.; Lewis, B. K.; Frank, J. A. A model of lysosomal metabolism of dextran coated superparamagnetic iron oxide (SPIO) nanoparticles: implications for cellular magnetic resonance imaging. *NMR Biomed.* **2005**, *18*, 383–389.
278. Shang, L.; Dong, S. Facile preparation of water-soluble fluorescent silver nanoclusters using a polyelectrolyte template. *Chem. Commun.* **2008**, 1088–1090.
279. Yuan, Z.; Cai, N.; Du, Y.; He, Y.; Yeung, E. S. Sensitive and selective detection of copper ions with highly stable polyethyleneimine-protected silver nanoclusters. *Anal. Chem.* **2014**, *86*, 419–426.
280. Eissa, A. M.; Abdulkarim, A.; Sharples, G. J.; Cameron, N. R. Glycosylated nanoparticles as efficient antimicrobial delivery agents. *Biomacromolecules* **2016**, *17*, 2672–2679.

281. Qu, F.; Li, N. B.; Luo, H. Q. Highly sensitive fluorescent and colorimetric pH sensor based on polyethylenimine-capped silver nanoclusters. *Langmuir* **2013**, *29*, 1199–1205.
282. Dai, X.; Guo, Q.; Zhao, Y.; Zhang, P.; Zhang, T.; Zhang, X.; Li, C., Functional Silver Nanoparticle as a Benign Antimicrobial Agent That Eradicates Antibiotic-Resistant Bacteria and Promotes Wound Healing. *ACS Applied Materials & Interfaces* **2016**, *10*, 1021-1067.
283. Kim, H.; Namgung, R.; Singha, K.; Oh, I.-K.; Kim, W. J., Graphene oxide–polyethylenimine nanoconstruct as a gene delivery vector and bioimaging tool. *Bioconjugate chemistry* **2011**, *22*, 2558-2567.
284. Worthington, R. J.; Melander, C., Combination approaches to combat multi-drug resistant bacteria. *Trends Biotechnol.* **2013**, *31*, 177–184.
285. Pauksch, L.; Hartmann, S.; Rohnke, M.; Szalay, G.; Alt, V.; Schnettler, R.; Lips, K. S. Biocompatibility of silver nanoparticles and silver ions in primary human mesenchymal stem cells and osteoblasts. *Acta Biomater.* **2014**, *10*, 439–449.
286. Li, X.; Robinson, S. M.; Akash, G.; Saha, K.; Jiang, Z.; Moyano, D. F.; Sahar, A.; Riley, M. A.; Vincent, M. R., Functional gold nanoparticles as potent antimicrobial agents against multi-drug resistant bacteria. *ACS Nano* **2014**, *8*, 10682–10686.
287. Padmos, J. D.; Boudreau, R. T. M.; Weaver, D. F.; Zhang, P. Structure of tiopronin-protected silver nanoclusters in a onedimensional assembly. *J. Phys. Chem. C* **2015**, *119*, 24627–24635.
288. Beyth, N.; Houry-Haddad, Y.; Domb, A.; Khan, W.; Hazan, R. Alternative antimicrobial approach: nano-antimicrobial materials. *J. Evidence-Based Complementary Altern. Med.* **2015**, 246012.
289. Eckhardt, S.; Brunetto, P. S.; Gagnon, J.; Priebe, M.; Giese, B.; Fromm, K. M., Nanobio silver: Its interactions with peptides and bacteria, and its uses in medicine. *Chem. Rev.* **2013**, *113*, 4708–4754.
290. Sangsuwan, A.; Kawasaki, H.; Matsumura, Y.; Iwasaki, Y. Antimicrobial Silver Nanoclusters Bearing Biocompatible Phosphorylcholine-Based Zwitterionic Protection. *Bioconjugate Chem.* **2016**, *27*, 2527–2533.

291. Godbey, W. T.; Wu, K.; Hirasaki, G.; Mikos, A. Improved packing of poly(ethylenimine)/DNA complexes increases transfection efficiency. *Gene Ther.* **1999**, *6*, 1380–1388.
292. Hou, Z.; Shankar, Y. V.; Liu, Y.; Ding, F.; Subramanion, J. L.; Ravikumar, V.; Zamudio, R.; Keogh, D.; Lim, K.; et al. Nanoparticles of short cationic peptidopolysaccharide self-assembled by hydrogen bonding with antibacterial effect against multidrug-resistant bacteria. *ACS Appl. Mater. Interfaces* **2017**, *9*, 38288–38303.
293. You, F.; Tang, W.; Yung, L. L. Real-time monitoring of Trojanhorse effect of silver nanoparticles by a genetically encoded fluorescent cell sensor. *Nanoscale* **2018**, *10*, 7726–7735.
294. Rajchakit, U.; Sarojini, V. Recent developments in antimicrobial-peptide-conjugated gold nanoparticles. *Bioconjugate Chem.* **2017**, *28*, 2673–2686.
295. Sadamoto, R.; Niikura, K.; Sears, P. S.; Liu, H.; Wong, C.; Suksomcheep, A.; et al. Cell wall engineering of living bacteria. *J. Am. Chem. Soc.* **2002**, *124*, 9018–9019.
296. Wiegand, I.; Hilpert, K.; Hancock, R. E. Agar and broth dilution methods to determine minimum inhibitory concentration (MIC) of antimicrobial substances. *Nat. Protoc.* **2008**, *3*, 163–175.
297. Wilson, M. R.; Jiang, Y.; Villalta, P. W.; Stornetta, A.; Boudreau, P. D.; Carrá, A.; Brennan, C. A.; Chun, E.; Ngo, L.; Samson, L. D., The human gut bacterial genotoxin colibactin alkylates DNA. *Science* **2019**, *363*, eaar7785.
298. Valles-Colomer, M.; Falony, G.; Darzi, Y.; Tigchelaar, E. F.; Wang, J.; Tito, R. Y.; Schiweck, C.; Kurilshikov, A.; Joossens, M.; Wijmenga, C., The neuroactive potential of the human gut microbiota in quality of life and depression. *Nat Microbiol* **2019**, *4*, 623.
299. Lebovitz, Y. Modulation of neurodevelopmental outcomes using *Lactobacillus* in a model of maternal microbiome dysbiosis. *Virginia Tech*, **2019**.
300. Meijnikman, A. S.; Gerdes, V. E.; Nieuwdorp, M.; Herrema, H., Evaluating causality of gut microbiota in obesity and diabetes in humans. *Endocr. Rev.* **2017**, *39*, 133-153.

301. Koh, A.; Molinaro, A.; Ståhlman, M.; Khan, M. T.; Schmidt, C.; Mannerås-Holm, L.; Wu, H.; Carreras, A.; Jeong, H.; Olofsson, L. E., Microbially produced imidazole propionate impairs insulin signaling through mTORC1. *Cell* **2018**, 175, 947-961. e17.
302. Taglialegna, A.; Lasa, I.; Valle, J., Amyloid structures as biofilm matrix scaffolds. *J. Bacteriol.* **2016**, 198, 2579-2588.
303. Wang, L.; Hu, C.; Shao, L., The antimicrobial activity of nanoparticles: present situation and prospects for the future. *Int. J. Nanomed.* **2017**, 12, 1227.
304. Pu, C. K.; Sani, M.-A.; Feng, D.; Alexander, K.; Ibrahim, J.; Separovic, F.; Thomas, P. D.; Mezzenga, R., Implications of peptide assemblies in amyloid diseases. *Chem. Soc. Rev.* **2017**, 46, 6492-6531.
305. Dueholm, M. S.; Petersen, S. V.; Sønderkær, M.; Larsen, P.; Christiansen, G.; Hein, K. L.; Enghild, J. J.; Nielsen, J. L.; Nielsen, K. L.; Nielsen, P. H., Functional amyloid in pseudomonas. *Mo. Microbiol.* **2010**, 77, 1009-1020.
306. Fowler, D. M.; Koulov, A. V.; Balch, W. E.; Kelly, J. W., Functional amyloid—From bacteria to humans. *Trends Biochem. Sci.* **2007**, 32, 217-224.
307. DePace, A. h., A critical role for amino-terminal glutamine/asparagine repeats in the formation and propagation of a yeast prion. *Cell* **1998**, 93,1241-1252.
308. Romero, D.; Valentin, E. S.; Vlamakis, H.; Kolter, R., Biofilm inhibitors that target amyloid proteins. *Chemistry & Biology* **2013**, 20, 102.
309. Flemming, H.-C.; Wingender, The biofilm matrix. *J., Nat. Rev. Microbiol.* **2010**, 8, 623.
310. Seviour, T.; Hansen, S. H.; Yang, L.; Yau, Y. H.; Wang, V. B.; Stenvang, M. R.; Christiansen, G.; Marsili, E.; Givskov, M.; Chen, Y., Functional amyloids keep quorum-sensing molecules in check. *J. Biol. Chem.* **2015**, 290, 6457-6469.
311. Smith, A. W., Biofilms and antibiotic therapy: Is there a role for combating bacterial resistance by the use of novel drug delivery systems? *Adv. Drug Deliv. Rev.* **2005**, 57, 1539-1550.
312. Toole, G. O.; Kaplan, H. B.; Kolter, R., Biofilm formation as microbial development. *Annu. Rev. Microbiol.* **2000**, 54, 49.

313. D. Davies, Understanding biofilm resistance to antibacterial agents. *Nat Rev Drug Discov.* **2003**, 2, 114.
314. L. H. Stoodley, J. W. Costerton, P. Stoodley, Bacterial biofilms: From the natural environment to infectious diseases. *Nat Rev Microbiol.* **2004**, 2, 95.
315. Dueholm, M. S.; Søndergaard, M. T.; Nilsson, M.; Christiansen, G.; Stensballe, A.; Overgaard, M. T.; Givskov, M.; Tolker-Nielsen, T.; Otzen, D. E.; Nielsen, P. H., Expression of Fap amyloids in pseudomonas aeruginosa, P. fluorescens, P. putida results in aggregation and increased biofilm formation. *Microbiologyopen* **2013**, 2, 365-382.
316. Evans, M. L.; Chorell, E.; Taylor, J. D.; Åden, J.; Göthesson, A.; Li, F.; Koch, M.; Sefer, L.; Matthews, S. J.; Wittung-Stafshede, P., The bacterial curli system possesses a potent and selective inhibitor of amyloid formation. *Mol. Cell* **2015**, 57, 445-455.
317. Zeng, G.; Vad, B. S.; Dueholm, M. S.; Christiansen, G.; Nilsson, M.; Tolker-Nielsen, T.; Nielsen, P. H.; Meyer, R. L.; Otzen, D. E., Functional bacterial amyloid increases Pseudomonas biofilm hydrophobicity and stiffness. *Front. Microbiol.* **2015**, 6, 1099.
318. Stenvang, M.; Dueholm, M. S.; Vad, B. S.; Seviour, T.; Zeng, G.; Geifman-Shochat, S.; Søndergaard, M. T.; Christiansen, G.; Meyer, R. L.; Kjelleberg, S.; Nielsen, P. H.; Otzen, D. E., Epigallocatechin gallate remodels overexpressed functional amyloids in Pseudomonas aeruginosa and increases biofilm susceptibility to antibiotic treatment. *J. Biol. Chem.* **2016**, 291, 26540-26553.
319. Najarzadeh, Z.; Mohammad-Beigi, H.; Pedersen, J. N.; Christiansen, G.; Sønderby, T. V.; Shojaosadati, S. A.; Morshedi, D.; Strømgaard, K.; Meisl, G.; Sutherland, D.; Pedersen, J. S.; Otzen, D. E., Plant polyphenols inhibit functional amyloid and biofilm formation in Pseudomonas strains by directing monomers to off-pathway oligomers. *Biomolecules* **2019**, In press.
320. Xie, Y.; Liu, Y.; Yang, J.; Liu, Y.; Hu, F.; Zhu, K.; Jiang, X., Gold nanoclusters for targeting Methicillin-resistant Staphylococcus Aureus In Vivo. *Angew. Chem. Int. Ed. Engl.* **2018**, 57, 3958-3962.

321. Yan, X.; He, B.; Liu, L.; Qu, G.; Shi, J.; Hu, L.; Jiang, G., Antibacterial mechanism of silver nanoparticles in *Pseudomonas aeruginosa*: proteomics approach. *Metallomics* **2018**, *10*, 557-564.
322. Sirelkhatim, A.; Mahmud, S.; Seeni, A.; Kaus, N.; Ann, L.; Bakhori, S.; Hasan, H.; Mohamad, D., Kinetics model Linear Equation Parameters Values at 0.15 mg mL<sup>-1</sup> DTT Values at 0.35 mg mL<sup>-1</sup> DTT 189, 110.
323. Kim, J. S.; Kuk, E.; Yu, K. N.; Kim, J.-H.; Park, S. J.; Lee, H. J.; Kim, S. H.; Park, Y. K.; Park, Y. H.; Hwang, C.-Y., Antimicrobial effects of silver nanoparticles. *Nanomedicine: NBM* **2007**, *3*, 95-101.
324. Sambhy, V.; MacBride, M. M.; Peterson, B. R.; Sen, A., Silver bromide nanoparticle/polymer composites: Dual action tunable antimicrobial materials. *J. Am. Chem. Soc.* **2006**, *128*, 9798-9808.
325. Zheng, H.; Ji, Z.; Roy, K. R.; Gao, M.; Pan, Y.; Cai, X.; Wang, L.; Li, W.; Chang, C. H.; Kaweeteerawat, C.; Chen, C.; Xia, T.; Zhao, Y.; Li, R., Engineered graphene oxide nanocomposite capable of preventing the evolution of antimicrobial resistance. *ACS Nano* **2019**, *13*, 11488-11499. DOI 10.1021/acsnano.9b04970.
326. John, T.; Gladytz, A.; Kubeil, C.; Martin, L.; Risselada, H. J.; Abel, B., Impact of nanoparticles on amyloid peptide and protein aggregation: a review with a focus on gold nanoparticles. *Nanoscale* **2018**, *10*, 20894.
327. Kim, Y.; Park, J.-H.; Lee, H.; Nam, J.-M., Erratum: How do the size, charge and shape of nanoparticles affect amyloid  $\beta$  aggregation on brain lipid bilayer. *Sci. Rep.* **2016**, *6*, 19548.
328. Pu, C. K.; Emily, H. P.; Sun, Y.; Ibrahim, J.; Alexander, K.; Gutao, P.; Feng, D.; Thomas, P. D., Mitigation of amyloidosis with nanomaterials. *Adv. Mater.* **2019**, *0*, 1901690.
329. Valery, N. B.; Dennis, L.; Adam, B., Application of helium ion microscopy to nanostructured polymer materials. *Nanotechnol Rev* **2014**, *3*, 361-387.
330. Ibrahim, J.; He, J.; Alexander, K.; Ava, F.; Yang, W.; Thomas, P. D.; Pu, C. K.; Chen, P., Probing the aggregation and immune response of human I $\kappa$ B amyloid polypeptides with ligand-stabilized gold nanoparticles. *ACS Appl. Mater. Interfaces* **2019**, *11*, 10462.

331. Gladysz, A.; Abel, B.; Risselada, H. J., Gold induced fibril growth: The mechanism of surface-facilitated amyloid aggregation. *Angew. Chem., Int. Ed.* **2016**, 55, 11242.
332. Ibrahim, J.; Sun, Y.; Adamcik, J.; Wang, B.; Alexander, K.; Emily, H. P.; Feng, D.; Mezzenga, R.; Thomas, P. D.; Pu, C. K., Cofibrillization of pathogenic and functional amyloid proteins with gold nanoparticles against amyloidogenesis. *Biomacromolecules* **2017**, 18, 4316.
333. Liao, Y. H.; Chang, Y. J.; Yoshiike, Y.; Chang, Y. C.; Chen, Y. R., Negatively charged gold nanoparticles inhibit Alzheimer's amyloid- $\beta$  fibrillization, induce fibril dissociation, and mitigate neurotoxicity. *Small* **2012**, 8, 3631.
334. Anand, B. G.; Dubey, K.; Shekhawat, D. S.; Kar, K., Capsaicin-coated silver nanoparticles inhibit amyloid fibril formation of serum albumin. *Biochemistry* **2016**, 55, 3345.
335. Sen, S.; Konar, S.; Das, B.; Pathak, A.; Dhara, S.; Dasgupta, S.; Gupta, S. D., Inhibition of fibrillation of human serum albumin through interaction with chitosan-based biocompatible silver nanoparticles. *RSC Adv.* **2016**, 6, 43104.
336. Wang, M.; Alexander, K.; Emily, H. P.; Thomas, P. D.; Pu, C. K., Differential effects of silver and iron oxide nanoparticles on IAPP amyloid aggregation. *Biomater. Sci.* **2017**, 5, 485.
337. Rizzello, L.; Pompa, P. P., Nanosilver-based antibacterial drugs and devices: Mechanisms, methodological drawbacks, and guidelines. *Chem. Soc. Rev.* **2014**, 43, 1501-1518.
338. Zil-e, H.; Akash, G.; Ibrahim, J.; Riddhe, D.; Sayed, Z. H.; Shazia, M.; Irshad, H.; Vincent, M. R.; Cationic silver nanoclusters as potent antimicrobials against multidrug resistant bacteria. *ACS Omega* **2018**, 3, 16721-16727.
339. Gutao, P.; Zil-e, H.; Umair, M.; Irshad, H.; Ibrahim, J.; In Metal nanoparticles for drug delivery and diagnostic applications (Eds: M. R. Shah, M. Imran, S. Ullah), *Elsevier, Amsterdam* **2019**, 119.
340. Durán, N.; Durán, M.; De Jesus, M. B.; Seabra, A. B.; Fávaro, W. J.; Nakazato, G., Silver nanoparticles: A new view on mechanistic aspects on antimicrobial activity. *Nanomedicine* **2016**, 12, 789.
341. Deshmukh, S.; Patil, S.; Mullani, S.; Delekar, S., Silver nanoparticles as effective disinfectant: A review. *Mater. Sci. Eng. C* **2019**, 97, 954.

342. Palmal, S.; Jana, N. R., Inhibition of amyloid fibril growth by nanoparticle coated with histidine-based polymer. *J. Phys. Chem. C* **2014**, 118, 21630.
343. Wagner, S. C.; Roskamp, M.; Pallerla, M.; R. Araghi, R.; Schlecht, S.; Kokschi, B., Nanoparticle-induced folding and fibril formation of coiled-coil-based model peptides. *Small* **2010**, 6, 1321.
344. Wu, M.; Ma, B.; Pan, T.; Chen, S.; Sun, J., Silver-nanoparticle-colored cotton fabrics with tunable colors and durable antibacterial and self-healing superhydrophobic properties. *Adv. Funct. Mater.* **2016**, 26, 569.
345. Park, J.; Kim, J.; Singha, K.; Han, D. K.; Park, H.; Kim, W. J., Nitric oxide integrated polyethylenimine-based tri-block copolymer for efficient antibacterial activity. *Biomaterials* **2013**, 34, 8766.
346. Xia, T.; Kovochich, M.; Liang, M.; Meng, H.; Kabehie, S.; George, S.; Zink, J. I.; Nel, A. E., Polyethylenimine coating enhances the cellular uptake of mesoporous silica nanoparticles and allows safe delivery of siRNA and DNA constructs. *ACS Nano* **2009**, 3, 3273-3286.
347. Díez, I.; Ras, R. H., Fluorescent silver nanoclusters. *Nanoscale* **2011**, 3, 1963-1970.
348. Ibrahim, J.; Yu, T.; Gutao, P.; Sánchez-Ferrer, A.; Ava, F.; Alexander, K.; Zhao, M.; Mezzenga, R.; Thomas, P. D.; Lin, S.; Pu, C. K., *In-vivo* mitigation of amyloidogenesis through functional-pathogenic double-protein coronae. *Nano Lett.* **2018**, 18, 5797-5804.
349. Wang, M.; Sun, Y.; Cao, X.; Peng, G.; Javed, I.; Kakinen, A.; Davis, T. P.; Lin, S.; Liu, J.; Ding, F.; Ke, P. C., Graphene quantum dots against human IAPP aggregation and toxicity in vivo. *Nanoscale* **2018**, 10, 19995-20006.
350. Wang, Y.; Kadiyala, U.; Qu, Z.; Elvati, P.; Altheim, C.; Kotov, N. A.; Violi, A.; VanEpps, J. S., Anti-biofilm activity of graphene quantum dots via self-assembly with bacterial amyloid proteins. *ACS Nano* **2019**, 13, 4278-4289.
351. Zhang, M.; Mao, X. Yu, Y.; Wang, C. X.; Yang, Y. L.; Wang, C., Nanomaterials for reducing amyloid cytotoxicity. *Adv. Mater.* **2013**, 25, 3780.
352. Vertegel, A. A.; Siegel, R. W.; Dordick, J. S., Silica nanoparticle size influences the structure and enzymatic activity of adsorbed lysozyme. *Langmuir* **2004**, 20, 6800.

353. Tang, S.; Zheng, J., Antibacterial activity of silver nanoparticles: structural effects. *Adv. Healthcare Mater.* **2018**, *7*, 1701503.
354. Jin, J.-C.; Wu, X.-J.; Xu, J.; Wang, B.-B.; Jiang, F.-L.; Liu, Y., Ultrasmall silver nanoclusters: Highly efficient antibacterial activity and their mechanisms. *Biomater. Sci* **2017**, *5*, 247-257.
355. Richards, R., Antimicrobial action of silver nitrate. *Microbios* **1981**, *31*, 83-91.
356. Gurunathan, S.; Han, J. W.; Kwon, D.-N.; Kim, J.-H., Enhanced antibacterial and anti-biofilm activities of silver nanoparticles against gram-negative and gram-positive bacteria. *Nanoscale Res. Lett.* **2014**, *9*, 373.
357. Shaper, M., Antibiotic Resistance in Streptococcus pneumonia : A Disaster in the making. *Epidemiol* **2011**, *1*, 1000102e.
358. Orihuela, C. J.; Gao, G.; Francis, K. P.; Yu, J.; Tuomanen, E. I., Tissue-specific contributions of pneumococcal virulence factors to pathogenesis. *Journal of Infectious Diseases* **2004**, *190*, 1661-1669.
359. Javier, A.; Olga, R.; Felipe, R. C.; Jose´ B.; Rafael, Z.; Asuncio´n, F.; Rosa, C.; Antonio, V.; Francisco, R. S.; Pedro, P. E.; Jordi, R.; Antoni, T., Drug-resistant pneumococcal pneumonia: Clinical relevance and related factors. *Clin Infect Dis* **2004**, *38*, 787-798.
360. World pneumonia day. *The Partnership, PMNCH* **2013**.
361. Daniel, M. M., Infections Caused by streptococcus pneumoniae: Clinical spectrum, pathogenesis, immunity, and treatment. *Clinical Infectious Diseases* **1992**, *14*, 801-807.
362. Moe, H. K.; Ruth, L.; William, S.; Allen, S. C.; James, H.; Arthur, R.; Ann, R. T.; Lee, H. H.; Nancy, M. B.; Monica, M. F.; Richard, R. F.; James, H. J.; John, B.; Elizabeth, R. Z.; Anne, S.; Cynthia, G. W., Effect of introduction of the pneumococcal conjugate vaccine on drug-resistant streptococcus pneumoniae. *The New England Journal of Medicine* **2006**, *354*, 1455-1463.
363. Susan, C., Pneumonia history. News medical life sciences
364. Chapter:17 Pneumococcal disease, immunology and vaccine-preventable diseases. *CDC.* **2015**, *17*, 279-296.

365. Yao, W.; Xiali, D.; Yuan, C.; Mingquan, G.; Yan, Z.; Xiaokui, G.; Hongchen, G., Antibiotic-loaded, silver core-embedded mesoporous silica nanovehicles as a synergistic antibacterial agent for the treatment of drug-resistant infections. *Biomaterials* **2016**, 101, 207-216.
366. Joseph, H.; Ying, J.; Emily, R. T.; Phaedra, C. G.; Gulen, Y. T.; Michelle, E. F.; Vincent, M. R., Simultaneous cytosolic delivery of a chemotherapeutic and siRNA using nanoparticle-stabilized nanocapsules. *Nanotechnology* **2016**, 27, 374001-372007.
367. Nijaporn, Y.; Brian, R. S.; Zhengrong, C., Nanoparticles engineered from lecithin-in-water emulsions as a potential delivery system for docetaxel. *Int J Pharm* **2009**, 379, 174–180.
368. Ronda, K. B.; Rhonda, D. H.; Veolanda, A. P.; Cleon, B.; Shree, R. S.; Vida, A. D.; Mamie, T. C., Silver polyvinyl pyrrolidone nanoparticles exhibit a capsular polysaccharide influenced bactericidal effect against *Streptococcus pneumoniae*. *Front. Microbiol* **2014**, 5, 1-9.
369. Catherine, H.; Emilie, C.; Jonathan, M. C.; Katie, B.; Jeremy, S. B., The streptococcus pneumoniae capsule inhibits complement activity and neutrophil phagocytosis by multiple mechanisms. *Infection And Immunity* **2010**, 78, 704–715.
370. Sven, H.; Sonja, W.; Andreas, H.; Simone, R.; Ellruth, M.; Manfred, R., Illustration of pneumococcal polysaccharide capsule during adherence and invasion of epithelial cells. *Infection And Immunity* **2005**, 73, 4653–4667.
371. Ibrahim, J.; Zhenzhen, Z.; Jozef, A.; Nicholas, A.; Yuhuan, L.; Daniel, E. O.; Sijie, L.; Raffaele, M.; Thomas, P. D.; Feng, D.; Pu, C. K., Accelerated amyloid beta pathogenesis by bacterial amyloid FapC. *Adv. Sci.* **2020**, 2001299-2001313.
372. Ibrahim, J.; Xuejing, C.; Xiaoyu, W.; Monika, M.; Nikolaos, A.; Yuhuan, L.; Thomas, P. D.; Yuliang, Z.; Pu, C. K.; Chunying, C., Implications of the human gut–brain and gut–cancer axes for future nanomedicine. *ACS Nano* **2020**, asap.
373. Kairi, K.; Huayuan, T.; Ibrahim, J.; Mehrdad, P.; Monika, M.; Thomas, P. D.; Sijie, L.; Alan, L. C.; Feng, D.; Pu C. K., Elevated amyloidoses of human IAPP and amyloid beta by lipopolysaccharide and their mitigation by carbon quantum dots. *Nanoscale* **2020**, asap.
374. Rubul, Mout.; Moumita, R.; Gulen, Y. T.; Yi-Wei, L.; Tristan, T.; Kanae, S.; Vincent, M. R., Direct cytosolic delivery of CRISPR/Cas9- Ribonucleoprotein for efficient gene editing. *ACS Nano* **2017**, 11, 2452–2458.